Department of Petroleum Engineering

Sand Production Simulation under True-Triaxial Stress Conditions

Ahmad Reza Younessi Sinaki

This thesis is presented for the Degree of
Doctor of Philosophy
of
Curtin University

October 2012

Declaration

To the best of my knowledge and belief this thesis contains no material previously published by any other person except where due acknowledgement has been made. This thesis contains no material which has been accepted for the award of any other degree or diploma in any university.

Ahmad Reza Younessi Sinaki
Signature: 
Date: 29 October 2012

Copyright

Abstract

Sand production in weakly consolidated sandstone reservoirs could result in damaging the production and surface facilities. Sanding includes two stages: the failure of sandstone around the borehole and sand grains being transported into the borehole. The first stage is related to stresses around the borehole whereas the second one is controlled by drawdown pressure. In order to avoid sanding, the stresses around the borehole and the drawdown pressure which initiate sanding are studied.

This research simulated sand production through laboratory experiments and numerical simulations. The effect of three independent far-field stresses was investigated which is contrary to most of the current studies being performed under a uniaxial or triaxial stress state. Accordingly, a unique experimental setup and procedure was introduced to conduct sand production experiments under true-triaxial stress conditions. The effect of drawdown pressure and state of far-field stresses on the sanding mechanism and development of the failure zone around a borehole were investigated. The experiments were conducted on $100\times100\times100$ mm^3 cubic samples of synthetic sandstones. The samples were manufactured using an established procedure developed to produce samples with properties similar to weakly consolidated sandstone. The properties of the synthetic sandstone samples were determined by conducting a series of standard rock mechanics tests on cylindrical plugs. Using a true-triaxial stress cell (TTSC), cubic samples were subjected to three independent boundary stresses and uniform lateral fluid flow from the outer boundaries. The fluid flows through the sample radially and discharges from a hole drilled at the centre of the sample: this allows the study of sanding initiation by changing the state of stress, sample material and fluid properties.

In this research, firstly, the concept of sand production from a geomechanics point of view and a summary of previous sanding experiments are explained. Thereafter, the procedure to prepare a sample suitable for sand production experiments is provided. Subsequently, the experimental equipment, setup and procedure are explained in detail. This is followed by presenting the results of two sets of experiments performed at different states of stress. The effect of changing the lateral stresses on the development

of the failure zone around borehole was investigated in these experiments. During these experiments it was observed that a minimum drawdown pressure is needed to initiate sand production, regardless of the state of the boundary stresses. In addition, it was observed that the geometry (i.e. width and depth) of the failure zone developed around the borehole is a function of the state of stresses.

The experiments were also simulated numerically using ABAQUS in order to gain a better understanding of sand production mechanisms. The numerical modelling procedure and results are presented in a separate section in this thesis. Good agreement was obtained between the results of both experimental and numerical methods which confirm the importance of the state of stresses on the evolution of sanding. Based on the experimental and numerical observations, it was shown that the effect of the magnitude of the maximum lateral stress on the depth of failure is more significant than the minimum lateral stress.

Contents

List of Figures

Preface

In early 2010 the Department of Petroleum Engineering of Curtin University manufactured a unique true-triaxial stress cell (TTSC) to conduct advanced geomechanics studies in the field of petroleum geomechanics. At that time, the author of this research and a colleague were assigned to set up the TTSC and establish a procedure to conduct sand production and hydraulic fracturing experimental studies. Since then, further equipment was developed and acquired for the purpose of these studies. Amongst them were a uniaxial compressive frame and a data acquisition system, which were designed, developed and set up by these two PhD students. By mid-2011, the geomechanics laboratory was fully operational and able to conduct standard rock mechanics tests and advanced geomechanical experiments using the TTSC.

The work presented in this thesis is the result of three years of laboratory work for the purpose of simulating sand production under true-triaxial stress conditions. The main objective of this work was to establish a new experimental procedure to conduct sand production studies using the TTSC. Thereafter, sand production experiments were conducted to study the effect of stresses and fluid flow on the sanding mechanism and geometry (i.e. width and depth) of the failure zone around a single borehole. To the best of my knowledge, this is one of the very few successful attempts to simulate sand production experimentally under true-triaxial stress conditions associated with fluid flow at the scale presented in this research.

During the course of this research, several papers were published in different conference proceedings and journals, all of which were relevant to the work carried out in this research. Every paper was peer-reviewed by at least two expert reviewers and their comments were applied to improve this work. These papers cover all aspects of this research. Consequently this PhD thesis is presented in the form of a series of published papers. Part I of this thesis contains an overview of the past literature, objectives and significance of this work, applied methodologies and the results are presented in brief. Detailed explanations can be found in the papers referred to in the different sections. Part II contains the published papers.

The following list provides the published papers in the order of their appearance in Part I:

Paper 1 *Younessi A, Rasouli V. A preliminary experimental study on sand production under true triaxial stress conditions. Australian Petroleum Production & Exploration Association Journal 2011:567-76.*

Paper 2 *Younessi A, Rasouli V, Wu B. Proposing a sample preparation procedure for sanding experiments. 2nd Southern Hemisphere International Rock Mechanics Symposium SHIRMS. Sun City, South Africa 2012.*

Paper 3 *Younessi A, Rasouli V, Wu B. Experimental sanding analysis: Thick walled cylinder versus true triaxial tests. 2nd Southern Hemisphere International Rock Mechanics Symposium SHIRMS. Sun City, South Africa2012.*

Paper 4 *Younessi A, Rasouli V, Wu B. The effect of stress anisotropy on sanding: An experimental study. The 46th US Rock Mechanics / Geomechanics Symposium. Chicago, IL 2012.*

Paper 5 *Younessi A, Rasouli V, Wu B. Numerical simulation of sanding under different stress regimes. The 46th US Rock Mechanics / Geomechanics Symposium. Chicago, IL 2012.*

Paper 6 *Younessi A, Rasouli V. A fracture sliding potential index for wellbore stability analysis. International Journal of Rock Mechanics and Mining Sciences. 2010;47:927-39.*

Paper 7 *Younessi A, Rasouli V. Rock Engineering Systems Adopted for Sanding Prediction in Perforation Tunnels. Australian Petroleum Production & Exploration Association Journal 2010:613-22.*

Paper 8 *Younessi A, Rasouli V. Representing rock engineering system to analyse sand production in perforation tunnels. European Rock Mechanics Symposium, EUROCK, Lausanne 2010. p. 845-8.*

At the beginning of each chapter the papers referred to in that chapter are named in the footnote on the first page. In addition, the papers are referred to where needed within each chapter. The material presented in Part I has also been submitted in a different format to the International Journal of Rock Mechanics and Mining Science.

Chapter 1 presents a brief introduction about the problems associated with sand production and a review of past experiments conducted by other researchers. The objectives and significance of this research are outlined in this chapter. In Chapter 2, the importance of sample preparation is described. The needs for using synthetically

manufactured samples for sanding experiments are discussed in this chapter. The procedure for preparing synthetic samples and the sample properties used in this study are presented in this chapter. A unique experiment setup and procedure is introduced to conduct sand production experiments under true-triaxial stress conditions in Chapter 3. In addition, the results of the sanding experiments conducted to investigate the effect of lateral stresses on the sanding mechanism and failure dimension are elaborated in this chapter. A finite element numerical program (ABAQUS) was used to simulate these experiments. The numerical modelling and results are presented in Chapter 4. In the last section of this chapter, a brief discussion is given to justify the observations from the experimental and numerical simulations. Finally, a summary of this work is presented in Chapter 5, followed by conclusions and recommendations for further work.

This work could not have been completed without the help and support of many individuals during these three years. I would like to express my gratitude to my supervisor Associate Professor Vamegh Rasouli who gave me this opportunity to pursue my PhD. His unlimited support and guidance made this project complete. It was a privilege for me to have Dr Bailin Wu, CSIRO Earth Science and Resource Engineering, as my associate supervisor in this work. His invaluable comments helped me to improve the quality of this research. I would like to acknowledge Dr Ali Saeedi, Curtin University Department of Petroleum Engineering, Dr Maxim Lebedev, Curtin University Department of Exploration Geophysics, Mr Bruce Maney and Dr Joel Sarout, CSIRO Earth Science and Resource Engineering, for their guidance in the development of the geomechanics laboratory tests. It was a pleasure for me to work together with Mr Mohammad Sarmadivaleh during the past few years to extend the capabilities of the geomechanics laboratory. A very special recognition goes to my friend Mr Amin Chamani who introduced me to priceless literatures. I would like to thank current staff and PhD students at the Department of Petroleum Engineering who helped me in different ways during the course of my PhD. Last but not least, I would like to acknowledge the non-stop support of both my parents and parents-in-law and their patience during these years.

To my beautiful wife Farnoosh.

Because of her, I managed to tick this off my bucket list.

Part I Research overview

1 Introduction to experimental sand production*

The stability of underground excavations is a significant concern in the field of civil, mining and petroleum engineering. In petroleum engineering, formation failure around a borehole may cause severe problems during different stages of drilling and hydrocarbon production. Amongst the problems is that of failure of the borehole in sandstone reservoirs during hydrocarbon production, known as *sand production*. Sand production not only causes several problems in maintaining borehole integrity but also is a problem during production where erosion-induced damage to the downhole and surface production facilities can occur.

A wide range of unconsolidated to consolidated sand reservoirs exists, each requires a different well completion system. In consolidated formations the sandstone is strong enough to resist failures. No sand control systems are required in these types of reservoirs. On the other hand, the unconsolidated sandstones are weak and sands are produced as soon as the hydrocarbon production begins. Sand control is essential in these types of reservoirs. The mechanics of weakly consolidated sandstones needs to be studied in more detail to optimise the completion system in order to reduce the costs associated with sand production (Veeken et al., 1991).

1.1 Sand production mechanism

In weakly consolidated sandstones, the onset of sanding occurs in two stages: *failure* and *transportation*. If the stresses induced around a borehole exceed the strength of the formations surrounding the borehole, the sandstone yields and fails eventually. Thereafter, the flow of hydrocarbon into the borehole transports the failed sands (Figure 1.1). Sand production can be prevented by predicting and mitigating the failure stage.

The majority of sand production problems occur in unconsolidated sands. In this type of formation the bonds between the sand grains are extremely weak, and borehole

* The contents given in this chapter are based on the following paper:
Paper 1. A preliminary experimental study on sand production under true triaxial stress conditions.

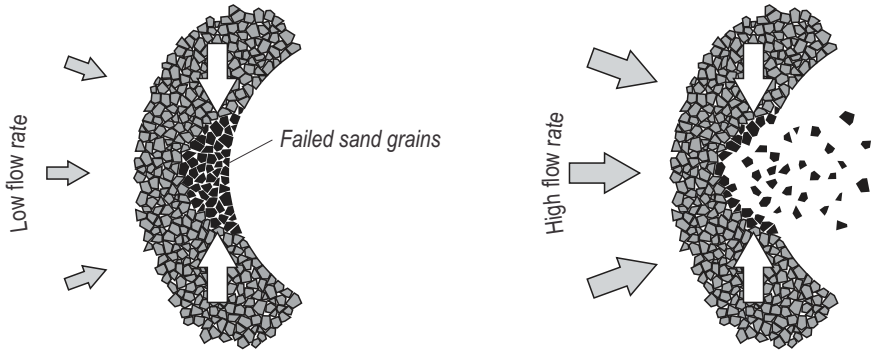

(1) Borehole wall fails when the induced stresses around the borehole exceed the sandstone strength.

(2) The failed sand grains are produced through the borehole, due to high rate of fluid flow.

Figure 1.1. Two stages of sand production mechanism.

stability is mainly governed by the sand-arch formed around the borehole (Hall and Harrisberger, 1970; Tippie and Kohlhaas, 1973; Clearly et al., 1979; Bratli and Risnes, 1981; Morita and Boyd, 1991). Sand production is also observed in weakly consolidated sandstones where sand production initiates due to stress induced failure of the sandstone in the vicinity of the borehole (Geertsma, 1985; Perkins and Weingarten, 1988). Once sandstone is in a state of failure, fluid flow applies a drag force to the sandstone resulting in some of the sand grains detaching from the wellbore wall and falling into the wellbore. In cased holes sand production is through the perforation tunnels but the mechanism (i.e. failure of sand formation and transportation of sand grains by the means of fluid flow) remains the same.

In the context of geomechanics, the state of stresses around a single borehole is a function of three principal far-field stresses; usually a vertical and two horizontal stress components. Different modes of failure have been observed around a circular opening. These modes of failure have been classified with respect to the state of stresses in vicinity of the borehole (Maury, 1987; Bratton et al., 1999). Figure 1.2 shows the main failure modes around a borehole with isotropic and anisotropic stresses perpendicular to the borehole axis.

Failure mode A, shown in Figure 1.2, is the most commonly observed failure mode around a borehole (Addis and Wu, 1993), where the tangential stress acting at the borehole wall (σ_θ) is the maximum stress, the radial stress (σ_r) is the minimum stress, and the axial stress (σ_a) is the intermediate stress ($\sigma_\theta > \sigma_a > \sigma_r$).

These modes of failure have been simulated in the laboratory for both isotropic and anisotropic states of stress. An extensive review of the past sanding laboratory

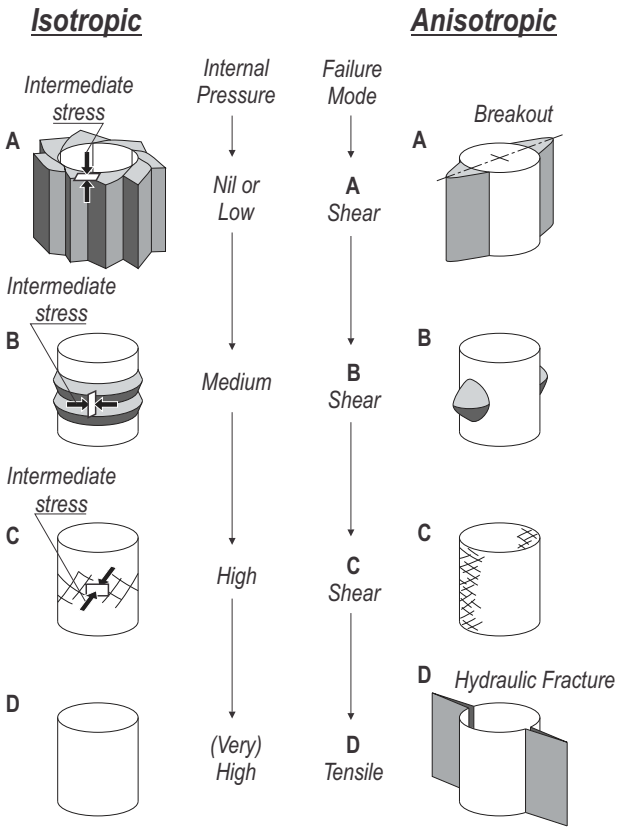

Figure 1.2. Different modes of failure around a borehole in isotropic (left) and anisotropic (right) state of stresses (after Maury, 1987).

experiments has been introduced in "*Paper 1. A Preliminary Experimental Study on Sand Production under True Triaxial Stress Conditions"*. In the following section a brief review of these experiments is presented.

1.2 Experimental sand production

It is more convenient to conduct experiments under isotropic stress conditions on cylindrical samples than under true-triaxial stress conditions (Santarelli and Brown, 1989; Ewy and Cook, 1990; Addis and Wu, 1993; Lee et al., 2002). This is due to the fact that sample preparation and equipment setup are easier for a cylindrical sample than for a rectangular prism sample which is required in true-triaxial tests. The isotropic boundary stresses lead to axisymmetric stress condition around the borehole. Nevertheless, the effect of the intermediate stress (axial) can be studied in the vicinity of the borehole wall (Addis and Wu, 1993; Lee et al., 2002).

A more realistic experiment should be the one which includes the effect of three independent stress components. In practice, this is only possible if the experiment is

conducted on rectangular prism samples. In this approach, the boundary stresses represent three principal far-field stresses, and the induced stresses around the borehole are not axisymmetric. Few experiments have been conducted under true-triaxial stress conditions to study borehole failure (Haimson and Song, 1993; Lee and Haimson, 1993; Mogi, 2006; Papamichos et al., 2010).

However, in order to study the borehole failure due to sand production, fluid flow must be presented through the sample and borehole during the tests. This has been practiced in cylindrical shape samples (Vriezen et al., 1975; Antheunis et al., 1979; Tronvoll et al., 1993; Khodaverdian et al., 1998; Papamichos et al., 2001; Wu and Tan, 2002; Nouri et al., 2006), but few attempts have been done to simulate sanding under true-triaxial boundary stress condition (Kooijman et al., 1992; Kooijman et al., 1996). This is the type of experiments which was performed to study sand production in this research.

1.3 Summary

The problem of sand production in the oil and gas industry requires further in-depth research. A major part of these studies was carried out through laboratory experiments. A brief overview of these attempts was introduced in this chapter.

Most of these studies were conducted on cylindrical shape samples, where the lateral stresses are applied uniformly around the borehole. However, a more realistic condition is where three independent principle stresses are applied to the boundary of a rectangular prism. In this study, the failure of a sand formation around a borehole was studied experimentally under true-triaxial stress conditions. This was achieved by establishing a unique experiment setup and procedure. In the following section the preparation and the properties of the samples used in this study are presented.

2 Sample preparation and properties*

Laboratory sand production experiments were conducted on synthetically manufactured samples. Although it is preferable to conduct the experiments on samples of natural sandstones, this is subject to some limitations. Firstly, it is practically impossible to collect an intact sample of weakly consolidated sandstone with sufficiently large size from downhole. Secondly, the physico-mechanical properties of rocks taken from outcrop (even if they are representative for downhole sandstones) may not be homogeneous while it is possible to make synthetic samples with reasonably homogeneous properties (Perkins and Weingarten, 1988).

Sophisticated methods have been proposed to generate realistic synthetic samples (Holt et al., 1994). To obtain a sample suitable for this purpose it is important to establish a consistent sample preparation procedure. In addition, prior to the sanding experiment, a series of conventional rock mechanical tests need to be carried out to obtain the physico-mechanical properties of the synthetic rocks. The details of sample preparation and a review of the equipment used for this purpose were reported in *Paper 2. Proposing a Sample Preparation Procedure for Sanding Experiments*. This procedure was used to make all samples used for the experiments in this study.

2.1 Sample preparation procedure

The synthetic sandstones are basically composed of sands, cement and water. Mechanical properties of the manufactured sample are a function of the ratio of the individual components used in the mixture. It has been observed that a small variation in the component ratio during sample preparation could result in a significant change in the properties of the final product. This indicates the importance of careful selection of the basic components. The synthetic samples used in the experiments were produced

* The contents given in this chapter are based on the following paper:
Paper 2. Proposing a sample preparation procedure for sanding experiments.

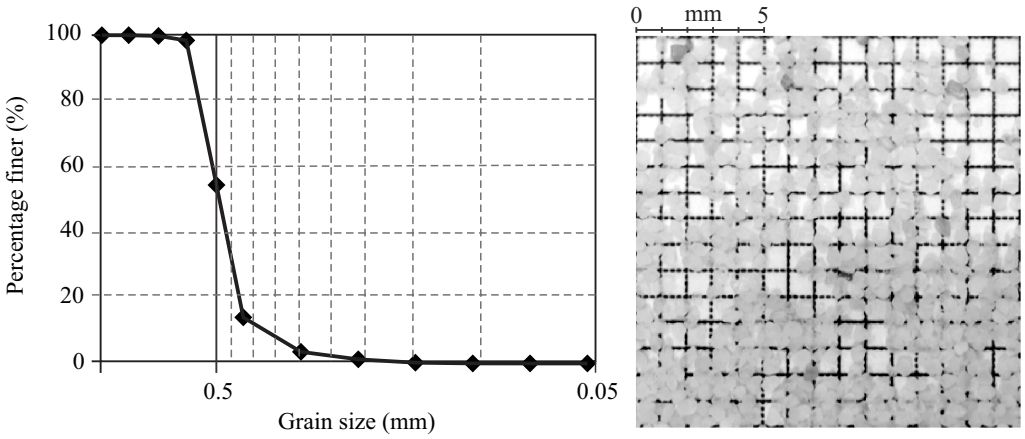

Figure 2.1. Grain size distribution curve for the synthetic sample made for sanding experiments.

following a consistent procedure to make samples with characteristics similar to weakly consolidated sandstones, i.e. the type of sandstone prone to sanding in fields.

Chemical analysis shows that the sand grains are 99.6% silica. The size of the grains selected for sample preparation depends solely on the purpose of the study to be performed. The grain size was selected to be 200-850 μm for the current study. Figure 2.1 shows the grain size distribution of the sand used for synthetic sample manufacturing.

Synthetic sandstones with different ratios of sand, Portland cement and water were produced and tested to obtain samples with desirable characteristics for sanding experiments. The proposed mixture was similar to what was proposed by Nouri et al. (2006), which consisted of sand-cement and water-cement weight ratio of 10 and 1.25, respectively.

Samples used for sand production experiments were $100\times100\times100\ mm^3$ cubes. These samples were cast in standard concrete moulds. The cement was not strong enough to bond sand particles in the early stage of curing. Hence, the samples were left in the moulds for three days (the sample loses its integrity if taken out of the mould earlier). The samples were then submerged into water and cured for 18 days. In order to reduce the effect of over-curing, the samples were dried in an oven at a temperature of 60°C for two days. Thereafter, to reduce the effect of weathering the samples were wrapped in plastic film and stored in a dry room environment.

2.2 Sample properties

The properties of the sample used for laboratory experiments were measured by conducting a series of laboratory tests on plugs of 38 mm in diameter following ISRM suggested methods (Bieniawski and Bernede, 1979; Bieniawski and Bernede, 1979; Franklin et al., 1979; Franklin, 1983). The mechanical properties of the sample were measured using a conventional triaxial stress cell, shown in Figure 2.2.

The stress-strain curves of the sample under different confining stresses are shown in Figure 2.3. This figure shows that the sample behaves more ductile in higher confining stresses. This is probably due to a low sand-cement ratio and/or the fact that the sample was cured under a free-stress environment. From Figure 2.3 it appears that the confining stress has a negligible effect on the Young's modulus for the range of confining stress studied. Figure 2.3 also shows the failure envelope of the sample in σ_1-σ_3 space. The tests were repeated in another set of samples to show the consistency of the sample properties and repeatability of the tests.

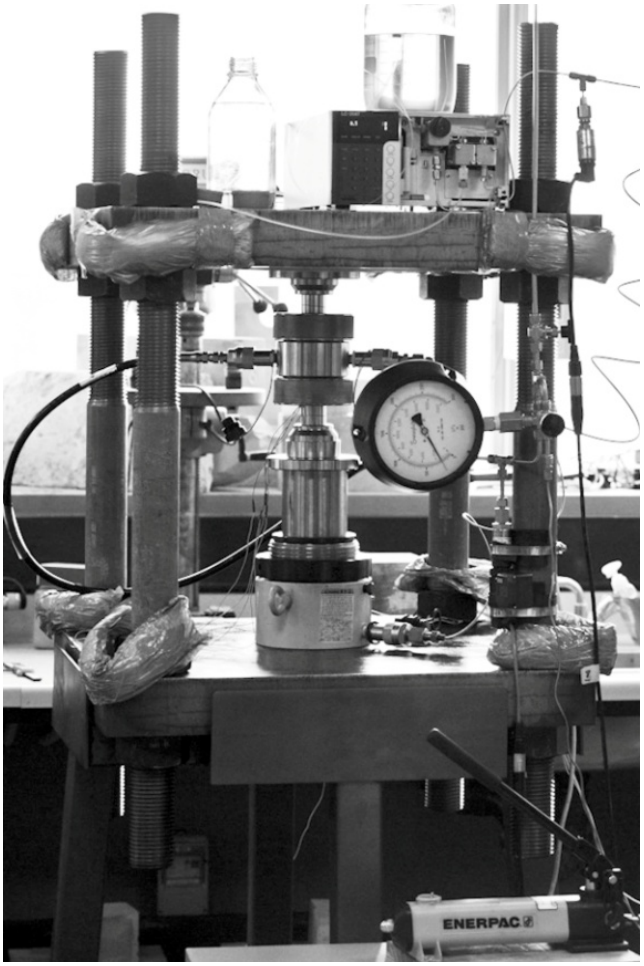

Figure 2.2. A conventional triaxial stress cell used to conduct standard rock mechanical tests.

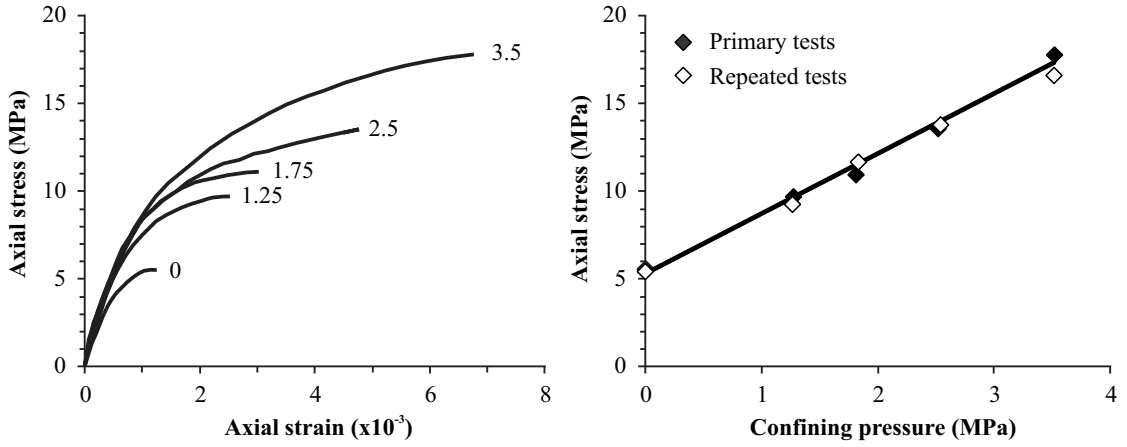

Figure 2.3. Stress-strain curves of the sample under different confining stresses (left), and failure envelope of the sample (right).

The physical and mechanical properties of the synthetic sandstone and the fluid properties of the oil used for sand production experiments are tabulated in Table 2.1. A sandstone with properties close to those given in Table 2.1 may be considered to be similar to weakly consolidated sandstones which are prone to sanding during production from a reservoir.

Table 2.1. Properties of the synthetic sandstone and fluid used in sanding simulations.

Fluid properties			
γ oil	Fluid weight density	7875.5	N/m^3
μ oil	Fluid dynamic viscosity	0.024	Pa.s
v oil	Fluid kinematic viscosity	2.99E-05	m^2/s
Physical properties			
ρb	Bulk density	1815	kg/m^3
ρg	Grain density	2500	kg/m^3
n	Porosity	0.274	-
k	Permeability	1.63E-13	m^2
Elastic properties			
E	Young's modulus	7.65	GPa
v	Poisson ratio	0.18	-
Strength parameters			
UCS	Uniaxial compressive strength	5.37	MPa
T_0	Tensile strength	0.7	MPa
Mohr-Coulomb parameters			
C	Cohesion	1.47	MPa
Φ	Friction angle	32.6	deg
Drucker-Prager parameters			
d	Shear yield stress	3	MPa
β	Friction angle	52.8	deg

2.3 Summary

Synthetic sandstones were manufactured using a consistent procedure to produce samples with identical properties for the purpose of sanding experiments. The samples were casted in 100×100×100 mm^3 cubes and 38 mm (diameter) cylindrical samples for sanding experiments and standard rock mechanical tests, respectively.

The properties of the samples were obtained following the ISRM suggested methods. The sanding experiment procedures were based on the properties of these samples (i.e. the rate and magnitude of the loads). In the following chapter the sanding experimental setup and procedure are described in detail.

3 Experimental simulations*

The main objective of this study was to establish an experimental procedure to simulate sand production under true-triaxial stress conditions. Thereafter, the sand production mechanism and the development of the failure zone around a single borehole were investigated by conducting a series of sanding experiments. These experiments were conducted on synthetically manufactured samples prepared according to the procedure explained in the preceding chapter. The sand production experiments were conducted using a true-triaxial stress cell (TTSC). The TTSC, as shown in Figure 3.1, was designed for conducting advanced geomechanical laboratory experiments under a true-triaxial state of stresses (Rasouli and Evans, 2010). In this study, for the first time the TTSC was used for sand production simulation.

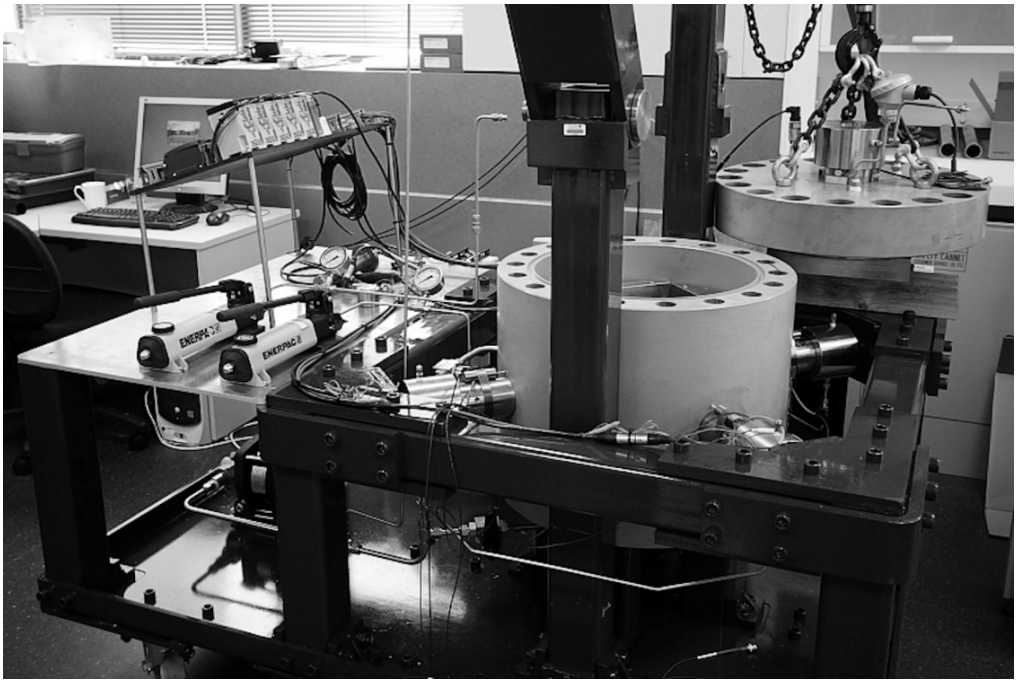

Figure 3.1. The true-triaxial stress cell (TTSC) used for sand production experiments.

* The contents given in this chapter are based on the following papers:
Paper 3. Experimental sanding analysis: thick walled cylinder versus true-triaxial tests.
Paper 4. The effect of stress anisotropy on sanding: an experimental study.

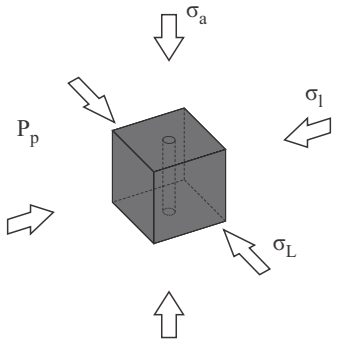

	Set 1	Set 2
σ_a	6.4 MPa	8 MPa
σ_l	6.4, 11.2, 16 MPa	8, 10, 12, 14 MPa
σ_L	16 MPa	14 MPa
P_p	3.2 MPa	4 MPa

Figure 3.2. State of stresses used in sanding simulations with respect to the borehole.

The effect of lateral boundary stresses on sanding was investigated by conducting two sets of stress sensitivity analysis. The state of stresses was chosen in a way that the intermediate stress was in the lateral direction in both sets of experiments. Sensitivity analyses were conducted to investigate the effect of the far field intermediate stress magnitude: this was done by increasing the magnitude of the intermediate stress from the minimum to the maximum principal stress (see Figure 3.2). The pattern and dimension of the failed zone due to sand production was studied and interpreted at the end of the physical simulations. In the following sections the procedure to conduct the experimental and numerical simulations will be described in detail.

3.1 Experimental setup

The TTSC consists of a pressure cell surrounded by a vertical and four horizontal hydraulic rams (Figure 3.3). The maximum operating loads are 450 kN and 250 kN for vertical and horizontal rams, respectively. The cell can be pressurized up to 21 MPa to simulate pore pressure by injecting fluid. The TTSC can accommodate a cubic sample of up to 300×300×300 mm^3 size for conducting various advanced laboratory experiments under true-triaxial stress conditions. An outlet hole is designed at the bottom of the cell to access the sample during the test for injection purposes in hydraulic fracturing experiments or disposal of the produced fluid and sand grains in a sanding test.

As shown in Figure 3.3 the produced sand grains are collected in a graduated measurement tube connected to a T-junction below the pressure cell. A cylindrical screen was mounted inside the T-junction to separate sand grains from the produced fluid. The separated sand grains deposit into the measurement tube due to gravitational forces during the test.

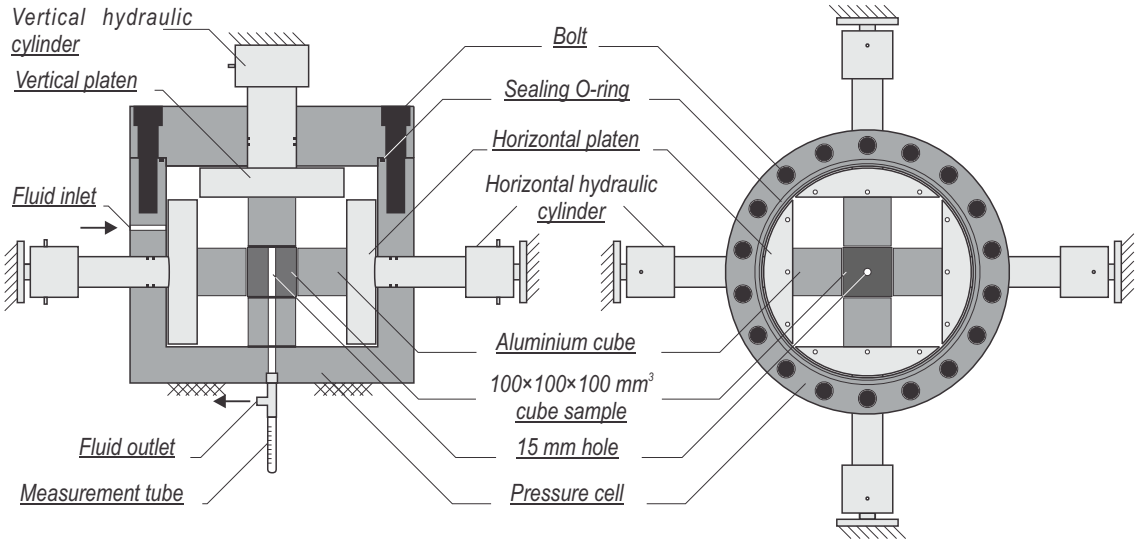

Figure 3.3. Side view (left) and top view (right) of the TTSC.

The special design of the hydraulic rams allows their independent control using manual or automatic hydraulic pumps. In this study, the fluid flow, which simulates the hydrocarbon production, was injected into the cell via an inlet, using a reciprocating pump with a maximum flow rate of 130 lit/hr and a maximum pressure of 36 MPa. Figure 3.4 shows the configuration of the pumps and arrangement of flow lines used for doing a sanding experiment using the TTSC.

A 15 mm diameter hole was drilled in the centre of the 100×100×100 mm^3 sample to represent a borehole. The size of the borehole was selected to minimise the effect of the sample boundary on failure around the borehole.

In order to accommodate a 100×100×100 mm^3 sample inside the TTSC the gap between the sample and platens must be filled. To do this, six aluminium blocks of size 97×97×100 mm^3 were placed around the sample to transmit the loads from the platens

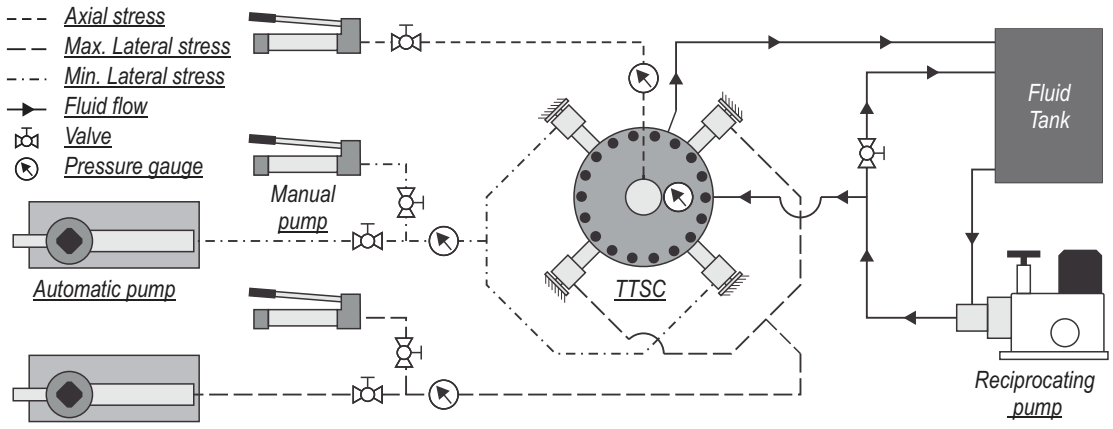

Figure 3.4. Laboratory sand production experiment configuration.

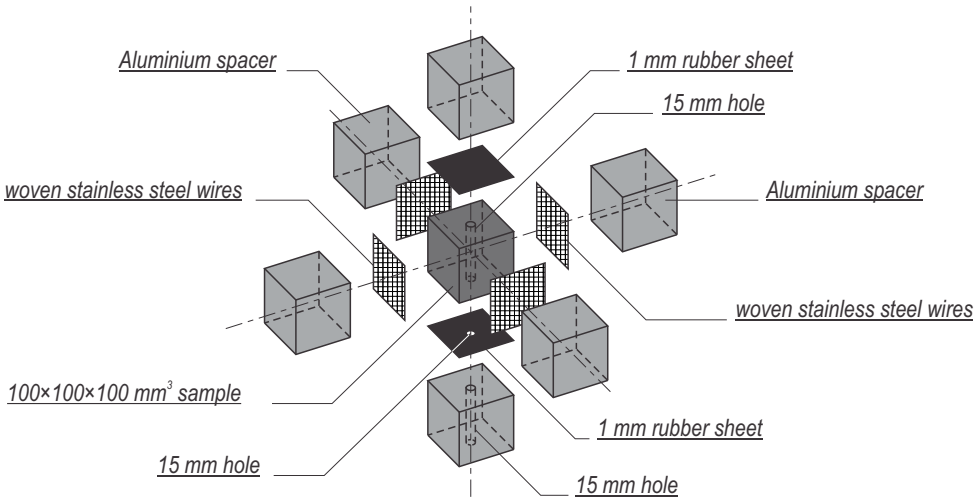

Figure 3.5. Schematic of positioning a sample for sanding experiment in the TTSC.

to the sample surfaces. A gap was formed between the neighbouring spacers as a result of the spacer size being smaller than the sample size. These gaps serve two purposes: firstly, it accommodates the sample deformation due to loading, and secondly, it allows the injected fluids to flood the sample. The stress concentration at the corner of the sample has negligible effect on the stress distribution around the borehole (see Section 4.2). The upper and lower faces of the sample were sealed using a 1 mm thick rubber sheet glued to these faces to simulate a radial flow around the borehole. The lower sheet had a 15 mm diameter hole at its centre to connect the hole to the outlet of the pressure cell. The lower aluminium spacer had the same diameter hole. To ensure that the fluid pressure was uniform at the boundary of the sample four woven stainless steel wire meshes were placed around the sample (Figure 3.5).

3.2 Experimental procedure

In a laboratory experiment, failure around a borehole is not only a function of rock properties and states of stress but also depends on the loading path. This is due to the non-linear behaviour of the sample material within the plastic zone. This suggests that depending on the purpose of the experiment, the loading path should be designed accordingly. The most realistic way to simulate downhole conditions is to apply the stresses on an intact sample and then drill the hole (Haimson and Kovacich, 2003).

In a laboratory experiment one may consider infinite loading paths to reach a specific state of stress. For instance, Figure 3.6 shows two different stress paths leading into the same final states of stress. From this figure it can be seen how different failure geometry and pattern could have developed around the borehole under different loading

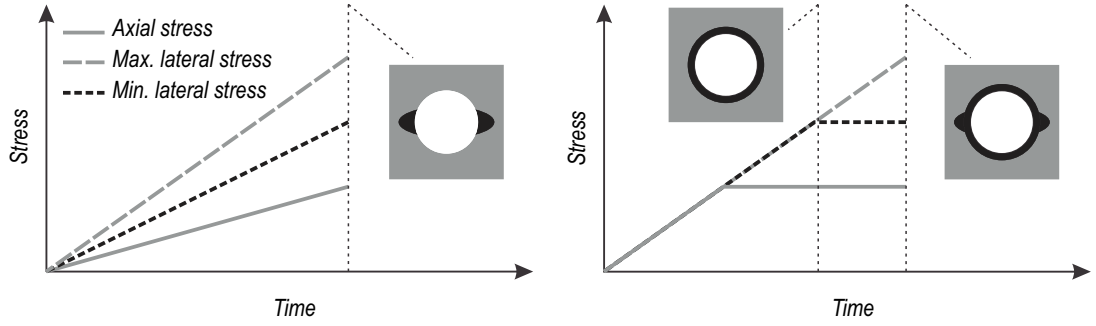

Figure 3.6. An example of stress path dependency of failure pattern.

paths. The left graph in Figure 3.6 shows the case in which the stress ratios are maintained constant during the entire experiment. In this case rock failure may develop gradually with a breakout pattern around the borehole wall. The right graph in Figure 3.6 shows that if the initial stresses are applied hydrostatically, the initial failure zone would be symmetrical. However, when stresses start deviating from hydrostatic, an additional failure zone in breakout pattern may form around the borehole wall.

In this study the main purpose was to investigate the geometry of the failure zone around a borehole which has resulted due to sanding. The experiments were conducted with specific stress ratios. During the experiments the stresses and pore pressure were increased in steps while their ratios were kept constant. This was due to the fact that it takes time to reach steady state fluid flow conditions.

After the sample was placed inside the TTSC a consistent procedure was followed in all tests to apply the stresses. The procedure includes:

(i) Sample sealing: To ensure that the area between sample and the upper and lower spacers are perfectly sealed, an axial stress (vertical stress) of 1.4 MPa was applied to the sample.

(ii) Sample saturation: After applying the vertical stress, the sample was saturated by a continuous flow of oil for at least 10 minutes until no air bubbles were observed in the fluid from the outlet.

(iii) Sand production: Stresses and fluid injection pressure were increased gradually in steps according to the stress ratios defined for the test. Each step lasted for at least 5 minutes.

(iv) Unloading: The unloading phase was similar but opposite to that of the preceding stage with shorter steps. This was done to ensure that the unloading stress path did not affect the pattern of the failure zone around the borehole.

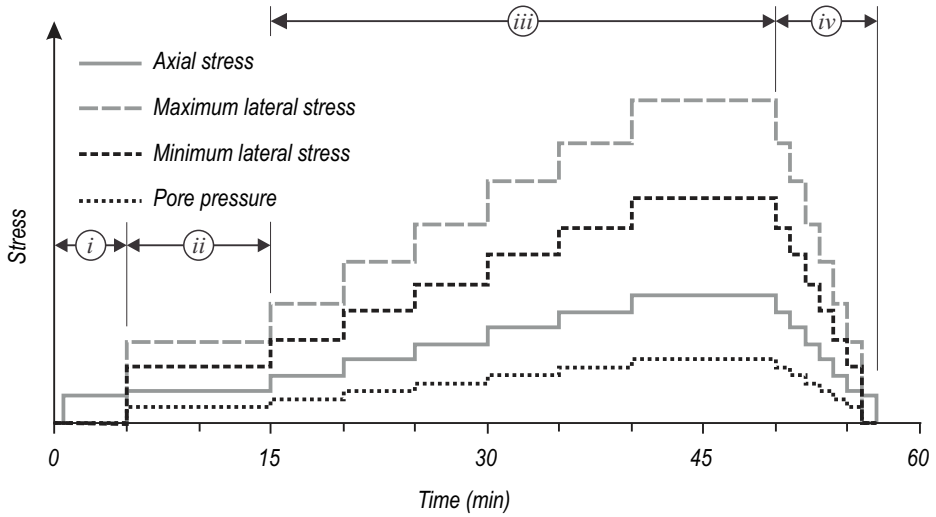

Figure 3.7. Loading and unloading stages in sanding experiments.

Figure 3.7 shows an example of the loading-unloading path for a typical test conducted for sanding experiments (different stages are marked on the chart).

3.3 Experimental results

Several preliminary tests were carried out to ensure that the experiment setup and procedure defined in the preceding sections were applied correctly. During these experiments the borehole failure and sanding were monitored in order for the author to have a better understating of the mechanism of the failure around the borehole. This information was used to design appropriate stress ratios and loading/unloading stages for the rest of the test program.

In the following sections the sanding mechanism observed in the preliminary tests (which was also observed in the main experiments) is explained in detail. Thereafter, the results of the main experiments will be presented and interpreted.

3.3.1 Sanding mechanism

Sanding was monitored by observing the produced sand grains collected in the measurement tube (described in Section 3.1). Since the borehole deformation was not monitored during the experiments, the yield point of the borehole could not be identified. However, the initiation of sanding was assumed to correspond with the observation of first sand grains in the measurement tube. Figure 3.8 shows the stress path of the preliminary experiments (test number B1600) and the amount of sand

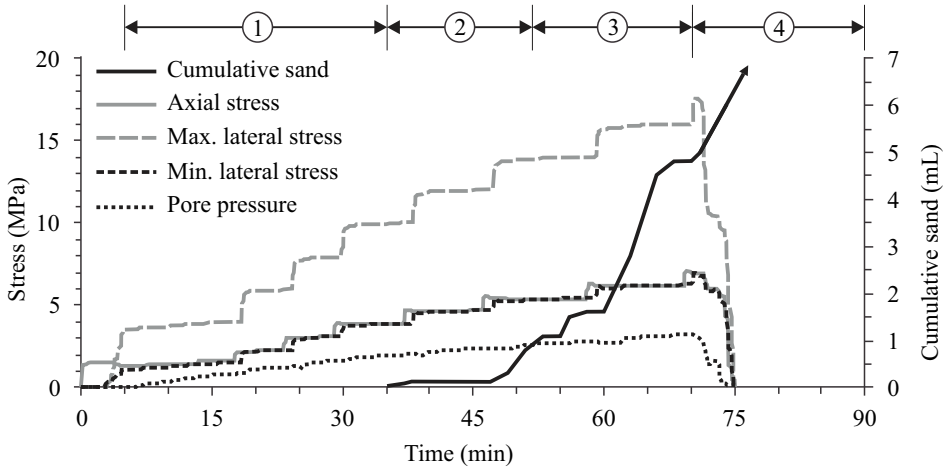

Figure 3.8. Loading diagram and sand volume produced in test B1600 (different stages are marked on the plot).

produced. From this figure the following conclusions can be drawn regarding the failure and sanding mechanism:

(1) The material surrounding the borehole yielded at the very early stage of loading (at the beginning of stage ii in the loading path). However, the residual bond strength between the sand grains prevented the grains from being displaced and fell into the borehole. The drag force of fluid flow appears to be inadequate to wash out the failed sand material from the borehole wall.

(2) By increasing the stresses and pore pressure at the boundaries, the size of the yield zone around the borehole increased. Sand production was initiated once the boundary pore pressure increased up to 2 MPa. This was when a small amount of sand grains were observed in the measurement tube. The drawdown pressure at the on-set of sanding is referred to as the *critical drawdown pressure* (Willson et al., 2002).

(3) A relatively large amount of sand grains were produced when the pore pressure reached 3.2 MPa. However, the rate of produced sand reduced after a certain period of time when the stresses around the borehole reached an equilibrium state. We refer to the drawdown pressure corresponding to this boundary pore pressure as the *destructive drawdown pressure*.

(4) Eventually, increase in the boundary stresses and pore pressure resulted in the yield of the entire sample. At this stage, a large amount of sand was produced and discharged through the outlet tube. The sand grains were produced continuously until the experiment was terminated. Large

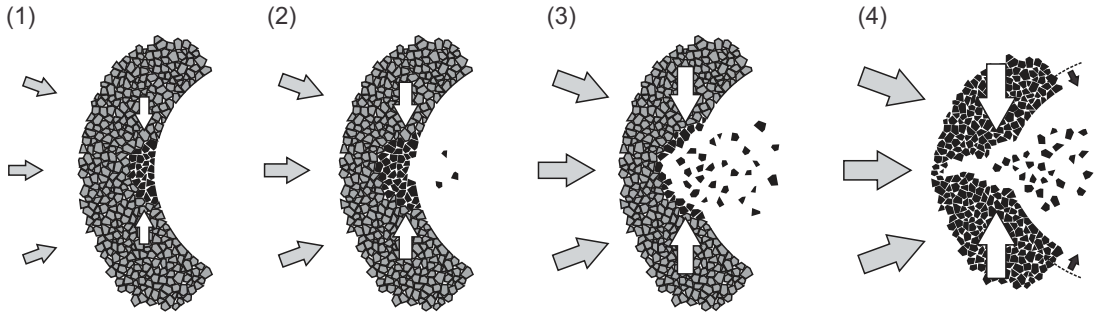

Figure 3.9. Evolution of sanding mechanism, Yielded grains are shown in black.

deformations were observed at the borehole wall in the direction of maximum lateral stress after the sample was removed from the TTSC. This stage, where sand grains are produced continuously and the borehole wall does not stabilize was referred to as *catastrophic* or *progressive sanding*.

Because the sample totally failed by the end of the loading stage, the experiment was terminated immediately without following the unloading procedure. The mechanism explained above is illustrated in Figure 3.9.

In the main experiments designed for this study, we only proceeded to stage 3 as the objective was to study the failure pattern and geometry of the failure zone around the borehole.

3.3.2 Geometry of failed zone

To investigate the geometry (i.e. width and depth) of the failure zone in the main experiments, the sample was unloaded (as explained in Section 2.3) and removed from the TTSC. A large amount of failed sand grains were still attached to the borehole wall due to residual strength. These grains were removed from the borehole wall by blowing pressurized air. This was done under free-stress state condition, so the cavity did not expand further. The shape of the failure zone was then captured precisely using a borescope (Figure 3.10). Table 3.1 summarizes the magnitudes of stresses and pore pressures applied to the boundary of the samples in each test, as well as the size of the corresponding failure zone.

The results presented in Table 3.1 imply that in each set of experiments the depth of the failure zones essentially did not change. This suggests that the minimum lateral stress (σ_l) has a minor effect on the depth of the failure zone for the conditions that we studied. On the other hand, the average depth of the failure zone in the two sets of experiments was quite different. The depth of the failure zone in the second set with

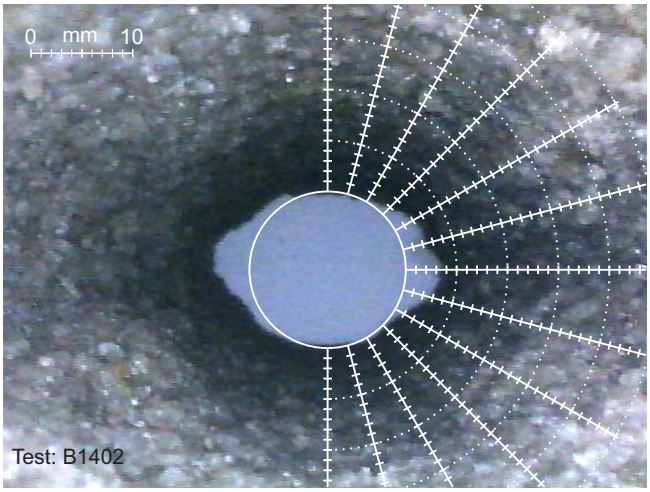

Figure 3.10. Failure zone developed in test number B1402.

maximum lateral stress (σ_L) of 16 MPa was larger than that of the first set of experiments. It may be postulated that the magnitude of the maximum lateral stress has a major impact on the depth of the failure zone. However, this needs further investigation for other cases to draw a more generic conclusion.

The results presented in Table 3.1 also show a noticeable change in the width of the failure zone corresponding to different minimum lateral stresses. It was seen that by increasing the stress anisotropy, the width of the failure zone decreased: this means that the width of the failure zone is inversely proportional to the difference between the minimum and maximum lateral stresses. The latter observations confirm the results reported in the literature (Haimson and Song, 1993; Papamichos et al., 2010).

For both sets of experiments, the results showed that in an anisotropic stress test the development of the failure zone was in the direction of minimum lateral stress, which is expected theoretically (Fjær et al., 2008). However, there was no preferred failure direction when the lateral stresses were isotropic. The main axis of wellbore ovalisation

Table 3.1. Applied stresses and the observed size of the failure zones in different sanding experiments.

Test Number	σ_L (MPa)	σ_l (MPa)	σ_l/σ_L (Pa/Pa)	σ_a (MPa)	P_p (MPa)	Width (deg)	Depth (mm)
B1401	14	8	0.57	8	4	120	3.4
B1402	14	10	0.71	8	4	140	3.6
B1403	14	12	0.86	8	4	170	3.2
B1404	14	14	1.00	8	4	180	2.3
B1601*	16	6.4	0.40	6.4	3.2	105	4.9
B1602*	16	11.2	0.70	6.4	3.2	150	4.6
B1603*	16	16	1.00	6.4	3.2	180	4.4

* These tests were presented and discussed in *Paper 3* and *Paper 4*.

in the test with isotropic stresses was not oriented to a preferred direction but was mainly influenced by the heterogeneity of the sample.

3.4 Summary

A new experimental setup and procedure was introduced to conduct sand production experiments under true-triaxial stress conditions. Several samples were tested to examine the experimental procedure and setup. These tests were also used to investigate the sanding mechanisms in different loading stages. The sand production mechanism was described in detail in this chapter.

Two sets of experiments were carried out to study the effect of lateral stresses on the development of failure around a borehole. The observations from the experiments showed that the width of the failure zone is reversely proportional to the degree of the lateral stresses anisotropy. Moreover, it was observed that the minimum lateral stress had a minor effect on the depth of the failure zone compared to that of the maximum lateral stress. These observations were theoretically supported when the experiments were simulated numerically using the finite element method (this is discussed in the next chapter).

4 Numerical modelling*

The observations from the main experiments presented in the previous Chapter were further investigated through the application of numerical simulations using ABAQUS software. The analytical solutions for stresses around a borehole can be implemented to model the laboratory experiments to some extent. These models, however, are only available for plane-strain conditions where a plane section perpendicular to the borehole is modelled (Risnes et al., 1982; Detournay and Fairhurst, 1987; Jaeger et al., 2007). In a plane-strain model the out-of-plane stress (in this study the axial stress) is a function of the in-plane stresses (Sadd, 2009), which means that the out-of-plane stresses cannot change independently. Therefore, in order to study the stresses and failure (i.e. yield) around a borehole under true-triaxial stress conditions, a 3D model must be employed.

The geometry and input parameters for the numerical model were based on sample properties and the experiment setup. These are discussed in more detail in the subsequent sections. The methodology used to numerically simulate the laboratory experiments in 3D is also explained. The results are discussed and compared to the laboratory observations.

4.1 Material properties

The material model which was used in the numerical modelling was based on the sample properties presented in Table 2.1 (see Section 2.2). A Drucker-Prager model with 0.8 flow stress ratio was found to be appropriate to model the synthetic sandstones (Figure 4.1). The results obtained from this model were found to have stronger correlation with the experimental results (see *Paper 5 Section 6.4*). Previous investigations show that a Mohr-Coulomb model results in a greater failure size than the experimentally observed, and the failure size observed from an original Drucker-Prager model is significantly smaller than the experimental results (see *Paper 5 Section 6.4*). A

* The contents given in this chapter are based on the contents presented in:
Paper 5. Numerical simulation of sanding under different stress regimes.

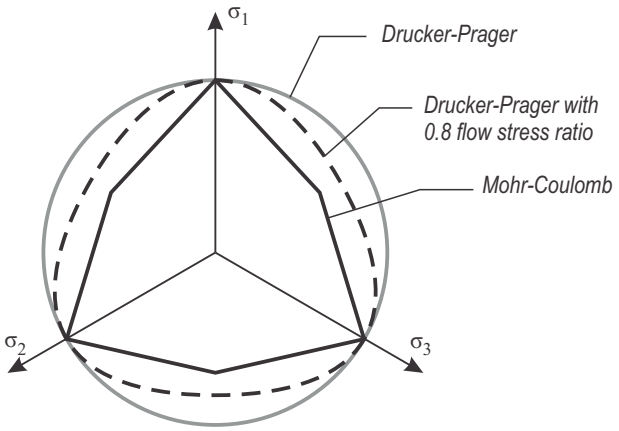

Figure 4.1. Comparison of failure criteria in a deviatoric stress plane.

linear elastic perfectly plastic constitutive model was assumed for the behaviour of the synthetic sandstone. The sample was assumed to deform in a linearly elastic manner prior to yielding and perfectly plastically after yielding. No strain hardening rule was assumed for the plastic model, i.e. yield function was assumed to coincide with the failure points. The plastic strain was not a concern in this study. Therefore, an associated plastic flow was presumed for ease of numerical modelling.

In Figure 4.2 the constitutive model used in the numerical model is overlaid on the stress-strain curves obtained from the triaxial tests. In this study, the average magnitude of the minimum and intermediate effective stresses on the borehole wall does not exceed 2.0 MPa. In this case, the error in higher confining stresses (above 1.75 MPa as seen in Figure 4.2) is not relevant.

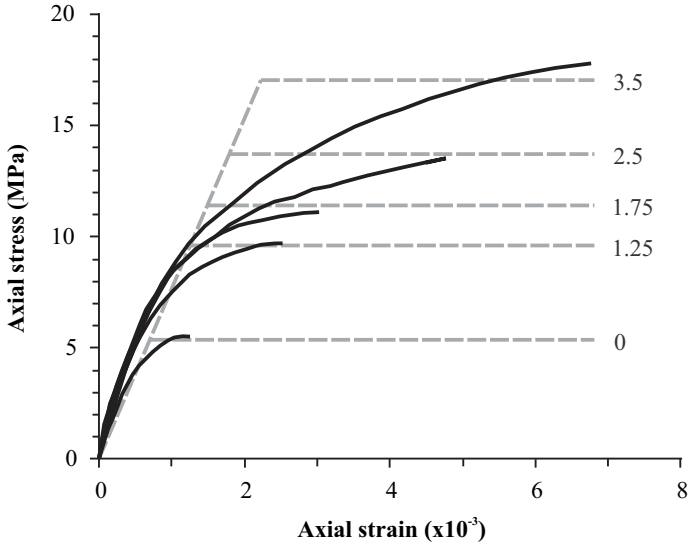

Figure 4.2. Comparison of the constitutive model and the stress-strain curve of the sample (the numbers next to the curves are the confining stresses in MPa).

The fluid was assumed to be inviscid and incompressible. The flow regime in sand production laboratory experiments was assumed to be in a steady-state condition. Finally, the pore fluid flow was assumed to be governed by Darcy's Law.

4.2 Modelling procedure

The geometry and boundary conditions of the numerical models were based on the sample geometry and experiment setup (see Figure 4.3). A thick-section perpendicular to the borehole axis was selected for the analysis. Due to the symmetrical nature of the problem only a quarter of the section was modelled. This reduces the number of elements required for the model and therefore less time for solution convergence. By contrast to the radial stresses that have a gradient along the lateral axis within the sample, the axial stress has no gradient along the vertical axis. Therefore, the axial dimension of the model can have any arbitrary dimension: in this study the model thickness was set to 10 mm.

The boundary conditions defined in the model must be representative of the loads and displacements applied to the boundary of the sample in the laboratory experiments. Uniform stresses were applied directly to the lateral boundaries. However, the vertical load was applied using a displacement boundary condition. The displacement corresponding to a specific stress was calculated from Hooke's Law for elastic material. The normal displacement of the symmetric faces (i.e. the two lateral and the bottom faces) and their rotation components were fixed in the model. These symmetric faces with fixed displacements eliminated the rigid body motion.

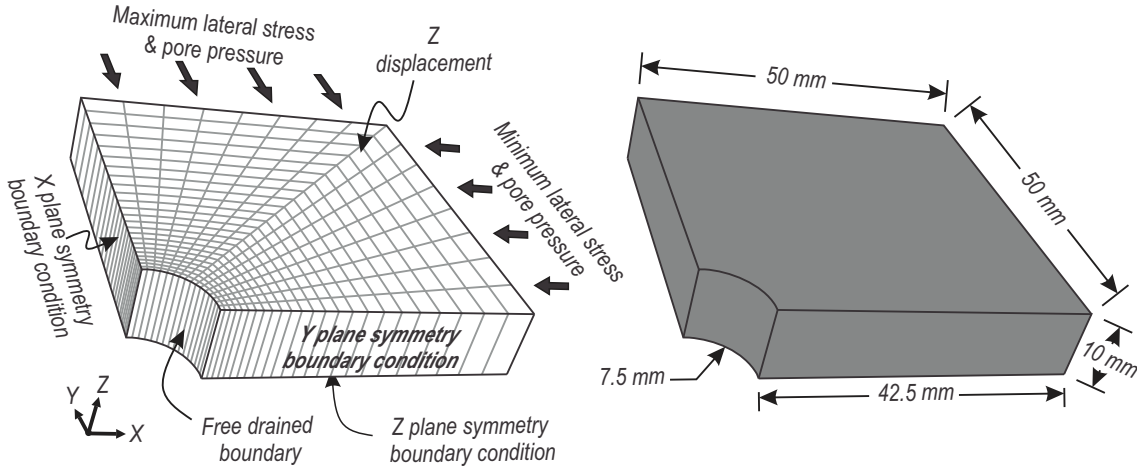

Figure 4.3. Geometry, mesh and boundary conditions of 3D numerical model built for sanding simulations of a cubic sample.

The fluid flow was simulated by considering a uniform pore pressure distribution on the lateral outer boundaries of the sample and the borehole wall was treated as a free-drained surface. The upper and lower sides of the sample were set to be impermeable. Figure 4.3 shows the geometry of the 3D numerical model constructed for this study.

The aluminium spacers were initially included in the numerical models. However, after comparing the results to a simpler case, where the boundary loads were directly applied to the sample, no significant differences were observed. Therefore, the aluminium spacers were excluded from the numerical model and the loads were directly applied to the sample boundaries. In addition, the effect of stress concentration at the corners of the sample which was generated due to the difference of the sample area and the spacer effective area was investigated. The results indicated that the stress distribution close to the borehole was not affected by these stress concentrations.

A mesh sensitivity analysis was conducted to obtain the optimum number of elements for the numerical modelling (see *Paper 5 Section 5.2*). Because there is no stress gradient in the axial direction only one element was considered along this dimension (see Figure 4.3).

4.3 Model validation

A plane-strain condition was considered as a special case for 3D modelling for validation purposes. Since the axial load was applied through displacement, it is plausible to simulate a 3D model in plane-strain mode by setting the axial displacement to zero. Therefore, the model was validated against available 2D analytical solutions for a borehole under isotropic stress conditions (see *Paper 5 Section 5.3* and *6.3*). Moreover, the stresses around a borehole in a cylindrical sample were compared to a cube sample. The results showed that the stresses are essentially identical except that a slight deviation in the results was observed close to the outer boundaries. This observation implied that laboratory experiments can be conducted on cubic samples with isotropic stresses to simulate a thick walled cylinder (TWC) test (see *Paper 3*).

4.4 Modelling results

Using ABAQUS software, 3D numerical modelling was performed to simulate the yield zones developed during the testing of synthetic samples in the laboratory. Width and depth of the failure zone are the two parameters to characterize the size of the failure

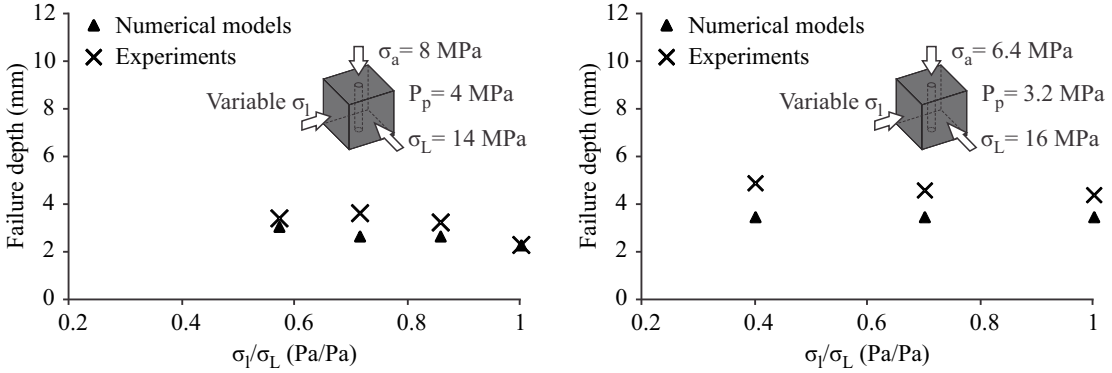

Figure 4.4. Failure depth comparison for set 1 (left) and set 2 (right) experiments.

zone. The results of the numerical models are shown in Figure 4.5 and Figure 4.4. For comparison purposes, the results of the experiments corresponding to these models are also plotted in these figures.

Figure 4.5 and Figure 4.4 show a close agreement between numerical models and experimental observations. It must be noted that in the experiments, the yield zone was assumed to be totally cleaned out by compressed air (see Section 3.3.2). These results show how experimental results may be reproduced by the means of numerical simulations, the benefit of which is to do a large number of sensitivity analyses using different parameters.

4.5 Discussion

The results presented in the preceding sections demonstrated the importance of the effect of lateral stress anisotropy on the characteristics of borehole failure. The results presented here confirm partly the previous observations made by other researches, for

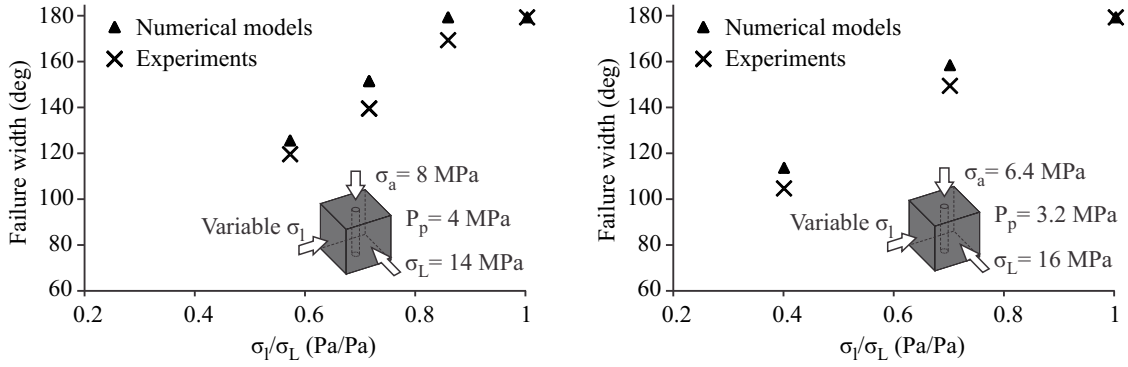

Figure 4.5. Failure width comparison for set 1 (left) and set 2 (right) of experiments.

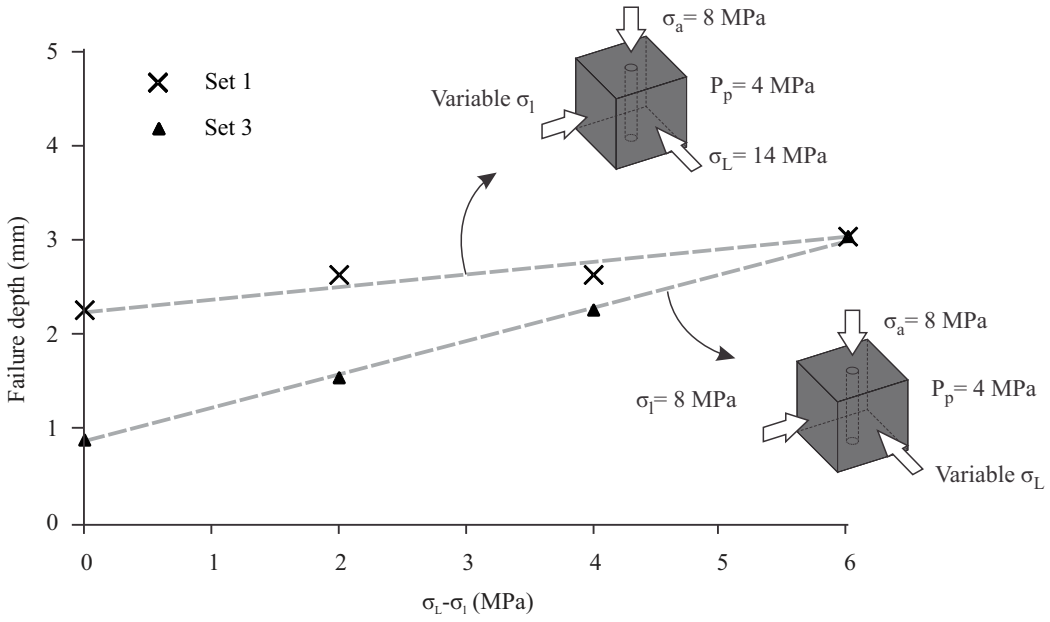

Figure 4.6. Comparison of depth of failure in set 1 and 3 of numerical simulations.

instance those who reported the effect of lateral stress anisotropy on failure width (Haimson and Song, 1993; Papamichos et al., 2010).

However, these results showed a different relationship between the depth of failure zone and lateral stresses. Previously, Haimson and Song (1993) showed that breakout depth increases as the minimum lateral stress was increased (Haimson and Song, 1993). However in their experiments, the maximum lateral stress was not constant, and it was increased relatively with the minimum lateral stress.

In this study, it was observed that the depth of the failure zone has more dependency on the maximum lateral stress (σ_L) than the minimum lateral stress (σ_l). This was initially noticed through the laboratory experiments (Section 3.3.2) but was later verified by numerical modelling (Section 4.4). These findings were also observed when numerical models were run for different material models, such as Mohr-Coulomb and the original Drucker-Prager (see *Paper 5* Section 6.4).

Although the numerical models presented in the preceding section show the effect of σ_L on depth of failure to some extent, a new set of numerical simulations (hereafter referred to as set 3) was run to show this effect more explicitly. In set 3, σ_a and σ_l were kept constant (8 MPa) while σ_L was changed (8, 10, 12 and 14 MPa). Figure 4.6 shows the results of the numerical simulations of set 3 along with the results of set 1. It can be clearly seen that changes in σ_L has more effect on depth of failure than changes in σ_l.

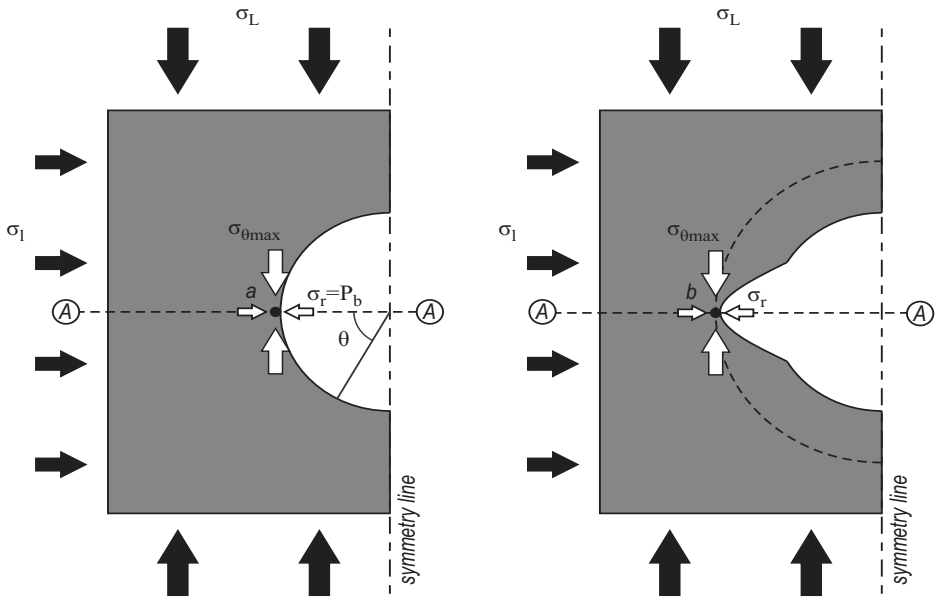

Figure 4.7. State of stress at failure initiation (left) and stabilization (right) stages.

In order to justify this observation, two different stages of failure were considered: initiation and stabilization of failure (Figure 4.7). For ease of explanation of the failure mechanism only the maximum and minimum principal stresses in the vicinity of borehole will be considered. For the case of failure mode A (as was illustrated in Figure 1.2) these stresses are the tangential and radial stresses (σ_θ and σ_r).

The failure initiates in the direction of σ_l at point *a*, where σ_θ is maximum ($\sigma_{\theta max}$) and σ_r is equal to borehole pressure (P_b). The magnitude of σ_θ in the direction σ_l (line *A-A*) when P_b=0 can be expressed as:

$$\sigma_{\theta(A\text{-}A)} = A\sigma_L + B\sigma_l,$$

where, considering Kirsch's equations (Jaeger et al., 2007) for θ = 0 we have:

$$A = \frac{1}{2}\left[2 + \frac{a^2}{r^2} + \frac{3a^4}{r^4}\right], \text{ and}$$

$$B = \frac{1}{2}\left[\frac{a^2}{r^2} - \frac{3a^4}{r^4}\right].$$

Figure 4.8 shows how parameters A and B vary along the radial distance from the borehole axis.

As anticipated, Figure 4.8 shows that A and B tends to become 1 and 0, respectively at distances further away from the borehole wall. This indicates that $\sigma_{\theta(A\text{-}A)}$ is independent from σ_l at the far-field. The effect of σ_l on $\sigma_{\theta(A\text{-}A)}$ increases in the vicinity

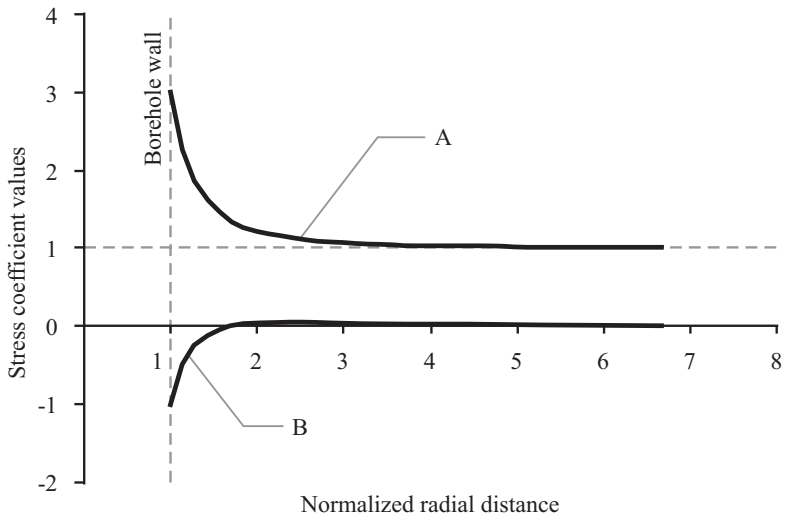

Figure 4.8. Lateral stresses coefficients for tangential stress.

of the borehole. Yet, the contribution of σ_L to the magnitude of $\sigma_{\theta(A\text{-}A)}$ at the borehole wall is three times more than σ_l.

The borehole wall failure propagates along line *A-A* till the stresses at the tip of the failure are equal to the material strength (point *b* in Figure 4.7). During the failure propagation phase, $\sigma_{r(A\text{-}A)}$ at the tip of failure is mainly governed by P_b and the residual strength in the yield zone. However, the magnitude of the $\sigma_{\theta(A\text{-}A)}$ is still a function of both σ_l and σ_L.

In order to understand the effect of lateral stresses on $\sigma_{\theta(A\text{-}A)}$ the stress profile along line *A-A* of the numerical models of set 1 and 3 were studied in more detail (Figure 4.9).

From Figure 4.9 it can be seen that the stress profile within the yield zone is independent of lateral stresses. Moreover as explained earlier, $\sigma_{r(A\text{-}A)}$ is independent of the lateral stresses at the elastic-plastic boundary (at the tip of failure, corresponding to point *b* in Figure 4.7). Overall, it can be seen that beyond the tip of failure (i.e. in the elastic zone), $\sigma_{r(A\text{-}A)}$ is mainly governed by σ_l, while $\sigma_{\theta(A\text{-}A)}$ is mainly governed by σ_L. Hence, it is plausible to assume that the contributions of σ_l and σ_L on $\sigma_{\theta(A\text{-}A)}$ in the elastic zone beyond the tip of failure along line *A-A* are similar to Kirsch's equation.

To summarize, the above discussion demonstrated that the contribution of σ_L is more than that of σ_l on the magnitude of $\sigma_{\theta(A\text{-}A)}$, and $\sigma_{r(A\text{-}A)}$ at the failure tip is mainly governed by P_b and the residual strength in the yield zone. Hence for a constant P_b the depth of failure, which is theoretically measured in the direction of *A-A*, is dependent more on σ_L than σ_l.

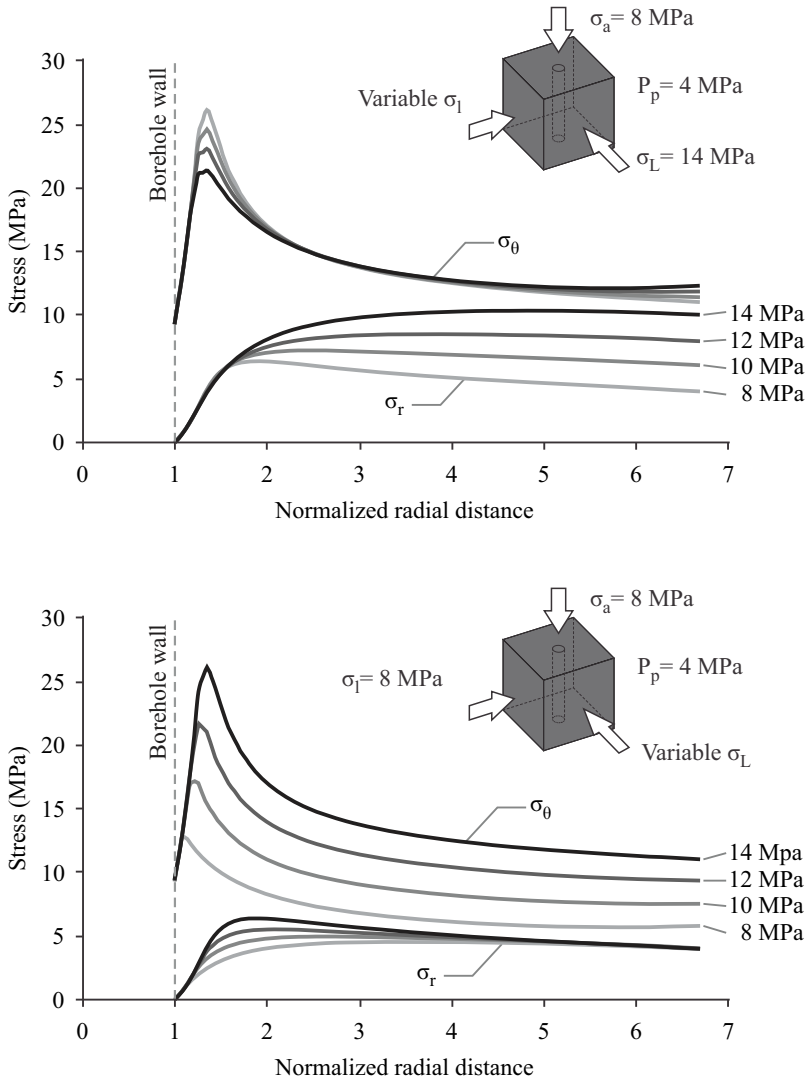

Figure 4.9. Stress profile along line *A-A* for set 1 (top) and set 3 (bottom) of numerical simulations.

4.6 Summary

The sand production experiments explained in Chapter 3 were simulated in a simplified manner using ABAQUS (an FEM program). The model was based on the material properties of the sample (described in Chapter 2), and the experimental setup and procedure (described in Chapter 3). The model was validated against the available analytical solutions for stress distribution around a borehole. Three different failure criteria were used to calibrate the model: Mohr-Coulomb, original Drucker-Pruger, and Drucker-Prager with 0.8 stress flow ratio. It was seen that the Drucker-Prager with 0.8 stress flow ratio material model gave the best agreement with the experimental results.

The geometry of the failure zone observed around the borehole was reproduced by the mean of these numerical models. Hence, it was confirmed that the width of the failure zone around a borehole increases as the lateral stresses become more isotropic. Moreover, the dependency of the depth of the failure zone to maximum lateral stress rather than minimum lateral stress was observed in the numerical models. The latter observation was justified using simple elastic equations for the stress distribution around a bore hole (Kirsch's equations).

In the following chapter, a brief summary of this work will be presented followed by conclusions made and recommendations for further work.

5 Conclusions and recommendations*

A large number of attempts have been made to simulate sand production in laboratories by geomechanics researchers in the past. However, most of these experiments have been carried out under uniform lateral stress applied to cylindrical samples. Few attempts have been made to simulate sanding under true-triaxial stress conditions. The few reported experiments were conducted under dry conditions with no fluid flow, which does not represent real field conditions for sanding.

In this thesis, we introduced a new experimental setup and procedure for sand production laboratory studies under true-triaxial stress conditions. Synthetically manufactured samples were used to conduct sanding experiments. A consistent procedure was introduced to prepare these samples. Two sets of experiments were designed to study the mechanism of sanding under different states of stress and flow conditions. Moreover, we investigated the effect of lateral stresses on the development of failure around the borehole.

In the following sections, the conclusions for this work are presented followed by some recommendations for further work.

5.1 Conclusions

A large amount of time was dedicated to find a proper procedure and composition to prepare synthetic samples for sanding experiments. Different mixes of sand, Portland cement and water were prepared and tested to obtain samples with desirable characteristics for sand production experiments. The main challenge was to obtain a mixture which was similar to weakly consolidated sandstone. We proposed a mixture suitable for sanding experiments which consisted of sand-cement and water-cement weight ratios of 10 and 1.25, respectively.

---

* The contents given in this chapter are based on the contents presented in previous chapters and the following papers:

Paper 6. A fracture sliding potential index for wellbore stability analysis.

Paper 7. Rock engineering systems adopted for sanding prediction in perforation tunnels.

Paper 8. Representing rock engineering system to analyse sand production in perforation tunnels.

Several tests were carried out to define an optimum experimental setup and procedure for sanding simulation under true-triaxial stress conditions. A unique experimental setup was proposed to conduct sanding experiments using the TTSC. The setup was designed to conducted experiments on 100×100×100 mm^3 cubes of synthetic sandstone. A comprehensive experimental procedure was proposed to apply loads and fluid flow to a cubic sample using the TTSC to simulate sanding which occurs under downhole conditions. The following is a summary of our findings with respect to the sand production mechanism:

- Yielding of the borehole wall was not necessarily associated with sanding in these experiments. A minimum drawdown pressure was needed to detach the yielded sands from the borehole wall.
- During loading of the sample at some point the fluid flow was strong enough to wash out a large amount of yielded sands, and we identified this point as the *destructive drawdown pressure*.
- When the entire sample yielded and the drawdown pressure exceeded its critical threshold, then continuous sanding with high deformation at the borehole wall was observed: we named this sanding mode as *catastrophic* or *progressive sanding*.
- The fluid flow on sanding under different state of true-triaxial stresses was examined and it was seen that the critical flow rate was not dependent on the stress regime.

The failure pattern and its geometry (i.e. width and depth) around the borehole were investigated experimentally and numerically. The following conclusions were obtained for the observations regarding the failure pattern and its size around the borehole:

- The geometry of the failed zone around the borehole was directly related to the difference and magnitude of the far-field lateral stresses.
- The width of the failure zone was inversely proportional to the lateral stress anisotropy, i.e. the width of the failure zone increases as the difference between the maximum and minimum lateral stresses decrease.
- The minimum lateral stress has a minor impact on the depth of the failure zone around the borehole. On the other hand, the extent of the depth of the failure zone was found to be mainly governed by the maximum lateral stresses for the given material.

- As anticipated, the failures developed in the direction of the minimum lateral stress. Also, the results showed that the direction of the failure zone under isotropic lateral stresses has an arbitrary direction which is mainly governed by heterogeneity of the sample.

The experiments were numerically simulated using an FEM program (ABAQUS). The following was concluded from the results of numerical modelling:

- The results of simulations in 2D and 3D were compared. It was shown that if the magnitude of the axial stress in 3D is relatively close to the magnitude of the out-of-plane stress in 2D (calculated from Hook's Law) the results are reasonably similar to each other.
- Investigations showed that Mohr-Coulomb material resulted in a greater failure size compared to the experimental results, and the original Drucker-Prager material results in a smaller failure size.
- Using different failure criteria it was concluded that for the samples used in the experiments, the Drucker-Prager with 0.8 flow stress ratio had the best correlation with experimental results.
- The direction of the failures simulated in numerical models was in good agreement with the laboratory experiment results.
- The results also confirm that the minimum lateral stress magnitude has a significant impact on the width of the failure zone. On the other hand, the depth of the failure zone seems to have a minor dependency on the minimum lateral stress magnitude and major dependency on the maximum lateral stress magnitude.

5.2 Recommendations

The failure mechanism observed in the laboratory during sand production can be modelled using PFC (Particle Flow Code) which is a DEM (Discrete Element Method) numerical-based code. The unique capabilities of PFC allow more realistic numerical simulations of sanding. The emphasis of this research was on laboratory experiments and simulations performed using ABAQUS were found adequate to model laboratory experiments.

Sand production can be studied using *rock engineering systems* (RES). The applications of the RES have been reported in petroleum related application. An example of this can be found in "*Paper 6. A fracture sliding potential index for*

wellbore stability analysis". The RES was implemented in sand production analysis in "*Paper 7. Rock engineering systems adopted for sanding prediction in perforation tunnels*" and "*Paper 8. Representing rock engineering system to analyse sand production in perforation tunnels*". However, further work is needed to define a sand production initiation index based on the RES interaction matrix.

Further experiments are suggested to be performed in order to have a better understanding of the effect of boundary stresses on failure geometry. The effect of sample properties can be studied by conducting experiments on different types of samples.

The deformation of the borehole was not recorded during our experiments. It is highly recommended that a series of experiments be conducted to specifically study the deformation of the borehole wall during the loading and unloading process.

References

Addis, M. A. and Wu, B. (1993). The role of the intermediate principal stress in wellbore stability studies: Evidence from hollow cylinder tests. International Journal of Rock Mechanics and Mining Sciences & Geomechanics Abstracts, 30, 1027-1030.

Antheunis, D., Fernandez Luque, R., van der Vlis, A. C. and Vriezen, P. B. (1979). The onset of sand influx from gas-producing friable sandstone formations - laboratory investigations, Society of Petroleum Engineers.

Bieniawski, Z. T. and Bernede, M. J. (1979). Suggested methods for determining the uniaxial compressive strength and deformability of rock materials: Part 1. Suggested method for determination of the uniaxial compressive strength of rock materials. International Journal of Rock Mechanics and Mining Sciences & Geomechanics Abstracts, 16, 137.

Bieniawski, Z. T. and Bernede, M. J. (1979). Suggested methods for determining the uniaxial compressive strength and deformability of rock materials: Part 1. Suggested method for determining deformability of rock materials in uniaxial compression. International Journal of Rock Mechanics and Mining Sciences & Geomechanics Abstracts, 16, 138-140.

Bratli, R. K. and Risnes, R. (1981). Stability and Failure of Sand Arches. SPE Journal, 21, 236-248.

Bratton, T., Bornemann, T., Li, Q., Plumb, D., Rasmus, J. and Krabbe, H. (1999). Logging-while-drilling images for Geomechanical, Geological and Petrophysical interpretations. SPWLA 40th Annual Logging Symposium, Society of Petrophysicists and Well-Log Analysts.

Cleary, M. P., Melvan, J. J. and Kohlhaas, C. A. (1979). The effect of confining stress and fluid properties on arch stability in unconsolidated sands. SPE Annual Technical Conference and Exhibition. Las Vegas, Nevada, American institute of Mining, Metallurgical, and Petroleum Engineers Inc.

Detournay, E. and Fairhurst, C. (1987). Two-dimensional elastoplastic analysis of a long, cylindrical cavity under non-hydrostatic loading. International Journal of Rock Mechanics and Mining Sciences & Geomechanics Abstracts, 24, 197-211.

Ewy, R. T. and Cook, N. G. W. (1990). Deformation and fracture around cylindrical openings in rock—I. Observations and analysis of deformations. International Journal of Rock Mechanics and Mining Sciences & Geomechanics Abstracts, 27, 387-407.

Fjær, E., Holt, R. M., Horsrud, P., Raaen, A. M. and Risnes, R. (2008). Petroleum related rock mechanics, Elsevier Science.

Franklin, J. A. (1983). Suggested methods for determining the strength of rock materials in triaxial compression: Revised version. International Journal of Rock Mechanics and Mining Sciences & Geomechanics Abstracts, 20, 285-290.

Franklin, J. A., Vogler, U. W., Szlavin, J., Edmond, J. M. and Bieniawski, Z. T. (1979). Suggested methods for determining water content, porosity, density, absorption and related properties and swelling and slake-durability index properties : Part 1: Suggested methods for determining water content, porosity, density, absorption and related properties. International Journal of Rock Mechanics and Mining Sciences & Geomechanics Abstracts, 16, 143-151.

Geertsma, J. (1985). Some Rock-Mechanical Aspects of Oil and Gas Well Completions. SPE Journal, 25, 848-856.

Haimson, B. and Kovacich, J. (2003). Borehole instability in high-porosity Berea sandstone and factors affecting dimensions and shape of fracture-like breakouts. Engineering Geology, 69, 219-231.

Haimson, B. C. and Song, I. (1993). Laboratory study of borehole breakouts in Cordova Cream: a case of shear failure mechanism. International Journal of Rock Mechanics and Mining Sciences & Geomechanics Abstracts, 30, 1047-1056.

Hall, C. D. and Harrisberger, W. H. (1970). Stability of Sand Arches: A Key to Sand Control. Journal of Petroleum Technology, 22.

Holt, R. M., Brignoli, M., Fjær, E., Unander, T. E. and Kenter, C. J. (1994). Core damage effects on compaction behaviour. Rock Mechanics in Petroleum Engineering. Delft, Netherlands, Society of Petroleum Engineers.

Jaeger, J. C., Cook, N. G. W. and Zimmerman, R. (2007). Fundamentals of Rock Mechanics, Wiley-Blackwell.

Khodaverdian, M., Abou-Sayed, A. S., Ramos, R., Guo, Q. and McLennan, J. D. (1998). Laboratory Simulation of Liner Loading and Near-Wellbore Permeability Variation in Poorly Consolidated Sandstones. SPE/ISRM Rock Mechanics in Petroleum Engineering. Trondheim, Norway, Society of Petroleum Engineers.

Kooijman, A. P., Halleck, P. M., de Bree, P., Veeken, C. A. M. and Kenter, C. J. (1992). Large-Scale Laboratory Sand Production Test. SPE Annual Technical Conference and Exhibition. Washington, D.C., 1992 Copyright 1992, Society of Petroleum Engineers Inc.

Kooijman, A. P., van den Hoek, P. J., de Bree, P., Kenter, C. J., Zheng, Z. and Khodaverdian, M. (1996). Horizontal Wellbore Stability and Sand Production in Weakly Consolidated Sandstones. SPE Annual Technical Conference and Exhibition. Denver, Colorado, 1996 Copyright 1996, Society of Petroleum Engineers, Inc.

Lee, D. H., Juang, C. H. and Lin, H. M. (2002). Yield Surface of Mu-San Sandstone by Hollow Cylinder Tests. Rock Mechanics and Rock Engineering, 35, 205-216.

Lee, M. and Haimson, B. (1993). Laboratory study of borehole breakouts in Lac du Bonnet granite: a case of extensile failure mechanism. International Journal of Rock Mechanics and Mining Sciences & Geomechanics Abstracts, 30, 1039-1045.

Maury, V. (1987). Observations, researches and recent results about failure mechanisms around single galleries. Report of the ISRM Comission on Failure mechanisms around underqround excavations.

Mogi, K. (2006). DEFORMATION AND FRACTURE OF ROCKS. Experimental Rock Mechanics, CRC Press.

Morita, N. and Boyd, P. A. (1991). Typical Sand Production Problems Case Studies and Strategies for Sand Control. SPE Annual Technical Conference and Exhibition. Dallas, Texas, Society of Petroleum Engineers, Inc.

Nouri, A., Vaziri, H., Kuru, E. and Islam, R. (2006). A comparison of two sanding criteria in physical and numerical modeling of sand production. Journal of Petroleum Science and Engineering, 50, 55-70.

Nouri, A., Vaziri, H. H., Belhaj, H. A. and Islam, M. R. (2006). Sand-Production Prediction: A New Set of Criteria for Modeling Based on Large-Scale Transient Experiments and Numerical Investigation. SPE Journal, pp. 227-237.

Papamichos, E., Tronvoll, J., Skjærstein, A. and Unander, T. E. (2010). Hole stability of Red Wildmoor sandstone under anisotropic stresses and sand production criterion. Journal of Petroleum Science and Engineering, 72, 78-92.

Papamichos, E., Vardoulakis, I., Tronvoll, J. and Skjærstein, A. (2001). Volumetric sand production model and experiment. International Journal for Numerical and Analytical Methods in Geomechanics, 25, 789-808.

Perkins, T. K. and Weingarten, J. S. (1988). Stability and Failure of Spherical Cavities in Unconsolidated Sand and Weakly Consolidated Rock. SPE Annual Technical Conference and Exhibition. Houston, Texas, Society of Petroleum Engineers.

Rasouli, V. and Evans, B. (2010). A true triaxial stress cell to simulate deep downhole drilling condition. Australian Petroleum Production & Exploration Association Journal, 61-70.

Risnes, R., Bratli, R. K. and Horsrud, P. (1982). Sand Stresses Around a Wellbore. SPE Journal, 22, 883-898.

Sadd, M. H. (2009). Elasticity: Theory, Applications, and Numerics, Academic Press.

Santarelli, F. J. and Brown, E. T. (1989). Failure of three sedimentary rocks in triaxial and hollow cylinder compression tests. International Journal of Rock Mechanics and Mining Sciences & Geomechanics Abstracts, 26, 401-413.

Tippie, D. B. and Kohlhaas, C. A. (1973). Effect of Flow Rate on Stability of Unconsolidated Producing Sands. Fall Meeting of the Society of Petroleum Engineers of AIME. Las Vegas, Nevada, American Institute of Mining, Metallurgical, and Petroleum Engineers, Inc.

Tronvoll, J., Kessler, N., Morita, N., Fjær, E. and Santarelli, F. J. (1993). The effect of anisotropic stress state on the stability of perforation cavities. International Journal of Rock Mechanics and Mining Sciences & Geomechanics Abstracts, 30, 1085-1089.

Veeken, C. A. M., Davies, D. R., Kenter, C. J. and Kooijman, A. P. (1991). Sand Production Prediction Review: Developing an Integrated Approach. SPE Annual Technical Conference and Exhibition. Dallas, Texas, 1991 Copyright 1991, Society of Petroleum Engineers, Inc.

Vriezen, P. B., Spijker, A. and van der Vlis, A. C. (1975). Erosion of Perforation Tunnels in Gas Wells. Fall Meeting of the Society of Petroleum Engineers of AIME. Dallas, Texas.

Willson, S. M., Moschovidis, Z. A., Cameron, J. R. and Palmer, I. D. (2002). New Model for Predicting the Rate of Sand Production. SPE/ISRM Rock Mechanics Conference. Irving, Texas, Society of Petroleum Engineers Inc.

Wu, B. and Tan, C. P. (2002). Sand Production Prediction of Gas Field - Methodology and Field Application. SPE/ISRM Rock Mechanics Conference. Irving, Texas, Copyright 2002, Society of Petroleum Engineers Inc.

Part II Published papers

Paper 1 A preliminary experimental study on sand production under true triaxial stress conditions

Lead author
Ahmadreza Younessi

A PRELIMINARY EXPERIMENTAL STUDY ON SAND PRODUCTION UNDER TRUE TRIAXIAL STRESS CONDITIONS

A. Younessi and V. Rasouli
Department of Petroleum Engineering
Curtin University of Technology
613 (Rear), Level 6, ARRC
26 Dick Perry Ave, Kensington
Perth WA 6151
Ahmadreza.YounessiSinaki@postgrad.curtin.edu.au
V.Rasouli@curtin.edu.au

ABSTRACT

Sand production prediction is becoming a regular study in reservoirs with weak or unconsolidated sands. Three main approaches for sanding prediction are analytical, numerical and experimental methods. Laboratory experiments have proven to provide more realistic results, with these being used to understand sanding mechanisms and validate analytical and numerical methods.

A large number of experimental studies have been carried out by researchers worldwide—most of which have been performed on cylindrical-shape samples under uniaxial (i.e. $\sigma_1 \neq 0, \sigma_2 = \sigma_3 = 0$) or triaxial (i.e. $\sigma_1 \neq 0, \sigma_2 = \sigma_3 \neq 0$) stress conditions. In general, a sanding experiment under true-triaxial stresses (i.e. $\sigma_1 \neq \sigma_2 \neq \sigma_3 \neq 0$) is more realistic in simulating downhole conditions. This stress condition can be simulated in the laboratory on a cubic sample.

The first part of this paper provides a comprehensive but brief literature review on past sanding laboratory experiments. This will be followed by the introducition of a unique true-triaxial stress cell (TTSC) which was modified and used for sanding simulations in the laboratory. The applied modifications will be illustrated and the test procedure described. The sample preparation for testing synthetic samples will be explained and some preliminary results obtained will be presented.

KEYWORDS

Sand production, experiment, true-triaxial stress, TTSC.

INTRODUCTION

By the early 1970s, a large number of fields prone to sand production problems were explored. Due to economic reasons, the strategy of the oil and gas industry shifted from past concerns with reservoir sand control to a higher production rate (Tippie and Kohlhaas, 1973). Hence, the wells drilled in such fields must have been designed specifically to reduce costs associated with sand production problems in higher production rates. To optimise well designs, engineers were persuaded to study the mechanisms of sand failure around wellbore and perforation, and factors that affect their stability. The majority of these studies were based on the laboratory tests. The results of these experiments were used to elucidate the mechanism of sand failures and helped to develop and validate theoretical models for sand production prediction.

Several laboratory testing apparatusus have been developed by researchers to simulate and study sand production. The authors could not find a short yet comprehensive literature on sanding studies carried out in the past, thus it was thought that providing such a text for future reference would benefit those who study this subject further. Accordingly, the first part of this paper gives a comprehensive review of the past experiments, including the objectives, findings and apparatus specifications. From this it can be seen that most of these studies were not conducted under a true-triaxial stress condition when simulating sanding. Instead, thick-walled cylinder (TWC) tests have been widely used for sanding simulation in the lab. During the TWC test, a hydrostatic (or at most, biaxial) pressure is applied to a cylindrical sample with a central hole to produce sand. Discarding the effect of three principal stresses being different from each other, however, could result in an unrealistic test condition compared to real field conditions.

A true-triaxial stress cell (TTSC), developed at the Petroleum Engineering Department of Curtin University of Technology (Rasouli and Evans, 2010) was modified to simulate sand production in the lab. The TTSC—originally designed for hydraulic fracturing studies—can accommodate a cubic sample with a maximum size of 30 cm while the three principal stresses are applied independently to it. The cell is completely sealed and therefore the pore pressure can be increased inside the cell up to 3,000 psi, which allows simulation of sanding. In the second part of this paper, the apparatus specifications, sample preparation procedure for testing synthetic samples, experimental setup and result of some preliminary tests will be discussed.

HISTORY OF SANDING LABORATORY EXPERIMENTS

It may be useful to review previously conducted sanding experiments to analyse sand failure around a borehole by

considering two categories of reservoir sand based on the sand consolidation status: that is, unconsolidated sand and friable (or weakly consolidated) sand. These are discussed in the following subsections.

Unconsolidated sand

Perhaps the first laboratory experiment conducted to analyse sand production was Terzaghi's famous trap-door experiment (Terzaghi, 1936). He simulated an arching phenomenon and showed its stabilisation against fluid flow. Since this first attempt, few researchers performed laboratory tests to study sand production until the 1970s. All of these tests, however, were conducted in the presence of very low stress magnitudes (Hall and Harrisberger, 1970). Hall and Harrisberger (1970) carried out further investigations to understand the stability mechanisms involved in sand arches. They concluded that dilatancy and cohesiveness are the two conditions required for the stability of an arch. They also showed the effect of wetting-phase and sand grains' shape on the onset of sand production; however, they did not consider the effect of fluid flow rate or rate changes in their experiments.

Tippie and Kohlhass (of the Colorado School of Mine) investigated the effect of fluid flow rate on arch formation and stability (Tippie and Kohlhass, 1973). The results of their experiments showed that fluid flow is a determining factor of arch size and stability. They also concluded that changes in permeability around the cavity have a strong influence on arch stability. Hence, they performed further investigations to study the effect of skin damage on the stability of sand arches (Tippie and Kohlhass, 1974). As a result of their studies they observed that flow rate indicated a strong damage effect due to fine migration. From their experiments' results they concluded that fines movement is associated with sand arch failure, and is in fact the mechanism that triggers the failure.

In the late 1970s, a more sophisticated large-scale apparatus was developed in the Colorado School of Mine to investigate the effects of different parameters on the stability of sand arches. A large number of tests were conducted to study the effect of overburden stress (Melvan, 1978), fluid properties (Cleary, 1978), and sand size (Wood, 1979) on arch stability, and the behaviour of arch stability in unconsolidated natural sands (Lasaki, 1980) and near wellbore stresses (Benton, 1984), which were discussed by Perkins and Weingarten (1988). One year later, the experimental results of Cleary and Melvan's (1978) work were published and discussed by Cleary et al (1979). They showed that arch structure and its size are both functions of confining stresses. They also concluded that different hydrocarbons alter the cohesive forces at the arch wall. The results of experiments by Wood (1979) and Lasaki (1980) can be found in a separate publication by Perkins and Weingarten (1988).

Bratli and Risnes (1981) analysed the effect of stress on arch stability. They developed a criterion to calculate the plastic zone and estimated the flow rate that causes tensile failure around a spherical cavity. The results of their laboratory tests confirm the applications of their analytical model, qualitatively.

In addition to Tippie and Kohlhaas's work, Selby and Ali (1988) of the University of Alberta performed a series of laboratory experiments to study the mechanics of fines movement and sand flow into the wellbore. Their experiments showed that grain size and shape can affect the onset of sand production.

At the time of writing, perhaps the latest experimental study on arch stability was by Bianco and Halleck (2001). Their study was basically an extension of Hall and Harrisberger's work, in which they investigated the problem of instability and sand production in poorly consolidated sandstones subjected to water influx. The result of the experiments showed the effect of the wetting-phase on the behaviour, morphology and stability of sand arches.

The specifications of the apparatus used in the above works are summarised in Table 1.

Friable (weakly consolidated) sand

For the first time, Vrizen et al (1975) conducted a series of experimental studies on friable sands, in which they evaluated the effect of erosion on perforation stability. From their studies, they concluded that stability of the perforation was mainly governed by the effective stress magnitude. The axial gas flow in perforation was found to have only a minor impact on the stability. Based on Vrizen et al's (1975) findings, Antheunis et al (1976) studied the stress dependency of perforated sandstones with various ratios of axial and radial loads. They also investigated the influence of perforation diameter on stability. From their experimental results they concluded that failure was mainly dominated by the radial rather than the axial load. They also observed that small perforations are more stable than larger-sized tunnels. Further results of their experiments were reported later (Antheunis et al, 1978).

Perkins and Weingarten (1988) investigated the conditions necessary for the stability of a spherical cavity in unconsolidated or weakly consolidated sand. Their experiments showed that a region of shear zone and disaggregated solids are generated around a cavity when the stresses increase. They concluded that when the porosity of cavity face increases to a critical value, the mechanical interaction of the particles is not sufficient, which leads to failure. They also developed a criterion based on critical porosity to estimate the onset of induced failure.

Wang et al (1991) conducted a laboratory sand production test with a similar method to that of Vriezen et al (1975). The results of their experiment were used to validate their proposed analytical approach.

In the early 1990s, a large-scale apparatus was developed in IKU, formerly SINTEF Petroleum Research. Several experimental studies were performed in IKU during the last two decades that used this equipment. The first set of experiments in IKU investigated the effect of stresses and fluid flow on perforation cavity stability (Tronvoll, 1992). The experiment results showed that fluid gradient does not have a large effect on the onset of non-linear deforma-

Table 1. Summary of experiment setup for laboratory studies of sand production in unconsolidated sands.

		Sample			Mechanical load		Fluid type
		Shape	Size	Cavity	Loading mechanism	Maximum axial load	
1970	Hall and Harrisberger	Cylindrical	8.26 cm (dia) × 5.08 cm	1.11 cm (dia) trap-door at bottom	Hydraulic ram	24 Mpa (3,450 psi)	Air/water/kerosene/mineral oil
1973	Tippie and Kohlhaas	Semi-hollow-cylindrical	23.5 cm (dia) × 40.64	5.08 cm (dia) cased wellbore with 1.27 cm (dia) perforation	Hydraulic pressure	2 Mpa (300 psi)	Oil (paint thinner)
1979	Clearly et al	Cylindrical	40.64 cm (dia) × 133.99 cm	10.16 cm (dia) cased wellbore with 1.27 cm (dia) perforation	Hydraulic ram	34 Mpa (5,000 psi)	Mineral spirits/ kerosene
1981	Bratli and Risnes	Cylindrical	19 cm (dia) × 38 cm	Trap-door at bottom	Hydraulic ram	5 Mpa (725 psi)	Air
1988	Selby and Farouq Ali	Cylindrical	20 cm (dia) × 17.7 cm	1.3 cm perforated tubing	Hydraulic pressure	1 Mpa (150 psi)	Distilled water
2001	Bianco and Halleck	Cylindrical	11.4 cm (dia) × 22.8 cm	1 cm open hole as outlet	Hydraulic pressure	14 Mpa (2,000 psi)*	Kerosene/3% KCL brine
		Planar	2.5 cm × 38 cm × 43 cm	0.6 cm open hole as outlet	Lever and weights	0.65 MPa (94 psi)	

* Hydrostatic

tion of the cavity wall. More laboratory investigations in IKU showed that the onset of sand production is mainly controlled by rock strength and the magnitude of in situ stresses (Tronvoll et al, 1992).

During 1991 and 1992, a more realistic set of experiments were conducted by Shell, British Petroleum, Elf Aquitaine and Schlumberger in TerraTek using large-scale true-triaxial stress equipment (Kooijman et al, 1992). These experiments were conducted to investigate the influences of both effective stresses and drawdown on sand production behaviour. In these studies, the presence of a wellbore with casing and cement, and actual perforations were taken into account. The secondary objective of these tests was to study the effect of water cut on sand production. The test behaved very realistically compared to the field condition. Further notes on these experiments were later published (Mason et al, 1994, and Behrmann et al, 1997).

At the same time, the onset of sanding was investigated at different stress conditions in IKU (Tronvoll et al, 1993). The experiment results showed that the cavity deformation, strength and failure mode depend on the ratio between the axial and radial stresses. Further notes on these experiments were reported by Morita (1994). Furthermore, the effect of fluid flow on cavity instability was investigated and showed that the evolution of a failure zone around a perforation tunnel is significantly affected by fluid flow (Tronvoll and Fjaer, 1994).

Kooijman et al (1996) at TerraTek, performed laboratory tests using a large-scale true-triaxial stress cell to study the stability of horizontal wellbore completions with uncemented liner in weakly-consolidated to unconsolidated sandstone formations. They also studied the effect of rock failure on well productivity. The experiment results showed that rock failure around the liner has a minor effect on productivity. It was also shown that a small percent of water cut resulted in massive sand production.

A vast number of experiments were conducted at IKU using field and outcrop material to investigate the effect of water breakthrough upon the onset of sand production (Skjaerstein et al, 1997). The results showed that sand production and water breakthrough could not be directly linked; however, once sand production was initiated, water production could accelerate the sand influx.

In TerraTek, Khodaverdian et al (1998) evaluated the effect of changing stress regimes on near wellbore permeability and liner loading. Their results showed the effect of sand ablation on load transfer mechanism to liner. They also observed that a negative skin is developed due to plastic deformation.

Papamichos et al (2001) at SINTEF, conducted a series of experiments to validate their volumetric sand production model. Fjaer et al (2004) used the same experimental setup to validate their analytical model for sand rate prediction.

A series of investigations on sand production were also conducted at CSIRO. Wu and Tan (2002) performed laboratory studies with gas flow. They observed that the sample could undergo stresses far beyond the amount predicted by linear elasticity. They also reported that initiation of some failure at the cavity wall is needed to trigger sand production.

Nouri et al (2004, 2005a) used the results of conducted laboratory tests to validate their proposed criteria in determining the onset of sanding and its severity of rate and duration. Using the same equipment, they investigated the effect of liner or stiffener with different perforation sizes on the rate of sand production (Nouri et al, 2005b). The results of their experiments indicated that the stiffener was effective in preventing any shear failure around the wellbore. It was also shown that the stiffener increased the mean effective stress around the wellbore, which in turn reduced the porosity and permeability.

The effect of water cut on sand production was also investigated by CSIRO researchers (Wu et al, 2005). The results of their work demonstrated that the effect of wa-

ter cut in sand production depends on the mineralogical composition and the amount of residual water saturation. From this work it was also concluded that rock strength reduction induced by water saturation is a significant factor on perforation failure.

As one of the latest experimental studies Papamichos et al (2008) at SINTEF, used the same laboratory apparatus as Tronvoll (1992) and presented three distinct failure patterns depending on the sandstone type. Sandstones were classified according to the failure pattern in three classes as brittle, ductile and compactive.

The above literature indicates a large volume of past laboratory based studies on sand production, each focusing on understanding specific parameters related to sanding. Table 2 gives a summary of all these attempts. From this table it is seen that few of these studies have considered true-triaxial stress conditions in their experimental studies. It is well known that depending on the relative magnitudes of three principal stress components, the shear failure around an opening could have different characteristics (Jaeger et al, 2007). As a result, an appropriate sanding simulation is one that includes the effect of three stress components independently. In practice, this is only possible if the experiment is conducted on cubic samples. This study initiated as a result of the above discussion.

In the following section the specifications of a TTSC that was used for sanding simulations will be briefly reviewed and the modification applied for this purpose will be explained.

SAND PRODUCTION UNDER TRUE-TRIAXIAL STRESS CONDITIONS

From the previous literature review, it has been shown that most of the customary sanding experiments were conducted on cylindrical samples in a uniaxial ($\sigma_1 \neq 0$, $\sigma_2 = \sigma_3 = 0$) or triaxial ($\sigma_1 \neq 0$, $\sigma_2 = \sigma_3 \neq 0$) cell. To simulate general subsurface stress conditions, however, the sample must be subjected to three independent stresses ($\sigma_1 \neq \sigma_2 \neq \sigma_3 \neq 0$)—this is called a polyaxial, or true-triaxial stress condition (Jaeger et al, 2007).

Several true-triaxial cells have been developed around the world for different purposes (Mogi, 2007, Rasouli and Evans, 2010), with few of them being capable to simulate the drawdown pressure for sanding analysis. The TTSC developed at Curtin University (Rasouli and Evans, 2010) has the potential capability for performing such experiments. The modifications applied for this purpose are briefly described below.

Table 2. Summary of experiment setup for laboratory studies of sand production in weakly consolidated sands.

		Sample			Mechanical load			Fluid type
		Shape	Size	Cavity	Loading mechanism	Maximum vertical/ axial load	Maximum horizontal/ radial load	
1975	Vriezen et al	Hollow cylindrical	0.4 cm (dia) × 0.64 cm	Cylindrical holes; 0.85, 1.25, 1.75 cm (dia)	Hydraulic pressure	69 Mpa (10,000 psi)*		Gas
1976	Antheunis	Hollow cylindrical	2.54 cm (dia) × 5.08 cm	Cylindrical holes; 0.6, 0.85, 1.25 cm (dia)	Hydraulic pressure	162 Mpa (23,500 psi)	54 Mpa (7,800 psi)	-
1988	Perkins and Weingarten	Cylindrical	9.84 cm (dia) × 9.84 cm	Hemispherical hole	Hydraulic pressure	28 Mpa (40,00 psi)*		Non-reactive mineral oil
1992	Tronvoll	Cylindrical	10 cm (dia) × 15 cm	Cylindrical hole; 2 cm (dia) × 6 cm	Hydraulic pressure	35 Mpa (5,000 psi)*		Oil
1992	Kooijman et al	Block	70 cm × 70 cm × 81 cm	Wellbore 10.2 cm (dia), cemented casing 7.36 cm (dia), and eight real perforations 0.6 cm (dia) × 14 cm	Flatjack	55 Mpa (8,000 psi)	55.1 Mpa (7,992 psi)	Oil (10 cp)
1996	Kooijman et al	Block	26.25 cm × 26.25 cm × 38 cm	Horizontal wellbore 2.44 cm (dia), with/without slotted or perforated liner	Flatjack	17 Mpa (2,500 psi)	8.618 Mpa (1,250 psi)	Odourless mineral spirit (OMS)
1998	Khodaverdian et al	Hollow cylindrical	25.4 cm (dia) × 38.1 cm	Wellbore 3.18 cm (dia), liner 1.91 cm (dia), and real perforations 0.13 cm (dia) and 60° phasing	Hydraulic pressure	69 Mpa (10,000 psi)*		Laboratory grade oil (26 cp)
2001	Papamichos et al	Hollow cylindrical	20 cm (dia) × 20 cm	Cylindrical hole; 2 cm (dia)	Hydraulic pressure	13 Mpa (1,885 psi)*		Oil
2002	Wu and Tan	Cylindrical	8.6 cm (dia) × 14 cm	Cylindrical hole; 1.6 cm (dia) × 10 cm	Hydraulic pressure	86.076 Mpa (12,484 psi)	70 Mpa (10,153 psi)	Gas
2004	Nouri et al	Hollow cylindrical	12.5 cm (dia) × 25 cm	Cylindrical hole; 2.54 cm (dia)	Hydraulic pressure	20.372 Mpa (2,955 psi)	64 Mpa (10,000 psi)	Odourless mineral spirit (OMS)

* Hydrostatic

TTSC modifications

The TTSC consists of a pressure vessel surrounded by a vertical and four horizontal hydraulic rams (Fig. 1). The cell can accommodate a block sample of up to 30 cm for conducting various advanced laboratory experiments under a true 3D stress condition. Tests can now be conducted on 5, 10, 15, 20 and 30 cm cubic samples (Fig. 2). The design of rams allows the independent control of ram to be made using manual hydraulic pumps. Hence, independent vertical and two horizontal stresses ($\sigma_v \neq \sigma_H \neq \sigma_h \neq 0$) can be simulated during the experiment. The maximum operation load of the rams is 50 MPa (8,000 psi); however, the maximum applicable stresses depend on the size of the sample. The vessel can be pressurised up to 21 MPa (3,000 psi) to simulate pore pressure by injecting fluid. An inlet/outlet hole is designed at the bottom of the vessel to access the sample during the test.

Sample preparation

Accurate sample preparation is significantly important as any undesired sample geometry could damage the cell, (e.g. by applying torsional forces to the rams and hydraulic plates) and make test result interpretation difficult. A wide range of weakly cemented sandstone cubic samples with different grain size distributions (150 µm to 1,000 µm) were made for the purpose of sanding analysis (Fig. 3). This was attempted to ensure that these synthetic samples could simulate the real sandstone formations seen in the field as closely as possible. Indeed, acquiring sandstone samples suitable for sanding studies are practically impossible, as they possess a very low strength (Perkins and Weingarten, 1988). On the other hand, the reproducibility of the physical and mechanical properties of synthetic samples allows performing several experiments to ensure that the results are consistent and not subjective. Sophisticated methods have been proposed to generate more realistic synthetic samples under different stress conditions (Holt et al, 1993); however, in this study synthetic sandstones with specific physical and mechanical properties were generated from a blend of Gingin sand, cement and water. A wide range of specimens were produced with different mixing designs (cement-to-sand ratio and water-to-cement ratio). The results presented in the following subsection were obtained from a sample with a uniaxial compressive strength of 3.7 MPa (540 psi). This was obtained by conducting a UCS test on a cylindrical sample with a diameter of 5 cm and length of 10 cm (Fig. 4).

Experiment setup and results

A preliminary test was conducted on a 10 cm block whose specification was given in the previous subsection. The following steps were taken to conduct the sanding experiment using the TTSC:

- A 1.6 cm diameter hole as deep as 5 cm was drilled at the centre of one face of the sample (Fig. 5). The sample was polished to ensure a good load distribution when stresses were applied through the rams.

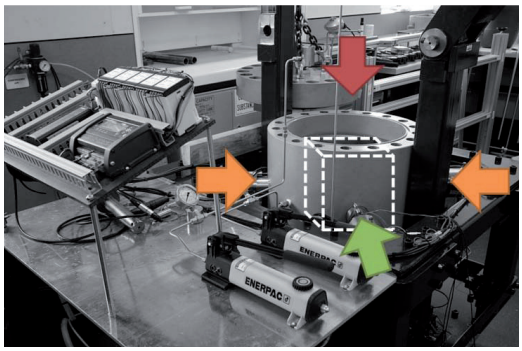

Figure 1. TTSC and the rams positions, one vertical and four horizontal rams applied three independent stresses.

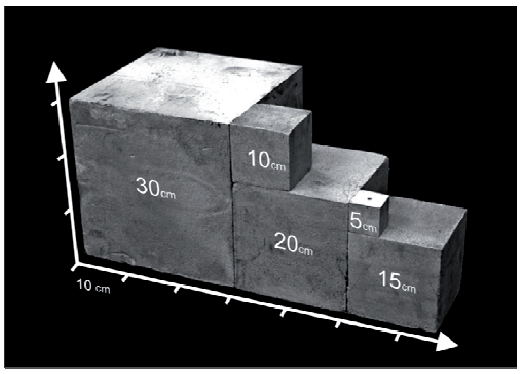

Figure 2. Different sample sizes prepared for sanding experiments.

- The pores of the drilled face were filled using acrylic gap filler to have a better seal and to prevent fluid invasion from this face.
- The sample was placed inside the pressure vessel using specific spacers (Fig. 6). The drilled hole was faced to the bottom of the cell where the pipe extended to the outside of the cell.
- Two thin plastic sheets were used between the sample and the bottom spacer, and also between the bottom spacer and the cell itself. These plates were used to act as a seal against the pressurised fluid inside the vessel. A small magnitude of vertical stress was applied to the sample to activate the seals and keep them in place.
- The fluid was then injected to the vessel at a low rate and pressurised until it was produced from the borehole. By fitting four sheets of mesh around the vertical sides of the sample, we could be sure that fluid flow into the sample was uniform from all the four vertical sides.
- The stresses were increased hydrostatically to a pre-specified value.
- One of the horizontal stresses was fixed and the other two stresses (i.e. vertical and maximum horizontal

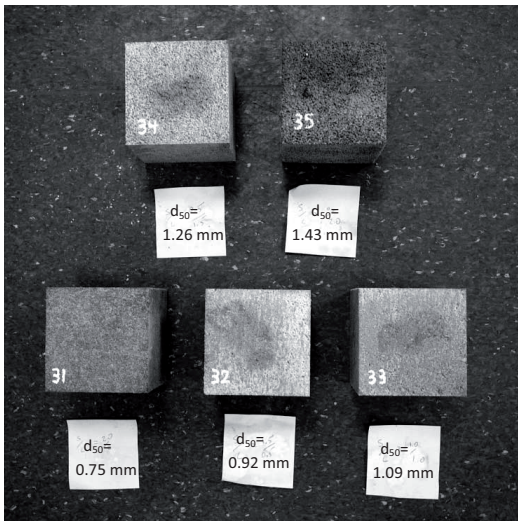

Figure 3. A series of samples with different grain size distributions prepared for sanding analysis.

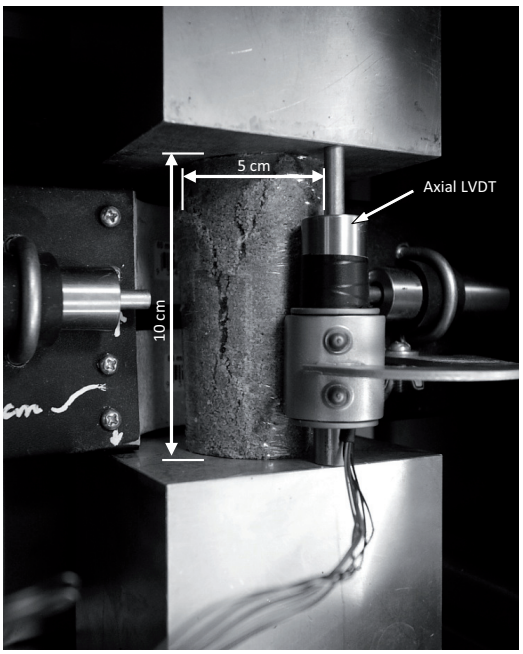

Figure 4. UCS tests are conducted to obtain the strength of the samples.

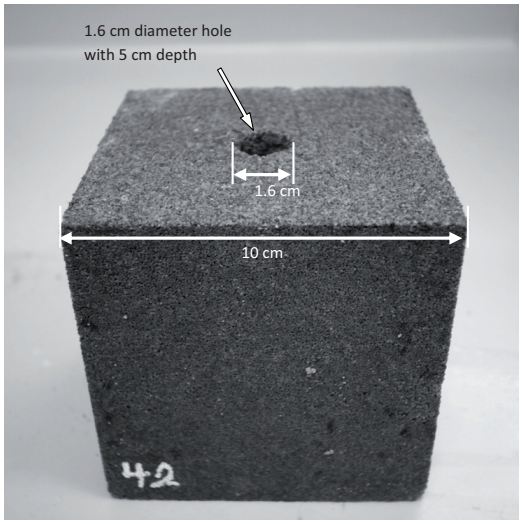

Figure 5. A 1.6 cm diameter hole as deep as 5 cm was drilled at the centre of one face of sample.

stresses) were increased in several steps.

- At each step the fluid flow rate was increased in five increments to observe the effect of flowing rate on sand stability.
- The test was terminated when a reasonable amount of sands were produced through the outlet.

The 10 cm sample was tested according to the above procedure. In the first few steps of loadings, under hydrostatic stress condition no sand was produced, even at high fluid rates. A minor volume of sand was produced in the following steps by increasing the stress anisotropy ratio. A sudden but temporary increase in sand production was observed due to an increase in fluid flow rate at this stage. The experiment was stopped when a considerable amount of sand was produced as a result of applying stresses, even at a low fluid flow rate (Fig. 7). A borescope was used to observe the perforation condition at the end of the test, as shown in Figure 8. This figure shows a clear shear failure around the borehole developing in the direction of the minimum horizontal stress.

This preliminary test result demonstrated the ability of the equipment and the present setup for performing valid sanding experiments. At this stage there is no intention to present quantitative results, as this requires several further tests to draw reliable conclusions. Following this work, it is planned to compare the results of sanding true-triaxial stress condition, as are performed using the TTSC, with the TWC test results. This would allow the investigation of differences between the two approaches.

CONCLUSION

A brief but thorough review of the past experimental studies of sand production was presented in the first part of

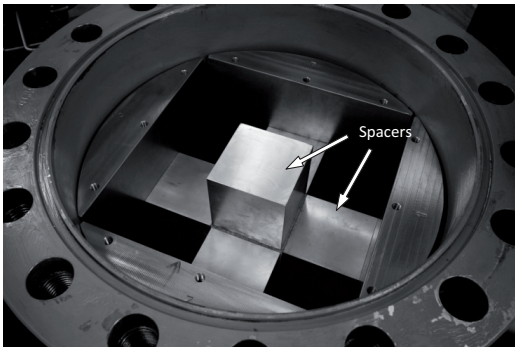

Figure 6. Setup of a 10 cm block sample using specific spacers.

Figure 7. Produced sands at the end of the test.

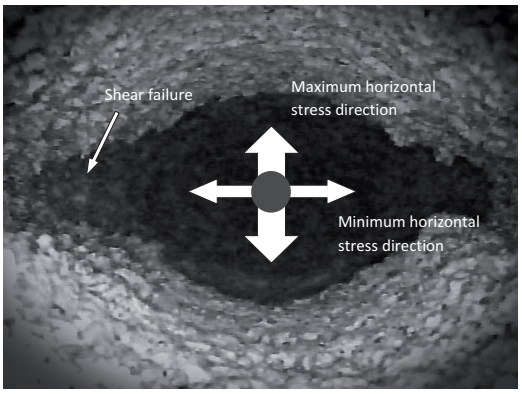

Figure 8. Shear failure observed in the direction of the minimum horizontal stress.

this paper. It was mentioned that in a TWC test the sample was subjected to only axial and radial loadings, which was not truly representative of general field stress condition. The TTSC, however, allowed applying three independently-controlled stresses to a cubic sample while the pore pressure could be varied separately. This allowed the simulation of sand production under true-triaxial stress condition. Although shear failure was observed in the previous experiments using the TWC, it appears that the direction of shear failure was governed by the inhomogeniety of the sample texture at a very small scale. In contrast, the present work shows the capability of the TTSC in simulating shear failure in the direction of minimum stress, which is a more realistic assumption in subsurface conditions. Although the conclusion from this experiment is already observed by many in the laboratory, it is the commencement of further work that will be unique.

REFERENCES

ANTHEUNIS, D., FERNANDEZ LUQUE, R., VAN DER VLIS, A.C. AND VRIEZEN, P.B, 1976—The onset of sand influx from gas-producing friable sandstone formations - laboratory investigations. SPE Journal, SPE 8031.

ANTHEUNIS, D., VRIEZEN, P.B, SCHIPPER, B.A. AND VAN DER VLIS, A.C., 1976—Perforation Collapse: Failure of Perforated Friable Sandstones. SPE European Spring Meeting, Amsterdam, Netherlands, 8–9 April, SPE 5750.

BEHRMANN, L.A., WILLSON, S.M., DE BREE, PH. AND PRESLES, C., 1997—Field Implications from Full-Scale Sand Production Experiments. SPE Annual Technical Conference and Exhibition, San Antonio, Texas, 5–8 October, SPE 38639.

BIANCO, L.C.B. AND HALLECK, P.M., 2001—Mechanisms of arch instability and sand production in two-phase saturated poorly consolidated sandstones. European Formation Damage Conference, The Hague, Netherlands, 21–22 May, SPE 68932.

BRATLI, R.K. AND RISNES, R., 1981—Stability and failure of sand arches. SPE Journal, 21 (2), 236–48.

CLEARY, M.P., MELVAN, J.J. AND KOHLHAAS, C.A., 1979—The Effect of Confining Stress and Fluid Properties on Arch Stability in Unconsolidated Sands. SPE Annual Technical Conference and Exhibition, Las Vegas, Nevada, 23–26 September, SPE 8426.

FJAER, E., CERASI, P., LI, L. AND PAPAMICHOS, P., 2004—Modeling the Rate Of Sand Production. The 6th North America Rock Mechanics Symposium, Houston, Texas, 5–9 June, ARMA/NARMS 04-588.

HALL, C.D. AND HARRISBURGER, W.H., 1970—Stability of sand arches: a key to sand control. Journal of Petroleum Technology, 22 (7), 821–9.

HOLT, R.M., UNANDER, T.E., KENTER, C.J. AND SANTARELLI, F.J, 1993—Unloading effects on mechanical properties of a very weak artificial sandstone: applications

to coring. In: Anagostopoulos et al (eds) Proc. Int. Symp. on Geotechnical Engineering of Hard Soil—Soft Rocks, 1609–14, Rotterdam: Balkema.

JAEGER, J.C., COOK, N.G.W. AND ZIMMERMAN, R.W., 2007—Fundamentals of Rock Mechanics (4th Edition). Oxford: Blackwell.

KHODAVERDIAN, M.F., ABOU-SAYED, A.S., RAMOS, R., GUO, Q. AND MCLENNAN, J.D., 1998—Laboratory Simulation of Liner Loading and Near-Wellbore Permeability Variation in Poorly Consolidated Sandstones. SPE/ISRM Rock Mechanics in Petroleum Engineering, Trondheim, Norway, 8–10 July, SPE 47291.

KOOIJMAN, A.P., HALLECK, P.M., DE BREE, P., VEEKEN, C.A.M. AND KENTER, C.J., 1992—Large-Scale Laboratory Sand Production Test. SPE Annual Technical Conference and Exhibition, Washington, D.C., 4–7 October, SPE 24798.

KOOIJMAN, A.P., VAN DEN HOEK, P.J., DE BREE, P., KENTER, C.J., ZHENG, Z. AND KHODAVERDIAN, M. 1996—Horizontal Wellbore Stability and Sand Production in Weakly Consolidated Sandstones. SPE Annual Technical Conference and Exhibition, Denver, Colorado, 6–9 October, SPE 36419.

MASON, J.N., BEHRMANN, L.A., DEES, J.M. AND KESSLER, N., 1994—Block Tests Model the Near-Wellbore in a Perforated Sandstone. SPE Annual Technical Conference and Exhibition, New Orleans, Louisiana, 25–28 September, SPE 28554.

MOGI, K., 2007—Experimental rock mechanics. London: Balkema.

MORITA, N., 1994—Field and laboratory verification of sand-production prediction models. SPE Drilling & Completion, 9 (4), 227–35.

NOURI, A., VAZIRI, H., BELHAJI, H. AND ISLAM, R., 2004—Sand Production Prediction: A New Set of Criteria for Modeling Based on Large-Scale Transient Experiments and Numerical Investigation. SPE Annual Technical Conference and Exhibition, Houston, Texas, 26–29 September, SPE 90273.

NOURI, A., VAZIRI, H., KURU, E. AND ISLAM, R., 2005a—A comparison of two sanding criteria in physical and numerical modeling of sand production. Journal of Petroleum Science and Engineering, 50, 55–70.

NOURI, A., VAZIRI, H., KURU, E. AND ISLAM, R., 2005b—A Laboratory Study of the Effect of Installation of Reticulated Expandable Liners on Sand Production in Weakly Consolidated Sandstone Formations. SPE Annual Technical Conference and Exhibition, Dallas, Texas, 9–12 October, SPE 96151.

PAPAMICHOS, E., STENEBRÅTEN, J., CERASI, P., LAVROV, A., VARDOULAKIS, I., FUH, G.F., BRIGNOLI, M., DE CASTRO, G.C.J. AND HAVMØLLER, O., 2008—Rock type and hole failure pattern effects on sand production. The 42nd U.S. Rock Mechanics Symposium, San Francisco, California, 29 June–2 July, ARMA 08-217.

PAPAMICHOS, E., VARDOULAKIS, I., TRONVOLL, J., AND SKJÆRSTEIN, A., 2001—Volumetric sand production model and experiment. International Journal for Numerical and Analytical Methods in Geomechanics, 25 (8), 789–808.

PERKINS, T.K. AND WEINGARTEN, J.S., 1988—Stability and Failure of Spherical Cavities in Unconsolidated Sand and Weakly Consolidated Rock. SPE Annual Technical Conference and Exhibition, Houston, Texas, 2–5 October, SPE 18244.

RASOULI, V. AND EVANS, B., 2010—A true triaxial stress cell to simulate deep downhole drilling condition. The APPEA Journal, 50, 61–70.

SELBY, R.J. AND FAROUQ ALI, S.M., 1988—Mechanics Of Sand Production And The Flow Of Fines In Porous Media. Journal of Canadian Petroleum Technology, 27 (3), 55–63.

SKJAERSTEIN, A., TRONVOLL, J., SANTARELLI, F.J. AND JORANSON, H., 1997—Effect of Water Breakthrough on Sand Production: Experimental and Field Evidence. SPE Annual Technical Conference and Exhibition, San Antonio, Texas, 5–8 October, SPE 38806.

TERZAGHI, K.V., 1936—Stress distribution in dry and in saturated sand above a yielding trap door. First International Conference on Soil Mechanics and Foundation Engineering, Harvard University, Cambridge, MA.

TIPPIE, D.B. AND KOHLHAAS, C.A., 1973—Effect of Flow Rate on Stability of Unconsolidated Producing Sands. Fall Meeting of the Society of Petroleum Engineers of AIME, Las Vegas, Nevada, 30 September–3 October, SPE 4533.

TIPPIE, D.B. AND KOHLHAAS, C.A., 1974—Variation of Skin Damage with Flow Rate Associated with Sand Flow or Stability in Unconsolidated-Sand Reservoirs. SPE California Regional Meeting, San Francisco, California, 4–5 April, SPE 4886.

TRONVOLL, J., 1992—Experimental investigation of perforation cavity stability. The 33rd U.S. Symposium on Rock Mechanics, Santa Fe, New Mexico, 3–5 June, 92-0365.

TRONVOLL, J. AND FJAER, E., 1994—Experimental study of sand production from perforation cavities. International Journal of Rock Mechanics and Mining Sciences & Geomechanics Abstracts, 31 (5), 393–410.

TRONVOLL, J., KESSLER, N., MORITA, N., FJAER, E. AND SANTARELLI, F.J., 1993—The effect of anisotropic stress

state on the stability of perforation cavities. International Journal of Rock Mechanics and Mining Sciences & Geomechanics Abstracts, 30 (7), 1085–9.

TRONVOLL, J., MORITA, N. AND SANTARELLI, F.J., 1992—Perforation Cavity Stability: Comprehensive Laboratory Experiments and Numerical Analysis. SPE Annual Technical Conference and Exhibition, Washington, DC, 4–7 October, SPE 24799.

VRIEZEN, P.B., SPIJKER, A. AND VAN DER VLIS, A.C., 1975—Erosion of Perforation Tunnels in Gas Wells. Fall Meeting of the Society of Petroleum Engineers of AIME, Dallas, Texas, 28 September–1 October, SPE 5661

WANG, Z., PEDEN, J.M. AND DAMASENA E.S.H., 1991—The Prediction of Operating Conditions To Constrain Sand Production From a Gas Well. SPE Production Operations Symposium, Oklahoma City, Oklahoma, 7–9 April, SPE 21681.

WU, B. AND TAN, C.P., 2002—Sand Production Prediction of Gas Field: Methodology and Laboratory Verification. SPE Asia Pacific Oil & Gas Conference and Exhibition, Melbourne, Australia, 8–10 October, SPE 77841.

WU, B., TAN, C.P. AND LU, N., 2005—Effect of Water Cut on Sand Production—An Experimental Study. SPE Asia Pacific Oil & Gas Conference and Exhibition, Jakarta, Indonesia, 5–7 April, SPE 92715.

Paper 2 Proposing a sample preparation procedure for sanding experiments

PROPOSING A SAMPLE PREPARATION PROCEDURE FOR SANDING EXPERIMENTS

A Younessi [a], V Rasouli [a], B Wu [b]

a. Curtin University, Perth, Australia
b. CSIRO, Melbourne, Australia

Abstract

The Authors, during past few years, have performed research on sand production under true triaxial stress conditions. To simulate sanding, 100×100×100 mm^3 cubic samples were placed in a true triaxial stress cell (TTSC) and three independent stresses were applied while the pore pressure was increased inside the cell. This resulted in sand grains to be produced through a drilled hole in the sample centre. The experiences obtained through testing several synthetic samples have indicated the significance of sample preparation to obtain valid results. Therefore, in this paper the procedure for preparation of synthetic samples suitable for a sanding experiment is proposed. Also, details of sample preparation for conventional rock mechanical tests to estimate rock physico-mechanical properties including deformability properties, strength parameters and permeability will be presented.

1. Introduction

Sand production mainly occurs in unconsolidated or weakly consolidated sand formations (Morita and Boyd, 1991). To investigate the impact of different parameters, sanding has been simulated in laboratories since 1930's (Terzaghi, 1936). Unconsolidated sands are mainly tested to study the arching effect while applying stresses and fluid flow through the sample (Hall and Harrisburger, 1970, Tippie and Kohlhaas, 1973, Bratli and Risnes, 1981). The unconsolidated samples consist of loose sands without any cementing bond. On the other hand, weak consolidated sands are tested to study the failure mechanism in the vicinity of a borehole under different states of stress and fluid flow conditions. Weakly consolidated sands used for laboratory experiments are either real sample taken from the outcrop or manufactured synthetically (Papamichos et al., 2010, Nouri et al. 2004).

Although it is preferable to conduct tests on real samples, this is subjected to some limitations. Firstly, it is not practically possible to collect an intact sample of weak-consolidated sandstone from underground due to the sample being highly incompetent. Secondly, the physico-mechanical properties of real rocks taken from outcrop are not identical while it is possible to make synthetic samples with reasonably similar properties (Perkins and Weingarten, 1988). Therefore, it is more advisable to use synthetic samples for sanding tests. Sophisticated methods have been proposed to generate more realistic synthetic samples under different stress conditions (Holt et al. 1993). To obtain a sample suitable for this purpose it is important to establish a

consistent sample preparation procedure. In addition, prior to the sanding experiment, a series of conventional rock mechanical tests need to be carried out to obtain the physico-mechanical properties of the synthetic rocks. In the following sections the details of sample preparation, a review of the equipment used and some results obtained are presented.

2. Mixture components

Synthetic sandstones are basically composed a mixture of sand, cement and water. The mechanical properties of the produced sample are a function of the individual components used in the mixture. The considerations to produce a synthetic sample for sand production experiments purposes are quite different from those used in civil engineering applications. For instance, in civil engineering concrete or mortar must have a minimum strength to sustain the loading when it is used in constructions; whereas in sand production experiments the sample must have a maximum strength limitation.

It has been observed that a small variation in properties of the initial components in sample preparation may have a significant change in the properties of the final product. This indicates the importance of careful selection the basic components.

The size of the grains selected for sample preparation depends solely on the purpose of the undergoing study. The size of the grains selected for our sanding experiments was selected to be 500 μm. This was decided based upon three main reasons. Firstly, the sanding experiments were conducted on 100×100×100 mm^3 cubic samples with a borehole drilled at its centre. A 15 mm hole was found adequately small relative to the sample size to avoid the boundary effects on the stresses around the borehole. Secondly, it was planned to model the experiments numerically using particle flow code (PFC), which is a discrete element based software. In PFC 2D discs in 2D (balls in 3D) are used to model the rock grains and having large number of grains increases the computation time. Choosing 500 μm for the size of sand grains was found to be within a reasonable range for having comparable simulation models converged in a timely manner. Thirdly,

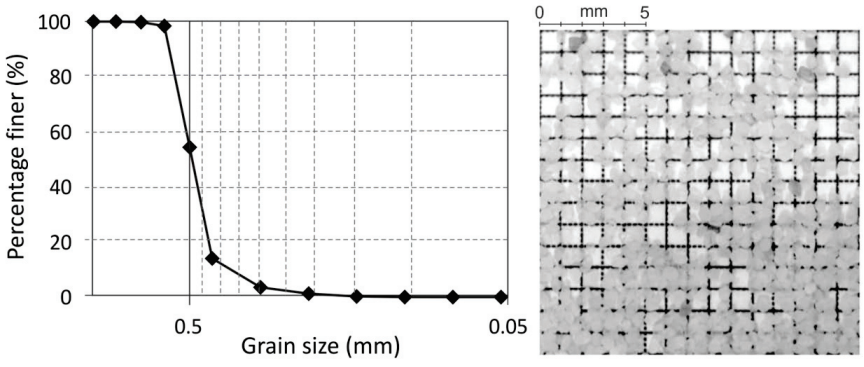

Figure 1. Grain size distribution curve for a typical synthetic sample made for sanding experiments.

this grain size distribution resulted in a porosity of 0.25 to 0.35, which gives the sample mechanical properties close to what is expected for weakly consolidated to unconsolidated sandstone, i.e. similar to real samples prone to sanding in the field. In Section 6 typical physico-mechanical properties for a synthetic sample used for sanding experiments are presented. Figure 1 shows the grain size distribution of a typical sample manufactured synthetically for sanding experiments.

3. Mixture preparation

Different mixes of sand, Portland cement and water were prepared and tested to obtain samples with desirable characteristics for sanding experiments. The main challenge was to obtain a mixing whose uniaxial compressive strength was less than about 7 MPa, which is similar to weakly consolidated sandstone. The proposed mixture was similar to what was proposed by Nouri et al. (2004), which consisted of sand-cement and water-cement weight ratio of 10 and 1.25, respectively.
The required volume of sand was estimated based on the number and size of the moulds used for sample preparation. Subsequently, the amount of cement and water were calculated. In Figure 2, the sequence of the mixing program followed in the lab is illustrated.

Figure 2. Mixture preparation steps.

4. Casting process

Synthetic sandstones were casted in moulds with different shapes and sizes for different tests. Samples used for sand production experiments were $100\times100\times100$ mm^3 cubes. These samples were casted in standard concrete moulds. The procedure of casting synthetic samples is illustrated in Figure 3.

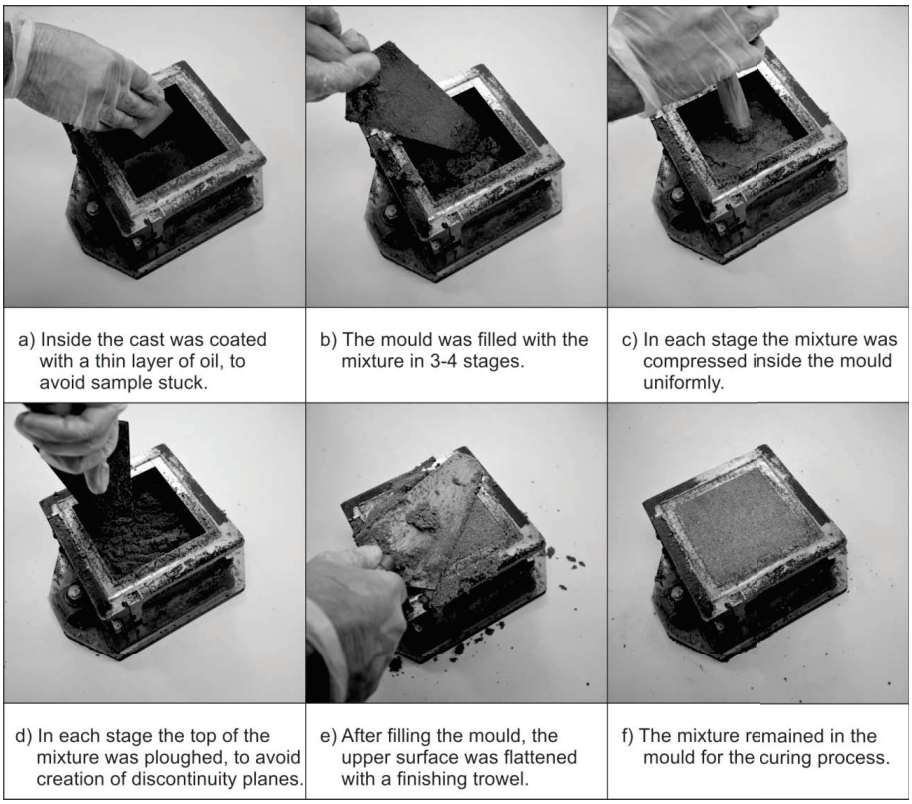

Figure 3. Casting procedure and considerations.

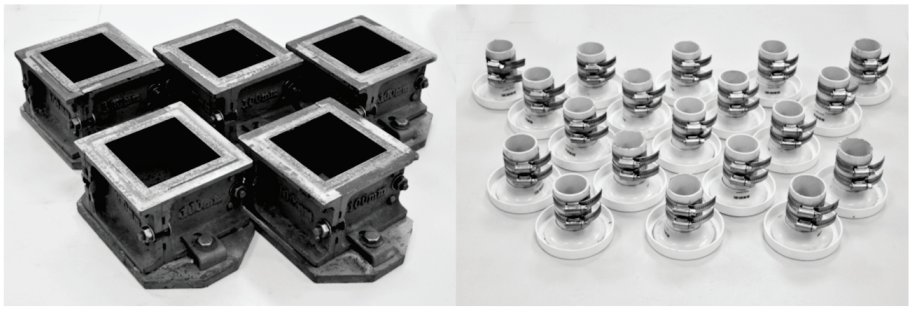

Figure 4. 10 cm cube (left) and cylindrical moulds (right) used for casting the samples.

Cylindrical samples were required to determine the physical and mechanical properties of the synthetic sandstones through performing standard laboratory tests. It was not possible to retrieve cylindrical cores from the cube samples. Due to low cement bonding strength, the outer surface of the sample was prone to severe damage during the process of coring, resulting in a rough surface. Therefore, customer-designed cylindrical moulds were manufactured to cast samples with similar dimensions of plugs used in petroleum applications, i.e. sample height of 7.62 cm and diameter of 3.81 cm. Figure 4 shows both cubic and cylindrical moulds used in this study.

5. Sample Curing

The cement was not strong enough to bond sand particles in the early stage of curing. Hence, the sample loses its integrity by taking it out of the mould earlier than three days. The samples were then submerged into water and cured for 18 days. In order to reduce the effect of over-curing, the samples must be dried after they were taken out of water. The samples were left in an oven with a temperature of 60°C for two days. Thereafter, to reduce the effect of weathering the samples were plastic wrapped and stored in a dry room environment. Figure 5 shows different steps of sample curing.

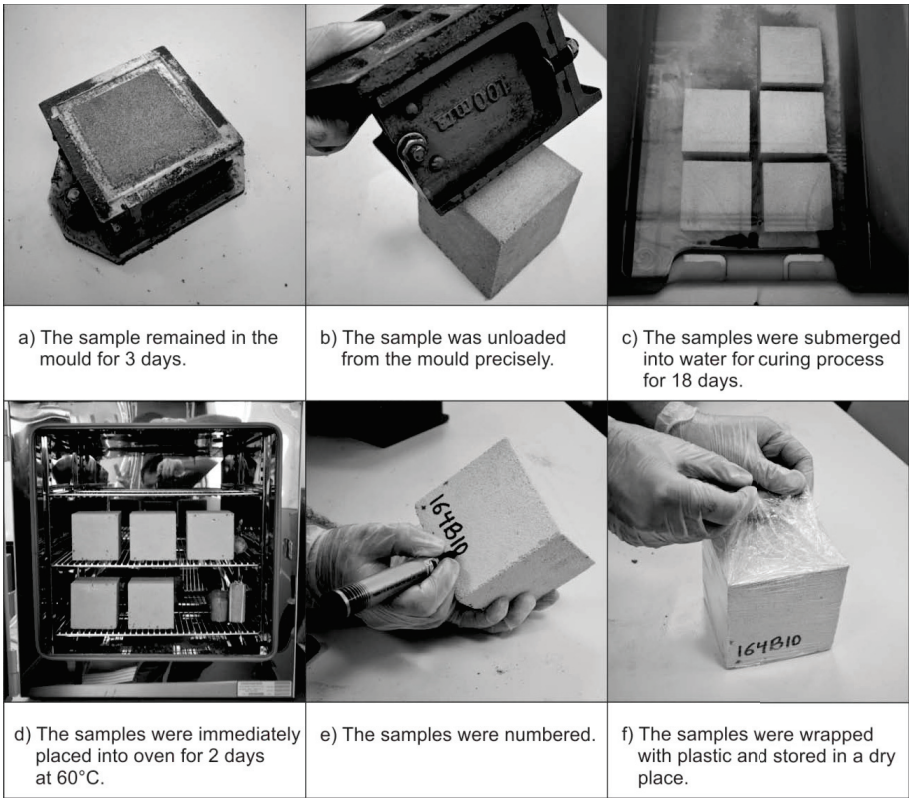

Figure 5. Sample curing and storing steps.

6. Sample properties

Properties of the synthetic sandstone made for sanding experiments were estimated through conducting series of standard tests. The density and porosity of the sample were measured using the method suggested by international society for rock mechanics ISRM (Franklin et al., 1979). The permeability of the sample was measured using a pulse decay permeameter where Helium gas is used as the injecting fluid. The physical properties and permeability of a typical sandstone sample suitable for sanding experiments is tabulated in Table 1. A sample with properties close to those given in Table 1 is seen to be similar to a weakly consolidated sandstone which is prone to sand production during drilling or production from a reservoir.

Table 1. Physical properties and permeability of a typical synthetic sandstone made for sanding experiments.

Bulk density	Grain density	Porosity	Void ratio	Permeability
1815 kg/m^3	2500 kg/m^3	0.274	0.377	1.6E-13 m^2

Deformation properties (e.g. Young's modulus, Poisson's ratio, etc) and strength parameters (e.g. cohesion, friction angle, etc) are essential information required to estimate the stress distribution and failure zone around the borehole in a sand production laboratory experiment. These parameters were estimated through uniaxial and triaxial tests conducted on cylindrical samples.
A uniaxial compressive frame equipped with a 3.81 cm size Hoek triaxial cell was used to do these tests. The axial compressive stress was applied using a hydraulic cylinder connected to a double-piston pump. The confining pressure was controlled in a servo-control manner using a plunger pump. Axial and confining stresses and deformation of the sample were monitored continuously using a data acquisition system.
The ISRM suggested methods were followed to determine the unconfined compressive stress-strain curve of the sample and deformation properties (Bieniawski et al. 1979). Table 2 shows the deformation properties of a typical synthetic sample made for sanding experiments.

Table 2. Deformation properties of a typical synthetic sandstone made for sanding experiments.

Young's modulus	Poisson's ratio	Shear modulus	Bulk modulus	Biot's constant
7.65 GPa	0.18	3.23 GPa	4.04 GPa	1

A series of triaxial tests were carried out under different confining stresses to derive the strength parameters of the synthetic sample. The tests followed the ISRM suggested methods (Franklin, 1983). The ultimate strengths for different confining stresses were used to define the failure envelope. The sample's yield envelope may also be defined from the yield points. However, in rock engineering problems it is more common to use the failure envelope in the analysis, in addition to the fact that here the failure of the synthetic sample around the borehole is the main study focus.

For the purpose of this study, two different failure criteria were used to model the sample failure in sand production laboratory experiments, i.e. Mohr-Coulomb and modified Drucker-Prager. These two failure models were used in the numerical analysis to simulate the laboratory experiments (Younessi et al. 2012). Table 3 shows the strength parameters of a typical synthetic sample made for sanding tests.

Table 3. Strength parameters of a typical synthetic sandstone made for sanding experiments.

Uniaxial compressive strength	Tensile strength	Mohr-Coulomb		Modified Drucker-Prager		
		Cohesion	Friction angle	Shear yield stress	Friction angle	Flow stress ratio
5.4 MPa	0.7 MPa	1.5 MPa	32.6 deg	3.0 MPa	52.8 deg	1 & 0.8

The triaxial tests were initially conducted according to a multi-stage scheme. The setup of this test was similar to the single stage tests. The tests procedure followed the method suggested by ISRM (Franklin, 1983). However, for several reasons it is recommended to conduct single-stage test to obtain the stress-strain curves when dealing with synthetic samples. Some of the reasoning for this is that:

- conducting the tests on different specimens and observing consistent results means that the samples have been generated uniformly. With synthetic samples there is access to many samples for testing purposes.
- The axial loading in multi-stage tests must be stopped before the sample reaches its ultimate strength, or practically its yield point. This means that the estimated strength is not a correct representation of the actual rock strength. If one wants to derive the rock yield envelope instead of the failure envelope this approach may be preferable.

7. Conclusion

In this paper the importance and the need for making synthetic samples for sanding lab experiments were discussed. A sample mixing program presented to prepare synthetic samples representing a weakly consolidated sandstone: this is the type of sandstone prone to sanding in real field conditions. The process of casting and curing the sample was explained in detail. Finally, mechanical properties as well as the range of porosity and permeability of a typical sample made through the proposed preparation scheme presented. The samples obtained from the proposed mixture has mechanical properties similar to a weakly consolidated sandstone which is prone to sanding.

8. References

MORITA, N., AND BOYD, P.A., 1991 – Typical sand production problems: case studies and strategies for sand control. 66th Annual Technical Conference and Exhibition of the SPE held in Dallas, TX, October 6-9.

TERZAGHI, K.V., 1936 - Stress distribution in dry and in saturated sand above a yielding trap door. First Intl. Conf. on Soil Mechanics and Foundation Engineering, Harvard U., Cambridge, MA.

HALL, C.D., AND HARRISBURGER, W.H., 1970 - Stability of sand arches: a key to sand control. J. Pet Technology, pp. 821-829, July 1970, SPE 2399-PA.

TIPPIE, D.B., AND KOHLHAAS, C.A., 1973 - Effect of flow rate on stability of unconsolidated producing sands. 48th annual fall meeting, Las Vegas, Nevada, SPE 4533.

BRATLI, R.K., AND RISNES, R., 1981 - Stability and failure of sand arches. SPE Journal, Vol. 21, No. 2, pp. 236-248, 8427-PA.

PAPAMICHOS, E., TRONVOLL, J., SKJÆRSTEIN, A., AND UNANDER, T.E., 2010 - Hole stability of Red Wildmoor sandstone under anisotropic stresses and sand production criterion, Journal of Petroleum Science and Engineering, 72 (2010) 78–92.

NOURI, A., VAZIRI, H., BELHAJI, H., AND ISLAM, R., 2004 - Sand production prediction: a new set of criteria for modeling based on large-scale transient experiments and numerical investigation. SPE annual technical conference and exhibition, Houston, Texas, SPE 90273.

PERKINS, T.K., AND WEINGARTEN, J.S., 1988 - Stability and failure of spherical cavities in unconsolidated sand and weakly consolidated rock. 63rd annual technical conference, Houston, Texas, SPE 18244.

HOLT, R.M., UNANDER, T.E., KENTER, C.J., AND SANTARELLI, F.J, 1993 - Unloading effects on mechanical properties of a very weak artificial sandstone: Applications to coring. Proc. Int. Symp. on Geotechnical Engineering of Hard Soil - Soft Rock, Anagostopoulos et al. (eds), 1609-1614, Rotterdam: Balkema.

FRANKLIN, J.A., VOLGER, U.W., SZLAVIN, J., EDMOND, J.M., AND BIENIAWSKI, Z.T., 1979 – Suggested methods for determining water content, porosity, density, absorption and related properties and swelling and slake-durability index properties. Int. J. of Rock Mech. & Mining Sci. & Geomechanics Abs., Vol. 16. No.2, pp. 141-156.

BIENIAWSKI, Z.T., FRANKLIN, J.A., BERNEDE, M.J., DUFAUT, P., RUMMEL, F., HORIBE, T., BROCH, E., RODRIGUES, E., VAN HEERDEN, W.L., VOLGER, U.W., HANSAGI, I., SZLAVIN, J., BRADY, B.T., DEERE, D.U., HAWKES, I., AND MILOVANOVIC, D., 1979 – Suggested methods for determining the uniaxial compressive strength and deformability of rock materials. Int. J. of Rock Mech. & Mining Sci. & Geomechanics Abs., Vol. 16. No.2, pp. 135-140.

FRANKLIN, J.A., 1983 – Suggested methods for determining the strength of rock materials in triaxial compression. Int. J. of Rock Mech. & Mining Sci. & Geomechanics Abs., Vol. 20. No.6, pp. 285-290.

YOUNESSI A., RASOULI V., AND WU B., 2012- Numerical simulation of sanding under different stress regimes, the 46th US Rock Mechanics / Geomechanics Symposium held in Chicago, IL, USA, 24-27 June 2012.

Paper 3 Experimental sanding analysis: Thick walled cylinder versus true triaxial tests

EXPERIMENTAL SANDING ANALYSIS: THICK WALLED CYLINDER VERSUS TRUE TRIAXIAL TESTS

A Younessi [a], V Rasouli [a], B Wu [b]

a. Curtin University, Perth, Australia
b. CSIRO, Melbourne, Australia

Abstract

Using a true triaxial stress cell (TTSC) the authors performed several sanding tests on cubes of synthetically made samples. The samples prepared based on an established procedure developed in the laboratory. Samples, with a dimension of $100\times100\times100$ mm^3, were subjected to far-field stresses while increasing the pore pressure inside the cell. Sands were produced from a borehole in the sample centre. An experiment was conducted with anisotropic lateral stress to investigate the effect of stress anisotropy on sand production. By applying uniform lateral stresses, an experiment analogy to TWC was performed for comparison purposes. Comparison of the results of these two experiments demonstrated the importance of considering the intermediate stress component in sanding analysis. The results of these experiments are presented in this paper.

1. Introduction

Sand production laboratory experiments have been conducted since 1930's (Terzaghi, 1936). The majority of the earlier tests were carried out on loose sands to study the effect of arching around a cavity (Hall and Harrisburger, 1970, Tippie and Kohlhaas, 1973, Bratli and Risnes, 1981). Later on, it was observed that even consolidated reservoirs may experience problems due to sand production. Since then, efforts have been made to simulate and study this phenomenon in laboratories (Vriezen et al., 1975, Antheunis et al., 1976, Perkins and Weingarten, 1988, Tronvoll et al., 1993, Papamichos et al., 2001, Wu and Tan, 2002, Nouri et al., 2004).

Most commonly, sanding experiments are performed on cylindrical shaped samples. The cylindrical sample, with a predrilled hole at its centre, is subjected to axial and lateral (i.e. radial) mechanical loads. A draw-down pressure is simulated by applying fluid pressure at the outer boundary of sample and producing from the borehole at the centre. This type of test commonly referred as thick walled cylinder (TWC) test, is the conventional test used to study sand production initiation in laboratories. However, one of the major limitations of such tests is that a uniform confining pressure is applied on the sample outer boundary, an unrealistic representation of the in-situ stress states surrounding a borehole or perforation in fields.

It is well known that depending on the relative magnitudes of three far-field principal stress components, different types of shear failures may occur around an opening

(Jaeger et al., 2007). Hence an appropriate laboratory sanding simulation should be the one which includes the effect of three independent stress components. In practice, this is only possible if the experiment is conducted on cubic samples. In this approach, the stresses represent three principal far-field stresses and the induced stresses around the borehole are not symmetric. This is a more realistic way to simulate sanding as happens in real situations. Only few attempts have been made so far to conduct sanding experiments on cube samples (Kooijman et al., 1992, Kooijman et al., 1996).
This study was motivated as a result of the above discussion. In the following sections the specifications of a true-triaxial stress cell (TTSC) which was used for sanding simulations will be briefly reviewed and the modification applied for this purpose will be explained. The results of sanding test under lateral stress anisotropy is reported and compared with a test corresponding to TWC.

2. Experiment setup

The true triaxial stress cell (TTSC) consists of a pressure cell surrounded by a vertical and four horizontal hydraulic cylinders (Figure 1). Independent vertical and two horizontal stresses ($\sigma_v \neq \sigma_H \neq \sigma_h \neq 0$) can be simulated during an experiment. The maximum operating loads are 450 kN and 250 kN for vertical and horizontal hydraulic cylinders, respectively. The cell can be pressurized up to 21 MPa to simulate pore pressure by injecting fluid. The cell can accommodate a cubic sample of up to 300×300×300 mm^3 for conducting various advanced laboratory experiments under a true 3D stress condition. An outlet hole is designed at the bottom of the cell to access the sample during the test for injection purposes or disposal of the produced sand grains.
The design of the hydraulic cylinders allows their independent control using manual or automatic hydraulic pumps. The fluid flow, which simulates the hydrocarbon production, was pumped with a reciprocating pump with a maximum flow rate of 130 lit/hr and a maximum pressure of 36 MPa. The fluid is injected via an inlet located on the body of the pressure cell. Figure 2 shows a schematic of the experiment configuration.

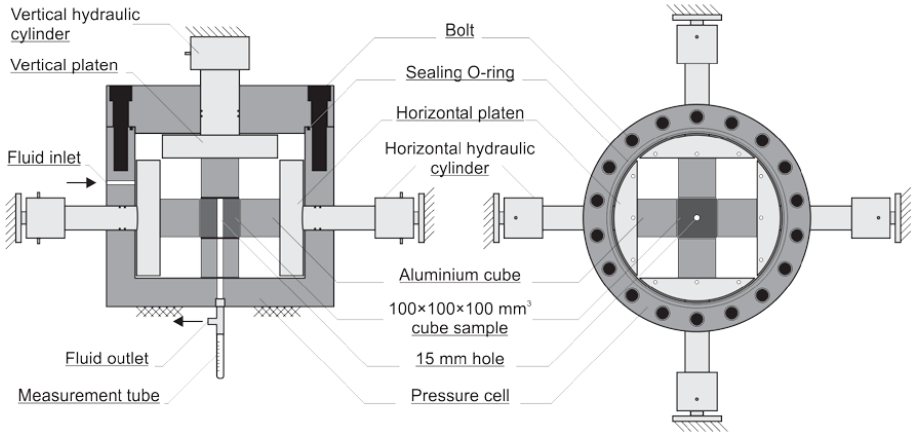

Figure 1. The side view (left) and top view (right) of the TTSC.

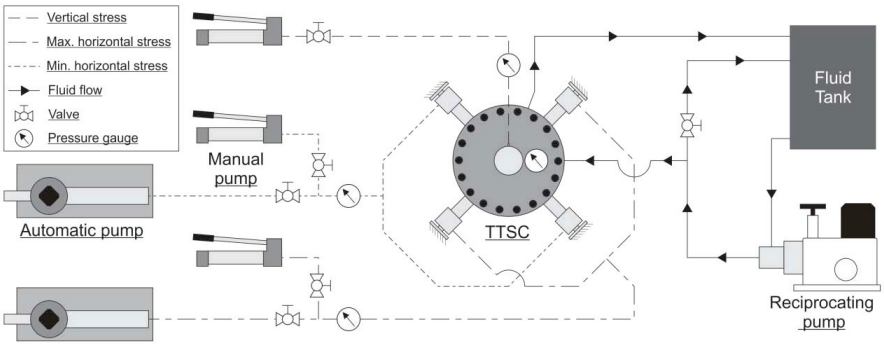

Figure 2. Laboratory sand production experiment configuration.

In this study, the experiments were conducted on 100×100×100 mm^3 cubic samples. Six aluminium block of size 97×97×100 mm^3 were placed around the sample to transmit the loads from the rams to the sample surfaces. A gap was formed between the neighbouring spacers as a result of the spacer size being smaller than the sample size. These gaps serve two purposes. Firstly, it accommodates the sample deformation due to loading, and secondly, it allows testing fluid to enter the sample. The stress concentration, introduced by the difference between the areas of the sample and spacers, at the corner of the sample is negligible (Younessi et al., 2012,a). The upper and lower faces of the sample were sealed using a 1 mm thick rubber sheet glued to their surfaces. The lower sheet has a 15 mm diameter hole in its centre to connect the hole to the outlet of the pressure cell. The lower Aluminium spacer has the same diameter hole. To make sure that the fluid pressure is uniform at the boundary of the sample four woven stainless steel wire meshes were placed between the sample and the spacer. Fluid is flowed through the sample to its borehole and then to the outlet of the cell. Figure 3 shows a schematic of the setup of the sample and the Aluminium spacers in TTSC.

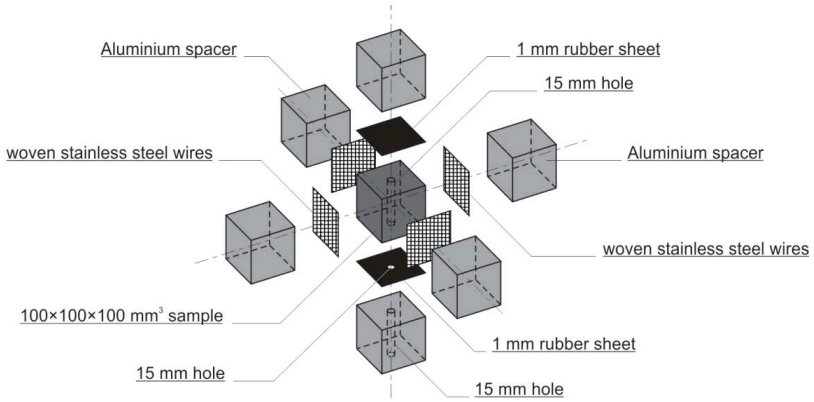

Figure 3. Setup of the sample and spacers inside the TTSC.

3. Sample material properties

The laboratory experiments were conducted on synthetic sandstones. The synthetic samples were produced following a procedure proposed by Younessi et al. (2012,b) to make samples with similar characteristics to a weak-consolidated sandstone. The properties of the sample and the fluid used for laboratory experiments were estimated by conducting a series of standard laboratory tests. Physical and mechanical properties of the synthetic sandstone and the fluid (which was a hydraulic oil) obtained in this study are tabulated in Table 1.

Table 1. Physical and mechanical properties of the synthetic sandstone and the fluid used for sanding studies.

Synthetic Sandstone					Hydraulic Oil	
Bulk density	Porosity	Permeability	Young's modulus	Poisson's ratio	Dynamic viscosity	Density
1815 kg/m^3	0.274	1.6E-13 m^2	7.65 GPa	0.184	0.024 Pa.s	803 kg/m^3

The material was assumed to have an elastic-perfectly plastic behaviour based on the observation from its stress-strain curve obtained in the triaxial tests. The rock was assumed to have a linear-elastic behaviour before its ultimate strength, hence the hardening phase was not considered. The mechanical parameters of two different strength models, Mohr-Coulomb and modified Drucker-Prager, were derived from triaxial tests. These properties and parameters are tabulated in Table 2.

Table 2. Mechanical strength parameters of the synthetic sandstone used for sanding studies.

Uniaxial compressive strength	Tensile strength	Mohr-Coulomb		Modified Drucker-Prager		
		Cohesion	Friction angle	Shear yield stress	Friction angle	Flow stress ratio
5.4 MPa	0.7 MPa	1.5 MPa	32.6 deg	3.0 MPa	52.8 deg	0.8

4. Test procedure

Due to the nonlinear behaviour of the testing material in the plastic zone, the propagation of the plastic zone depends on the stress path. Therefore, to achieve the desirable far-field stresses, the stresses must be applied to the sample following a consistent procedure as explained in four stages below and illustrated in Figure 4:
Stage 1. Sample sealing: After a test sample is set up in the cell, a small vertical stress (1.4 MPa) is applied to the sample to make sure that a good seal between the sample surfaces and the vertical aluminium blocks is achieved.

Stage 2. Sample saturation: Small horizontal stresses and pore fluid pressure are applied on the sample outer boundary hold constant for at least 10 minutes to make sure that the sample is fully saturated with fluid.
Stage 3. Sand production: The stresses are increased step by step following the stress ratio defined for the test program (here in this study minimum to maximum lateral stress ratios were 0.4 and 1). In each step the vertical stress is increased prior to increasing the two horizontal stresses, and the pore pressure was increased after all the three stresses were applied. The sand produced in each step was monitored and measured using a measurement tube located at the outlet of the vessel. Each step lasts for at least 5 minutes.
Stage 4. Unloading: The unloading phase is quite similar to the loading stage but in reverse order, where pore pressure, horizontal and vertical stresses are reduced, respectively. This is done to ensure that the unloading stress path does not induce further extension of the failure zone around the borehole.
Figure 4 shows an example of loading-unloading path for a test (the stages has been marked on the chart).

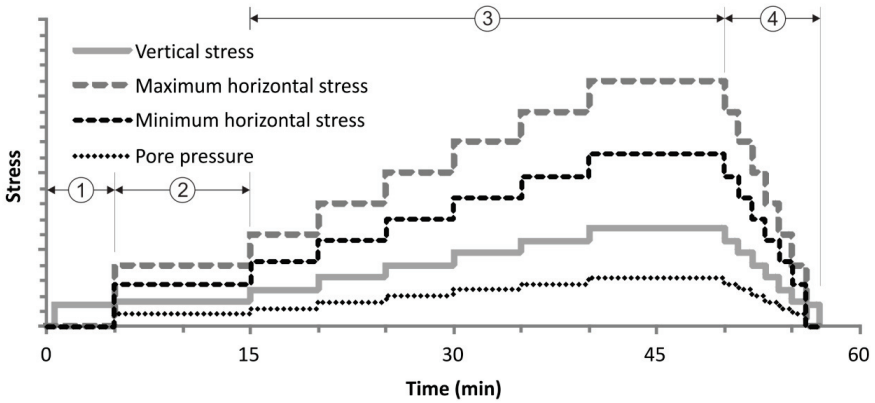

Figure 4. Loading and unloading stages applied in sanding experiments.

5. Results and discussions

Two tests were conducted on two identical samples. The tests were designed to compare the results of borehole failure under both isotropic and anisotropic lateral stress conditions. In both experiments the test procedure presented in the preceding section was followed.
Figure 5 shows the loading path and the amount of sand produced in each experiment. Theoretically the sand around the borehole reaches its yield stress at the very beginning stage of loading (at the beginning of stage 2). However, the fluid flow seems to be inadequate to detach failed sand grains from borehole wall. For both experiments the initiation of sanding was mainly governed by the rate of fluid flow. Sand production was initiated once the boundary pore pressure increased to 2 MP when small amount of sand grains were observed at the measurement tube. A noticeable amount of sand was produced at pore pressure of 2.8 MPa. Finally a relatively large amount of sand grains

were produced when pore pressure reached 3.2 MPa, i.e. at the last step of loading stage.

The rate of sand production may also have a correlation with the size of the failure zone. To investigate the dimension of the failure zone, the stresses were unloaded (as explained in the preceding section) and the sample was taken out from the TTSC. Large amount of failed sands were still attached to the borehole wall when the samples were taken out of the TTSC. These have been removed by blowing pressurized air into the borehole.

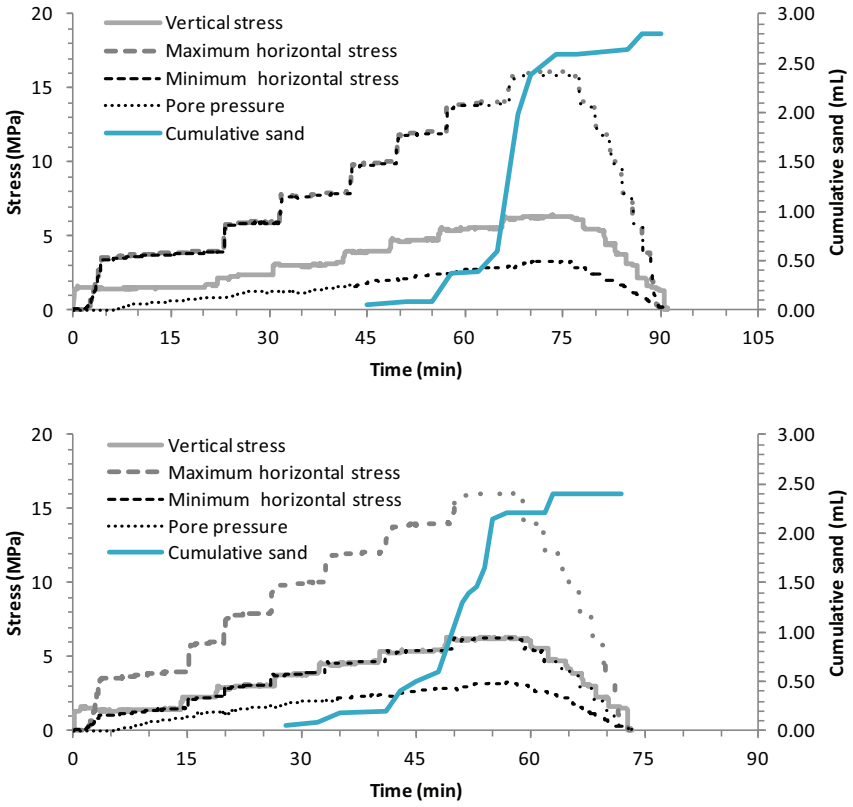

Figure 5. Loading path and the amount of sand produced in experiments with isotropic (top) and anisotropic (bottom) lateral stresses.

The shape of the failure zone was then captured precisely using a borescope. Figure 6 shows the failure zones developed around the borehole for the two experiments. This figure shows that the average depth of the failure zones is reasonably equal in the two tests while it is the width of the failure zone which shows an increase in the case of isotropic test.

The results showed that in an anisotropic stress test the development of the failure is in the direction of minimum horizontal stress. However, there is no preferred failure direction when the two horizontal stresses are isotropic. The main axis of wellbore

ovalisation in the test with isotropic stresses was not oriented to the minimum stress direction. The authors believe this is due to heterogeneity of the sample.

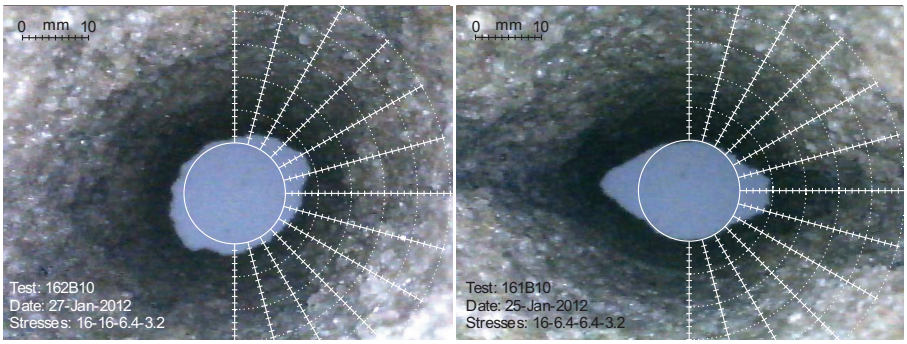

Figure 6. Experimental results: sanding under isotropic (left) and anisotropic (right) state of stresses.

6. Conclusions

Two experiments were conducted to study the difference between the conventional sanding test results (i.e. TWC) and test under true triaxial stress conditions. The tests were conducted on $100\times100\times100$ mm^3 synthetic sandstone. The test setup and procedure for a cube sample subjected to true triaxial stresses and fluid flow was discussed in detail. The followings can be concluded from this investigation:

- The sand production initiation point does not necessarily coincide failure point. The observations indicated that a minimum fluid flow rate is needed to detach the failed sands around the borehole.
- A critical fluid flow rate can be defined as when a significant sand production rate is observed.
- The amount of sands produced at the critical flow rate depends on the geometry of the failed zone, which is a function of the sample mechanical properties and far-field stresses.
- The results showed how the direction of the failure zone in a TWC test has an arbitrary direction which is mainly governed by sample heterogeneity. Oriented breakouts in the direction of minimum stress can only be simulated on a cube shaped sample which was studied here.

Following recommendations are presented for the future work in this research area:

- In all experiments conducted in this study the borehole pressure was atmospheric. Applying a back pressure at the outlet line would allow tests to be conducted under a more realistic downhole condition.
- The tests may be performed on different samples with different mechanical properties to investigate how rock properties (e.g. mechanical strength) may impact sanding.
- The tests may be performed on samples with different sizes and to investigate the effect of the sample size on sanding. The effect of the borehole size is another parameter which could be studied.

7. References

TERZAGHI, K.V., 1936 - Stress distribution in dry and in saturated sand above a yielding trap door. First Intl. Conf. on Soil Mechanics and Foundation Engineering, Harvard U., Cambridge, MA.

HALL, C.D., AND HARRISBURGER, W.H., 1970 - Stability of sand arches: a key to sand control. J. Pet Technology, pp. 821-829, July 1970, SPE 2399-PA.

TIPPIE, D.B., AND KOHLHAAS, C.A., 1973 - Effect of flow rate on stability of unconsolidated producing sands. 48th annual fall meeting, Las Vegas, Nevada, SPE 4533.

BRATLI, R.K., AND RISNES, R., 1981 - Stability and failure of sand arches. SPE Journal, Vol. 21, No. 2, pp. 236-248, 8427-PA.

VRIEZEN, P.B., SPIJKER, A., AND VAN DER VLIS, A.C., 1975 - Erosion of perforation tunnels in gas wells. 50th annual fall meeting, Dallas, Texas, SPE 5661

ANTHEUNIS, D., FERNANDEZ LUQUE, R., VAN DER VLIS, A. C., AND VRIEZEN, P.B, 1976 - The onset of sand Influx from gas-producing friable sandstone formations - laboratory Investigations. SPE Journal, SPE 8031.

PERKINS, T.K., AND WEINGARTEN, J.S., 1988 - Stability and failure of spherical cavities in unconsolidated sand and weakly consolidated rock. 63rd annual technical conference, Houston, Texas, SPE 18244.

TRONVOLL, J., KESSLER, N., MORITA, N., FJAER, E., AND SANTARELLI, F.J., 1993 - The effect of anisotropic stress state on the stability of perforation cavities. Int. J. Rock Mech. Min. Sci. & Geomech. Abstr., Vol. 30, No. 7, pp. 1085-1089.

PAPAMICHOS, E., VARDOULAKIS, I., TRONVOLL, J., AND SKJAERSTEIN, A., 2001 - Volumetric sand production model and experiment. Int. J. Numer. Anal. Meth. Geomech., Vol. 25, pp. 789-808.

WU, B., AND TAN, C.P., 2002 - Sand production prediction of gas field: methodology and laboratory verification. Asia Pacific Oil & Gas Conference and Exhibition, Melbourne, Australia, SPE 77841.

NOURI, A., VAZIRI, H., BELHAJI, H., AND ISLAM, R., 2004 - Sand production prediction: a new set of criteria for modeling based on large-scale transient experiments and numerical investigation. SPE annual technical conference and exhibition, Houston, Texas, SPE 90273.

JAEGER, J.C., COOK, N.G.W., AND ZIMMERMAN, R.W., 2007 - Fundamental of rock mechanics 4th edition. Blackwell.

KOOIJMAN, A.P., HALLECK, P.M., DE BREE, PH., VEEKEN, C.A.M., AND KENTER, C.J., 1992 - Large-scale laboratory sand production test. 67th SPE annual technical conference and exhibition, Washington, DC, SPE 24798.

KOOIJMAN, A.P., VAN DEN HOEK, P.J., DE BEER, PH., KENTER, C.J., ZHENG, Z., AND KHODAVERDIAN, M., 1996 - Horizontal wellbore stability and sand production in weakly consolidated sandstone. SPE annual technical conference and exhibition, Denver, Colorado, SPE 36419.

YOUNESSI A., RASOULI V., AND WU B. 2012(a)- Numerical simulation of sanding under different stress regimes, the 46th US Rock Mechanics / Geomechanics Symposium held in Chicago, IL, USA, 24-27 June 2012.

YOUNESSI A., RASOULI V., AND WU B. 2012(b)- Proposing a sample preparation procedure for sanding experiments, Southern Hemisphere International Rock Mechanics Symposium SHIRMS 2012.

Paper 4 The effect of stress anisotropy on sanding: An experimental study

ARMA 12-374

The effect of stress anisotropy on sanding: An experimental study

Younessi, A. and Rasouli, V.
Curtin University, Perth, Western Australia, Australia
Wu, B.
CSIRO, Melbourne, Victoria, Australia

This paper was prepared for presentation at the 46th US Rock Mechanics / Geomechanics Symposium held in Chicago, IL, USA, 24-27 June 2012.

ABSTRACT: Sand production experiments were carried out under true-triaxial stress conditions. The experiments were conducted on 100×100×100 mm^3 cubes of synthetically made samples. The samples were prepared base on an established procedure developed in the laboratory to produce samples with identical physico-mechanical properties and representing weakly consolidated sandstone. Using a true-triaxial stress cell (TTSC), the samples were subjected to 3D far-field stresses and radial fluid flow from the boundaries. The fluid flows through the sample uniformly and discharges from a hole drilled at the center of the sample. The experiment setup and procedure are explained in detail in this paper. The experiments were performed under three different states of stress to study the effect of the intermediated principal stress (here in this study the minimum lateral stress) on the development of the failure zone. The dimension (i.e. width and depth) of the failure zone developed around the borehole were investigated at the end of the experiments. The results of these experiments will be presented and discussed.

1. INTRODUCTION

Laboratory sand production experiments were initially carried out to study the effect of arching on stability of cavities in unconsolidated sandstones [1]. This aspect of sanding was investigated extensively in the past[2, 3, 4]. However, sanding problems are not limited to unconsolidated sandstone. It has been shown that if the stresses around a perforation tunnel exceed the formation strength, sanding may occur [5]. Also, the effect of stresses and flow rate has been investigated by other researchers on sand production in consolidated sandstones [5 - 11].

The majority of these studies have been conducted on cylindrical samples with a hole drilled at center, and is subjected to axial and lateral (i.e. radial) mechanical loads. Pressure draw-down may be simulated by applying fluid pressure at the outer boundary of sample and producing from the borehole. In this arrangement it is not practically possible to conduct test under real stress conditions (i.e. with three independent far-field stress magnitudes applied to the sample).

An appropriate sanding simulation is the one which includes effect of three independent stress components. In practice, this is only possible if the experiment is conducted on cubic samples. In this approach, the stresses represent three principal far-field stresses and the induced stresses around the borehole are not symmetric. This is a more realistic way to simulate sanding as happens in real situations. Only few attempts have been made to conduct sanding experiments on cube samples [12, 13].

In this study, a series of tests were conducted under true triaxial stress conditions on synthetically manufactured samples to investigate the effect of intermediate principal stress (here in this study the minimum lateral stress) on the size of the failure zone developed due to sand production around the borehole. These tests were conducted using a triaxial stress cell (TTSC). In the following sections the experiment setup and procedure to conduct the experiment are explained in detail. The experimental results are reported and discussed.

2. EXPERIMENT SETUP

The true triaxial stress cell (TTSC) consists of a pressure cell surrounded by a vertical and four horizontal hydraulic cylinders (Figure 1). The maximum operating loads are 450 kN and 250 kN for vertical and horizontal hydraulic cylinders, respectively. The cell can be pressurized up to 21 MPa to simulate pore pressure by injecting fluid. The cell can accommodate a cubic sample of up to 300×300×300 mm^3 for conducting various advanced laboratory experiments under true stress conditions. An outlet hole is designed at the bottom of the cell to access the sample during the test for injection purposes or disposal of the produced sand grains.

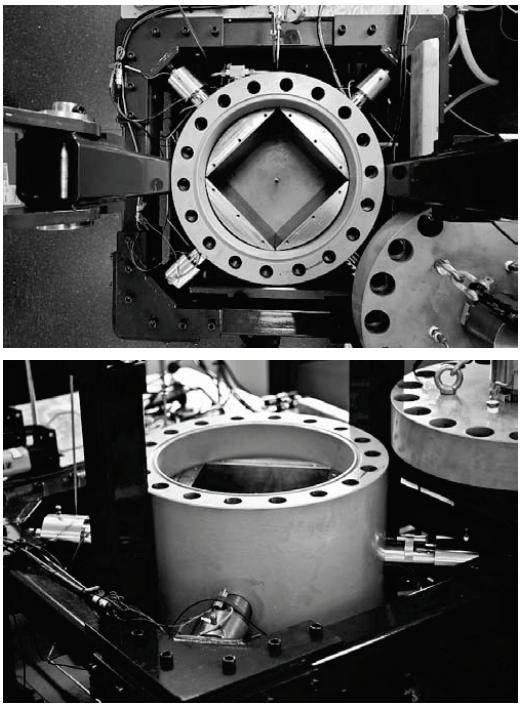

Fig. 1. The top and side view of the TTSC.

The design of the hydraulic cylinders allows their independent control using manual or automatic hydraulic pumps. The fluid flow, which simulates the hydrocarbon production, was injected into the cell via an inlet, using a reciprocating pump with a maximum flow rate of 130 lit/hr and a maximum pressure of 36 MPa.

The experiments were conducted on 100×100×100 mm^3 cubic samples. Six Aluminum blocks of size 97×97×100 mm^3 were placed around the sample to transmit the loads from the rams to the sample surfaces. A gap was formed between the neighboring spacers as a result of the spacer size being smaller than the sample size. These gaps serve two purposes. Firstly, it accommodates the sample deformation due to loading, and secondly, it allows testing fluid to enter the sample. The stress concentration, introduced by the difference between the areas of the sample and spacers, at the corner of the sample is negligible [14]. The upper and lower faces of the sample were sealed using a 1 mm thick rubber sheet glued to their surfaces to simulate a radial flow around the borehole. The lower sheet has a 15 mm diameter hole at its center to connect the hole to the outlet of the pressure cell. The lower Aluminum spacer has the same diameter hole. To ensure that the fluid pressure is uniform at the boundary of the sample four woven stainless steel wire meshes were placed around the sample (Figure 2).

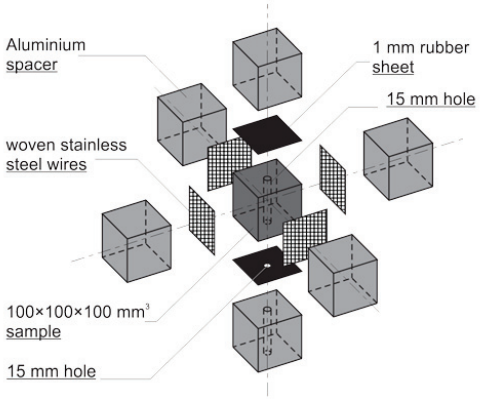

Fig. 2. Setup of the sample and spacers inside the TTSC.

3. SAMPLE PROPERTIES

The synthetic samples used in the experiments were produced following a procedure proposed by Younessi et al. [15] to make samples with similar characteristics to weakly consolidated sandstones, i.e. the type of sandstone prone to sanding in field conditions. The properties of the sample and the fluid used for laboratory experiments were measured by conducting a series of standard laboratory tests. These properties are tabulated in Table 1.

Table 1. Detail properties of a synthetic sample and the fluid used in sand production laboratory experiments.

Fluid Properties			
γ oil	Fluid Weight density	7875.5	N/m^3
μ oil	Fluid Dynamic viscosity	0.024	Pa.s
Physical Properties			
ρb	Bulk density	1815	kg/m^3
n	Porosity	0.274	-
k	Permeability	1.628E-13	m^2
Elastic Properties			
E	Young's modulus	7.65	GPa
ν	Poisson ratio	0.18	-
Strength Parameters			
UCS	Uniaxial compressive strength	5.37	MPa
T0	Tensile strength	0.70	MPa
Mohr-Coulomb parameters			
S0	Cohesion	1.47	MPa
φ	Internal friction angle	32.6	Deg
Drucker-Prager Parameters			
d	Shear yield stress	3.00	MPa
β	Friction angle	52.8	Deg
k	Flow stress ratio	1 & 0.8	-

4. TEST PROCEDURE

Due to the nonlinear behavior of the sample within the plastic zone, the propagation of the plastic zone depends on the stress path. Consistent procedures which were followed in all tests for applying the stresses are listed below:

- **(i)** Sample sealing: To ensure that a good sealing was achieved between the sample and spacers, an axial stress of 1.4 MPa was applied to the sample.
- **(ii)** Sample saturation: The sample was saturated by flowing fluid for at least 10 minutes.
- **(iii)** Sand production: Stresses were increased gradually following the stress ratio defined for the test. Each step lasts for at least 5 minutes.
- **(iv)** Unloading: The unloading phase was similar but opposite to that of the loading stage with shorter steps. This is done to ensure that the unloading stress path does not affect the characteristics of the failure zone around the borehole.

Figure 3 shows an example of the loading-unloading path for a typical test conducted for sanding studies (the stages has been marked on the chart).

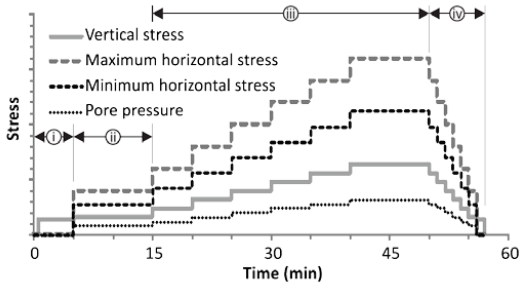

Fig. 3. Sample loading and unloading stages followed in sanding experiments.

5. RESULTS AND DISCUSSIONS

Three individual tests were conducted on identical samples. The tests were designed to investigate the effect of intermediate lateral stress on borehole failure. Hence, the axial and maximum lateral stresses were kept equal in all tests. The fluid flow was simulated similarly in all tests and the test procedure presented in the previous section was followed throughout the whole experiments.

Failed sand grains were observed to be still attached to the borehole after the sample was removed from the TTSC. These have been removed by blowing pressurized air into the borehole. The shape of the failure zone was then captured precisely using a borescope (Figure 4). Table 2 summarizes the magnitudes of stresses and pore pressures applied to the boundary of the samples in each tests, as well as the dimension of the corresponding failure zone.

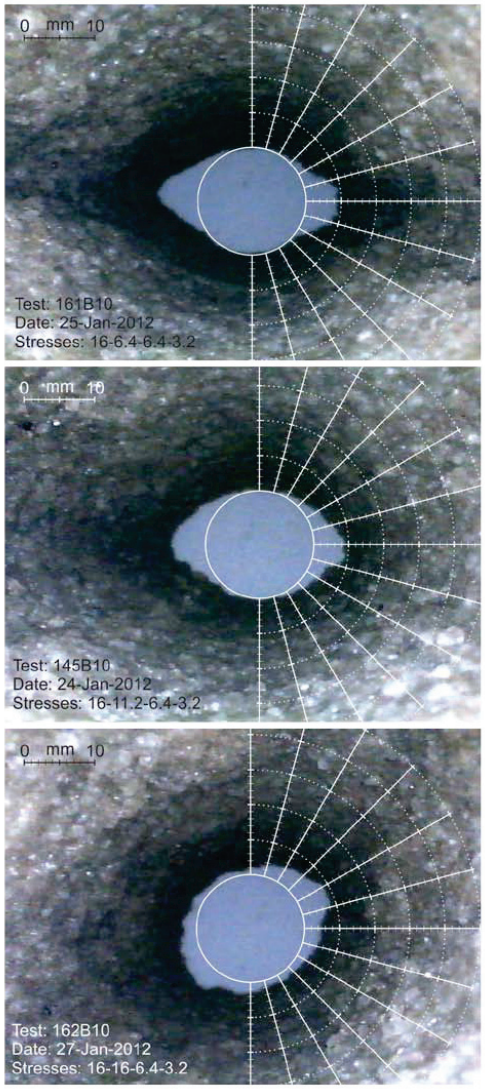

Fig. 4. Failure zone developed in sanding experiments under 0.4 (top), 0.7 (middle) and 1.0 (bottom) lateral stress ratios.

Table 2. Applied stresses and observed dimension for the failure zones in different sanding experiments.

Test name	B1601	B1602	B1603
Max. lateral stress (MPa)	16	16	16
Min. lateral stress (MPa)	6.4	11.2	16
Lateral stress ratio (Pa/Pa)	0.4	0.7	1
Axial stress (MPa)	6.4	6.4	6.4
Pore pressure (MPa)	3.2	3.2	3.2
Failure width (deg)	105	150	180
Failure depth (mm)	4.9	4.6	4.4

The results of Table 2 show that the depth of the failure zones did not change in different experiments. This suggests that the minimum lateral stress does not have any effect on the depth of failure zone for the condition that we studied. This may be postulated that the magnitude of the maximum lateral stress has the main impact on the depth of failure zone. However, this needs further investigations for other cases to reach a general conclusion.

Table 2 also shows a noticeable change in the width of the failure zone corresponding to different minimum lateral stresses. The results show that by increasing the stress anisotropy, the width of the failure zone decrease: this means that the width of the failure zone is reversely proportional to the difference between the minimum and maximum lateral stress. Both observations were supported when the experiments were simulated numerically using a finite element method [14].

The results showed that in an anisotropic stress test the development of the failure is in the direction of minimum horizontal stress. However, there is no preferred failure direction when the two horizontal stresses are isotropic. The main axis of wellbore ovalisation in the test with isotropic stresses was not oriented to an preferred direction. The authors believe this could be due to heterogeneity of the sample.

6. CONCLUSIONS

Three experiments were conducted on identical cubic samples under different horizontal stress anisotropies to investigate the importance of the intermediate principal stress (in this study the minimum lateral stress). The tests were done on $100\times100\times100$ mm^3 synthetic sandstones. The test setup and procedure for a cubic sample subjected to true triaxial stresses and fluid flow was discussed in detail. The following may be concluded from this investigation:

- The geometry of the failed zone around the borehole is directly related to the difference and magnitude of the far-field stresses.
- The depth of the failure zone was independent of the amount of lateral stress anisotropy in the condition that the tests were conducted. This may indicate that the extent of the depth of the failure zone might be mainly governed by the axial and maximum lateral stresses for a given material.
- The width of the failure zone is reversely proportional to the lateral stress anisotropy. The width of failure zone increases as the difference between the maximum and minimum lateral stresses decrease.
- The results showed that the direction of the failure zone in an isotropic test has an arbitrary direction which is mainly governed by heterogeneity of the sample. The failure in the direction of minimum stress can only be simulated on a cube shaped sample which was studied here.

Following recommendations are presented for the future work in this research area:

- A new set of experiments may be conducted to investigate the effect of the maximum lateral stress on the depth of the failure zone.
- The authors believe that the axial stress may have significant impacts on the dimension of the failure zone. More investigations are needed to study this effect.

7. REFERENCES

1. Terzaghi, K.V., 1936 - Stress distribution in dry and in saturated sand above a yielding trap door. First Intl. Conf. on Soil Mechanics and Foundation Engineering, Harvard U., Cambridge, MA.
2. Hall, C.D., and Harrisburger, W.H., 1970 - Stability of sand arches: a key to sand control. J. Pet Technology, pp. 821-829, July 1970, SPE 2399-PA.
3. Tippie, D.B., and Kohlhaas, C.A., 1973 - Effect of flow rate on stability of unconsolidated producing sands. 48th annual fall meeting, Las Vegas, Nevada, SPE 4533.
4. Bratli, R.K., And Risnes, R., 1981 - Stability and failure of sand arches. SPE Journal, Vol. 21, No. 2, pp. 236-248, 8427-PA.
5. Vriezen, P.B., Spijker, A., And Van Der Vlis, A.C., 1975 - Erosion of perforation tunnels in gas wells. 50th annual fall meeting, Dallas, Texas, SPE 5661
6. Antheunis, D., Fernandez Luque, R., Van Der Vlis, A. C., and Vriezen, P.B, 1976 - The onset of sand Influx from gas-producing friable sandstone formations - laboratory Investigations. SPE Journal, SPE 8031.
7. Perkins, T.K., And Weingarten, J.S., 1988 - Stability and failure of spherical cavities in unconsolidated sand and weakly consolidated rock. 63rd annual technical conference, Houston, Texas, SPE 18244.
8. Tronvoll, J., Kessler, N., Morita, N., Fjaer, E., and Santarelli, F.J., 1993 - The effect of anisotropic stress state on the stability of perforation cavities. Int. J. Rock Mech. Min. Sci. & Geomech. Abstr., Vol. 30, No. 7, pp. 1085-1089.
9. Papamichos, E., Vardoulakis, I., Tronvoll, J., and Skjaerstein, A., 2001 - Volumetric sand production model and experiment. Int. J. Numer. Anal. Meth. Geomech., Vol. 25, pp. 789-808.
10. Wu, B., and Tan, C.P., 2002 - Sand production prediction of gas field: methodology and laboratory verification. Asia Pacific Oil & Gas Conference and Exhibition, Melbourne, Australia, SPE 77841.
11. Nouri, A., Vaziri, H., Belhaji, H., And Islam, R., 2004 - Sand production prediction: a new set of criteria for

modeling based on large-scale transient experiments and numerical investigation. SPE annual technical conference and exhibition, Houston, Texas, SPE 90273.

12. Kooijman, A.P., Halleck, P.M., De Bree, Ph., Veeken, C.A.M., and Kenter, C.J., 1992 - Large-scale laboratory sand production test. 67th SPE annual technical conference and exhibition, Washington, DC, SPE 24798.

13. Kooijman, A.P., Van Den Hoek, P.J., De Beer, Ph., Kenter, C.J., Zheng, Z., and Khodaverdian, M., 1996 - Horizontal wellbore stability and sand production in weakly consolidated sandstone. SPE annual technical conference and exhibition, Denver, Colorado, SPE 36419.

14. Younessi A., Rasouli V., and Wu B. 2012- Numerical simulation of sanding under different stress regimes, the 46th US Rock Mechanics / Geomechanics Symposium held in Chicago, IL, USA, 24-27 June 2012

15. Younessi A., Rasouli V., and Wu B. 2012- Proposing A Sample Preparation Procedure For Sanding Experiments, Southern Hemisphere International Rock Mechanics Symposium SHIRMS 2012

Paper 5 Numerical simulation of sanding under different stress regimes

ARMA 12-373

Numerical simulations of sanding under different stress regimes

Younessi, A. and Rasouli, V.
Curtin University, Perth, Western Australia, Australia
Wu, B.
CSIRO, Melbourne, Victoria, Australia

This paper was prepared for presentation at the 46th US Rock Mechanics / Geomechanics Symposium held in Chicago, IL, USA, 24-27 June 2012.

ABSTRACT: Laboratory experiments of sand production conducted under true-triaxial stress conditions were simulated numerically using ABAQUS program. The experiments were performed in a true-triaxial stress cell on 100×100×100 mm^3 cubes of synthetic sandstones. Two and three dimensional numerical analyses were conducted to investigate the impact of the magnitude of far-field intermediated principal stress and pore pressure on the failure in the vicinity of a borehole. Different stress boundary conditions were modeled for this purpose. The results provide a better understanding on how the stress anisotropy may have an impact on borehole failure and sand production mechanism. The simulation was used as a tool to optimize and plan the future tests conducted in the laboratory on cube samples. The results of the numerical models will be presented and interpreted.

1. INTRODUCTION

A borehole drilled or perforated in a formation composed of unconsolidated sands prone to sanding problems during its production life. Sand production may occur in consolidated sandstones if the stresses induced around the borehole wall exceed the formation strength.

In the context of geomechanics, the magnitude of stresses induced around a single borehole is a function of three principal far-field stresses; usually a vertical and two horizontal stresses, and pore pressure. Several theoretical models have been developed to use these stresses to predict sand production in a borehole [1, 2, 3, 4]. In addition, the extent of the failure zone developed in the vicinity of the borehole wall is a function of these stresses. The dimension of the failure zone is directly proportional to the rate of sand production. The effect of these stresses on failure dimension can be investigated either by experimental or theoretical approaches.

The common practice to simulate sanding in laboratories is to conduct thick walled cylinder (TWC) experiments on a hallow cylindrical shaped sample [3, 5, 6, 7]. This type of experiment, however, is not a realistic simulation of downhole condition for sanding as the sample is subjected to axial and uniform lateral stresses. In real situation three different principal stresses often exist in the formation. Sanding experiments under true 3D stress conditions have been conducted by the authors using a true triaxial stress cell [8]. The setup and results of these experiments will be presented briefly in the following sections.

The effect of stress anisotropy on the development of the plastic zone during the experiment was investigated through the application of theoretical models. The plane-strain analytical solutions for a borehole in an elasto-plastic material subjected to uniform lateral stresses may be used to estimate the dimension of the induced plastic zone around a borehole [9]. However, due to symmetric nature of this solution the induced plastic zone is assumed to be circular. This is opposed to real situation where the borehole is subjected to three different far-field principal stresses, i.e. stress anisotropy perpendicular to the axis of the borehole, which results in the plastic zone to be induced in the direction of the minimum horizontal stress. Therefore, in order to theoretically study the effect of stress anisotropy on the induced plastic zone, numerical simulations are required to be carried out.

The geometry and input parameters for the numerical model are set based on sample properties and experiment setup. These are discussed briefly in the subsequent sections. The methodology used to numerically simulate the lab experiments in both two and three dimension are explained in detail. The results are discussed and compared to the laboratory observations.

2. SAMPLE PROPERTIES

Sample properties define the material model to be used in the numerical modeling. The experiments were conducted on synthetic samples whose mechanical characteristics are similar to typical weak consolidated sandstones. A consistent sample preparation procedure was established and used for the purpose of this study, the details of which can be found in [10]. The sample and fluid properties were obtained by conducting a series of laboratory tests using triaxial and porosity-permeability apparatus, respectively. Strength parameters of the samples were extracted from the results of lab tests based on two failure criteria, i.e. Mohr-Coulomb and Drucker-Prager. Table 1 shows the detail properties of one of the representative samples used for simulations in this paper.

Table 1. Detail properties of a synthetic sample and the fluid used in sand production laboratory experiments.

Fluid Properties			
γ oil	Fluid Weight density	7875.5	N/m^3
μ oil	Fluid Dynamic viscosity	0.024	Pa.s
ν oil	Fluid Kinematic viscosity	2.99E-05	m^2/s
Physical Properties			
ρb	Bulk density	1815	kg/m^3
ρg	Grain density	2500	kg/m^3
n	Porosity	0.274	-
k	Permeability	1.628E-13	m^2
Elastic Properties			
E	Young's modulus	7.65	GPa
ν	Poisson ratio	0.18	-
G	Shear modulus	3.23	GPa
K	Bulk modulus	4.04	GPa
α	Biot's constant	1	-
Strength Parameters			
UCS	Uniaxial compressive strength	5.37	MPa
T0	Tensile strength	0.70	MPa
Mohr-Coulomb parameters			
S0	Cohesion	1.47	MPa
φ	Internal friction angle	32.6	deg
ψ	Dilation angle	32.6	deg
Drucker-Prager Parameters			
d	Shear yield stress	3.00	MPa
β	Friction angle	52.8	deg
k	Flow stress ratio	1 & 0.8	-
ψ	Dilation angle	52.8	deg

Linear elastic-perfectly plastic constitutive model was assumed for the behavior of synthetic sandstone. The sample was assumed to deform linearly prior to yielding and no hardening rule was assumed for the model, i.e. yield function was assumed to coincide with the failure points. The plastic strain was not a concern in this study and therefore using any flow rule was acceptable. However, associated plastic flow was presumed for ease of numerical modeling. The fluid is assumed to be inviscid, and incompressible. The flow regime in the sand production laboratory experiment was assumed to be in steady-state condition. Finally, the constitutive behavior for pore fluid flow was assumed to be governed by the Darcy's law.

3. LABORATORY EXPERIMENT SETUP

The experiments were conducted in a true triaxial stress cell (TTSC) developed for the purpose of sand production and hydraulic fracturing laboratory experiments [11]. The TTSC applies three independent stresses to sides of a cubic sample by the means of five independent rams (Figure 1).

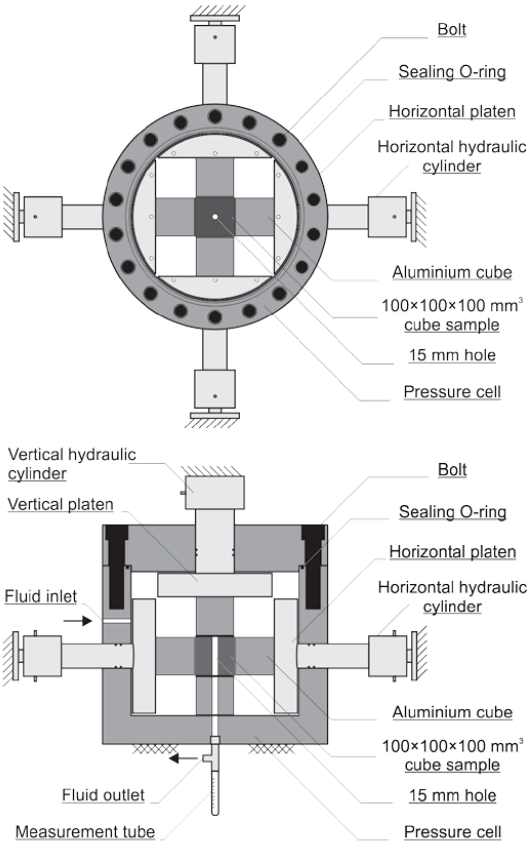

Fig. 1. Polyaxial sand production laboratory experiment setup, top and side view, with 100x100x100 mm^3 cube sample.

The samples tested were cubes of 100×100×100 mm^3 with 15 mm diameter borehole drilled at centre of the sample. The borehole was connected to an outlet at the bottom of the pressure cell. Fluid production was simulated by increasing fluid pressure at the outer boundaries of the sample. Therefore, the fluid flows through the sample, i.e. from the boundaries to the borehole. The fluid pressure at the boundary of the sample is controlled by a pump while the pressure at the borehole is atmospheric. The produced sand is collected and measured at the outlet of TTSC (Figure 1).

The TTSC was designed to accommodate up to a maximum of 300×300×300 mm^3 cubic sample size. In order to conduct tests on 100×100×100 mm^3 samples, six Aluminum cubes were placed in each side of the sample, between the sample and rams. The effective area of these spacers (97×97 mm^2), where the loads were applied, is slightly smaller than the sample sides area (100×100 mm^2) to make sure that the sample is loaded instead of the spacers interacting with each other during the loading process.

The details of sample setup and test procedure of sand production laboratory experiments conducted using the TTSC is presented in [8].

4. EXPERIMENT RESULTS

Failure around borehole was studied in three dimensions. In this case three experiments were conducted under different stress conditions. The far-field intermediate stress (i.e. minimum lateral stress) was changed for each stress regime to investigate the effect of intermediate stress on failure zone around the borehole. Therefore, two principal stresses (i.e. maximum lateral and axial stresses) were maintained constant for the analysis. Table 2 tabulates the stresses and failure dimension for these experiments.

Table 2. Results of the laboratory experiments.

Test name	B1601	B1602	B1603
Max. lateral stress (MPa)	16	16	16
Min. lateral stress (MPa)	6.4	11.2	16
Lateral stress ratio (Pa/Pa)	0.4	0.7	1
Axial stress (MPa)	6.4	6.4	6.4
Pore pressure (MPa)	3.2	3.2	3.2
Failure width (deg)	105	150	180
Failure depth (mm)	4.9	4.6	4.4

The complete results are presented in a separate paper [8]. In the following sections the methodology implemented to simulate these experiments using finite element method is explained.

5. 2D NUMERICAL SIMULATIONS

Comparing to 3D, performing 2D numerical simulations is more time and cost effective. This may, however, be at the expense of gaining less accurate results. Several analytical solutions have been derived to calculate stresses around a borehole in plane-strain conditions where 2D simulations provide reasonable estimations of 3D results [1, 9]. In this case, it is assumed that the axial dimension of borehole has an infinite length and the out of plane stress has no effect on in-plane stresses. It must be noted that in this case the out of plane stress is not completely vanished, but it is a function of the magnitude of in-plane stresses [12].

The analytical solutions of stresses around a borehole can be implemented to model the laboratory experiments to some extent. These models, however, are constrained in their assumptions to simple boundary conditions and/or constitutive models. For instance, the analytical models derived for elastic-plastic materials are limited to isotropic boundary stress conditions [9] or the ratio of lateral stresses [13]. As another example, the solutions for biaxial boundary stresses are only available for elastic materials [12]. Therefore, for cases with more complicated boundary conditions and constitutive models, the solutions need to be obtained through numerical simulations.

The sand production laboratory experiments conducted in the TTSC were simulated using ABAQUS in 2D. For this, a horizontal plane section perpendicular to the borehole axis was simulated. Although the length of the borehole in the sample is limited (100 mm), it is much larger than its diameter (15 mm). Therefore, it was thought to be plausible to assume a plane strain condition for this problem. Here, the effects of lateral boundary stresses (i.e. in-plane stresses) on development of failure zone (i.e. yield zone in the numerical simulation) around the borehole were investigated. It must be noted that the effect of the axial stress (i.e. out of plane stress) was not explicitly studied in 2D models but was studied in three dimensional analysis which will be discussed in the next section.

5.1. Geometry and boundary conditions

The geometry and boundary conditions of the numerical models were defined based on the sample geometry and experiment setup. A plane section perpendicular to the borehole axis was selected for the plane-strain analysis. Due to the symmetrical nature of the problem only a quarter of the sample was modeled. This reduces the number of elements required for the model and therefore a less time for solution convergence.

The normal displacement of the two symmetric faces and their rotation components were fixed in the model. These two symmetric faces with fixed displacements eliminated the rigid body motion.

The boundary conditions defined in numerical simulation must be representative of the loads and displacements applied to the boundary of the sample in the laboratory experiments. Same boundary conditions were applied in the numerical simulation, i.e. biaxial stresses and uniform pore pressure were considered at the outer boundary of the sample and the borehole wall were treated as a free-draining surface. Figure 2 shows the geometry of the 2D numerical model built in this study.

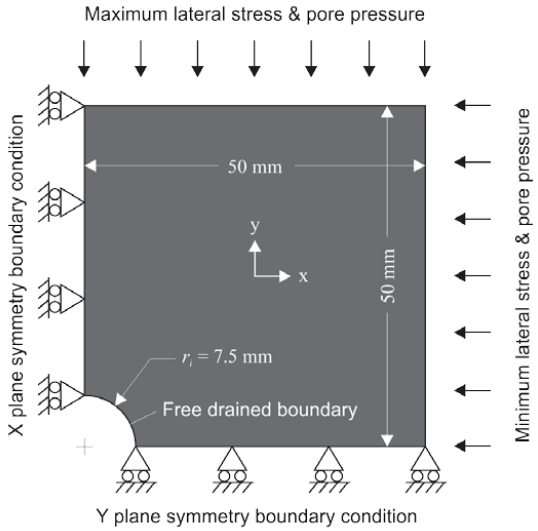

Fig. 2. 2D numerical model geometry built for sanding simulations of a cubic sample.

The Aluminum spacers were initially included in the numerical models. However, after comparing the results to a simpler case, where the boundary loads are directly applied to the sample, no significant differences were observed. Therefore, the Aluminum spacers were excluded from the numerical model and loads were directly applied to the sample boundaries, and later models were developed with no spacer. In addition, the effect of stress concentration in the corners of the sample which was generated due to the difference of the sample area and the spacer effective area was investigated. The results indicated no significant stress distribution changes close to the borehole due to this stress concentration around the sample periphery.

5.2. Elements and mesh

A mesh sensitivity analysis was conducted. Five different mesh densities were examined in the model and the changes in magnitude of stresses at borehole wall were monitored. A linear elastic material with deformation properties tabulated in Table 1 was used for this purpose. The models were subjected to uniform lateral stress of 10 MPa and pore pressure of 2 MPa. The results for each of the five mesh densities are compared in Table 3. It was observed that very coarse, coarse and moderate mesh sizes predict less accurate stress values at the borehole wall, but the fine and very fine meshes result in similar answers. The convergence of the results is plotted in Figure 3 which supports this statement.

Table 3. Results of mesh refinement study.

Mesh	Number of elements	Relative stresses at wellbore wall (ratio to "very coarse" results)	
		Radial stress	Tangential stress
Very coarse	6	1.00E+00	1.00E+00
Coarse	24	2.09E-01	9.20E-01
Moderate	96	3.69E-02	9.06E-01
Fine	384	5.52E-03	9.04E-01
Very fine	1536	8.75E-04	9.03E-01

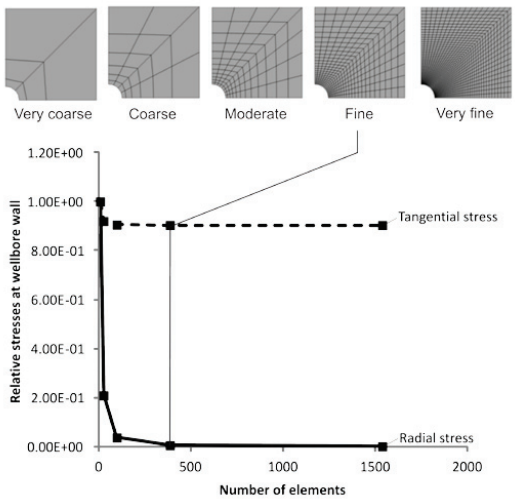

Fig. 3. Convergence of results in a mesh refinement study.

It might be better to run the 2D model with very fine meshes, as this has no significant influence in solution time required for analysis. However, this requires a significant amount of memory and solution time in 3D analysis. As in this study the idea was to compare the results of 2D versus 3D models it was decided to use similar mesh densities. Therefore, fine mesh with 384 elements was used in all our models.

5.3. Model validation

Elastic solutions for a hole in an infinite plane subjected to biaxial stresses assuming plane-strain conditions are widely used to calculate the stress distribution around the borehole [12]. It can be shown that the induced

stresses around the borehole reach to 98% of the far-field stress magnitudes in a distance of $6r_i$ away from the borehole axis, where r_i is borehole radius. Therefore, in current experimental setup, where the minimum distance of the boundaries to the centre of the borehole is $6.7r_i$ (0.05 m/0.0075 m), the applied boundary stresses can be assumed as far-field stresses.

In order to validate the model, a cylinder which was inscribed in a cubic sample with an identical hole at its centre was used in this study. The cylindrical model with Mohr-Coulomb material was validated against the analytical stress solutions derived by [9]. Figure 4 shows the stress profile in the radial direction of a cylinder with Mohr-Coulomb material subjected to 16 MPa lateral load at its outer boundary. The model pore pressure was also 3.2 MPa. Because the geometry and the boundary conditions were axisymmetric in the cylindrical model, the stress profile is similar in all radial directions.

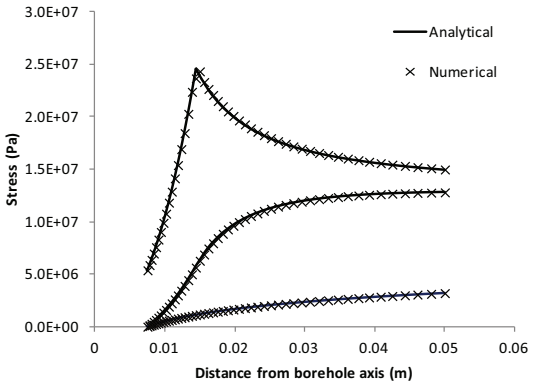

Fig. 4. Validation of numerical results of stresses applied to a cylindrical sample.

The cubic sample was subjected to hydrostatic boundary stresses to compare the results with that of cylindrical model. The results are shown in Figure 5, with the boundary conditions of 16 MPa uniform lateral loads and 3.2 MPa pore pressure. The results show that the stresses are essentially identical except a slight deviation close to the outer boundaries. Because the main objective of this study was to investigate the stresses and failure near the borehole, this deviation can be ignored. This observation implies that laboratory experiments can be conducted on cube samples with isotropic stresses to simulate a thick wall cylinder (TWC) test.

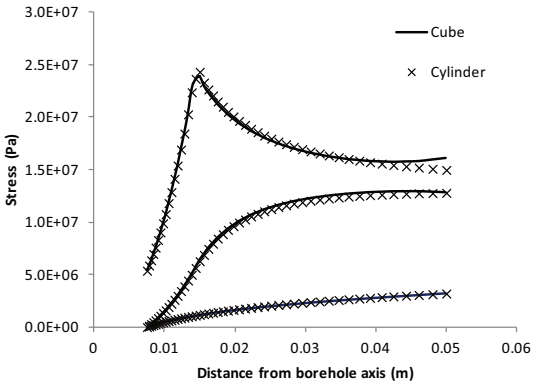

Fig. 5. Comparison of numerical simulations of stresses for a cube and a cylinder under isotropic stress conditions.

5.4. Stress sensitivity analysis

The 2D numerical models were used to simulate the failure zones (Breakouts) developed during testing synthetic samples in the laboratory. The failure zone may represent the volume of sands produced during production from the borehole. Width and depth of the failure zone were the two parameters to characterize the size of the failure zone. The results of the simulations are presented in Figure 6 and Figure 7.

The Drcuker-Prager criterion predicted a very minor failure zone around the borehole. In comparison, Mohr-Coulomb criteria predicted a much larger zone of failure, i.e. is a more conservative failure predictor. Therefore, modified Drucker-Prager (with 0.8 flow stress ratio) was used and found to provide the best correlation with the experimental results. This is the failure criterion used in this study.

From Figure 6, it can be seen that the difference between the lateral stresses has a significant impact on the failure width. As the stress anisotropy reduces, the failure width tends to cover the entire borehole wall. This must be noted that in thick walled cylinder experiments the lateral stresses are isotropic and it is not possible to study the effect of the intermediate stress (minimum lateral stress).

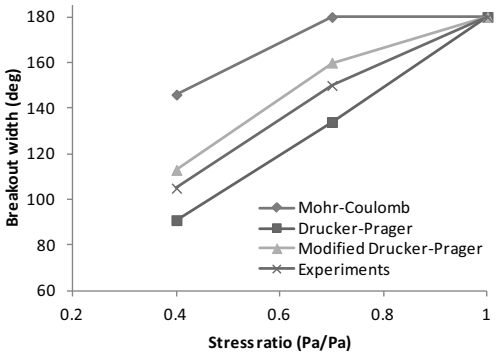

Fig. 6. The failure zone (i.e. yield zone) width as a function of stress anisotropy.

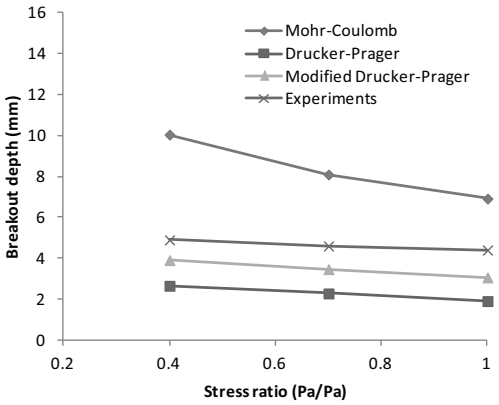

Fig. 7. Depth of failure zone (i.e. yield zone) as a function of stress anisotropy.

However, it seems that the stress anisotropy has less impact on the failure depth (Figure 7). It is important to note that these are 2D plane-strain models in which the axial stress is calculated from the Hoek's law. In contrary, in full 3D models the axial stress is not a function of the magnitude of the lateral stresses and can be applied independently. This concludes that to investigate the impact of the axial stress 3D or axisymmetric models must be employed. However, in this study as the two lateral stresses were unequal 3D model was used for simulations. This is discussed in the following section.

6. 3D NUMERICAL SIMULATIONS

There are no analytical solutions available to estimate the induced stresses around a borehole subjected to three independent far-field stresses. In order to study the failure (i.e. yield) around the borehole in true-triaxial stress conditions, i.e. where three independent principal stresses are applied to the sample, a 3D model must be developed. In this case the axial stress, which is a function of the lateral stresses in plane-strain, can be changed independently. However, the plane-strain condition can be considered as a special case of 3D model and it will be discussed later on.

6.1. Geometry and boundary conditions

As discussed earlier in this paper the geometry and boundary conditions of the numerical models are governed by sample geometry and experiments setup. The 3D model is basically an extended 2D model in the axial dimension. However the axial dimension of the model needs to be considered carefully. In contrary to the radial stresses that have a gradient along the lateral axes within the sample, the axial stress has no gradient due to the axi-symmetrical nature of the borehole. Therefore, the axial dimension can have any arbitrary dimension: in this study the model thickness was assumed to be 10 mm. The symmetric faces, including two lateral and the bottom faces of the model were fixed in the direction of their axes, similar to the 2D model.

The axial load applied to the sample should represent the load applied through the vertical platen in the TTSC tests. Although the load is controlled by the hydraulic pressure behind the hydraulic cylinder, the load is applied through the Aluminum spacers around the boundary of the sample. The Aluminum spacer has a significantly higher stiffness than that of the sample. This means that the deformation of the spacer can be ignored compared to the sample deformation. Therefore, it is plausible to apply the vertical load by a displacement boundary condition. The displacement associated with a specific load can be calculated from the Hook's law for elastic material.

Similar to the 2D analysis the fluid flow is simulated by considering a uniform pore pressure on the lateral boundary of the sample and the borehole wall was freely drained. The upper and lower sides of the sample were impermeable. Figure 8 shows the geometry of a 3D numerical model constructed for this study.

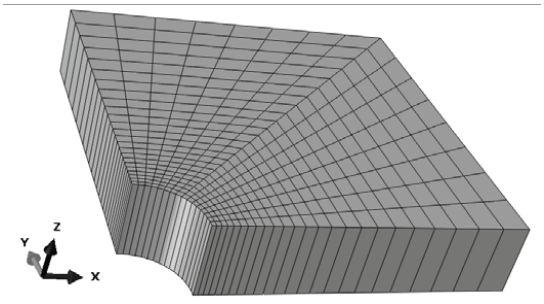

Fig. 8. A 3D model geometry constructed for stress analysis of a cubic sample.

Similar to the 2D model the effect of including the axial Aluminum spacer in the model and the stress concentration at sample corners were found negligible and hence discarded in further simulations.

6.2. Elements and mesh

The meshing in horizontal plane is similar to the 2D model. Because there is no stress gradient in the axial direction only one element was considered along this dimension (see Figure 8).

6.3. Model validation

Plane-strain condition was considered as a special case of 3D model for validation purposes. As the axial load is applied through displacement, it is quite easy to simulate a 3D model in plane-strain by setting the axial displacement to zero. Therefore, the model was validated against 2D solutions obtained from the results presented in the previous section.

6.4. Stress sensitivity analysis

Similar to 2D analyses, 3D models were used to simulate the failure zone (i.e. yield zone) as observed in the experiments conducted on synthetic samples. To investigate the dimension of the failure zone, the width and depth of the failure zone were determined and the results are presented in Figure 9 and Figure 10.

Similar to 2D analysis the modified Drucker-Prager (with 0.8 flow stress ratio) showed the best correlation with the experimental results. The Mohr-Coulomb criterion yielded a large zone of failure whereas the Drcuker-Prager criterion resulted in a very small size for the breakout zone.

The impact of the lateral stress anisotropy is quite similar to the 2D analysis as is seen from Figure 9. As the state of stresses becomes less anisotropic, the failure width tends to spread around the entire borehole wall. Again, it is emphasized that the effect of intermediate stress on failure zone dimension cannot be studied had one used the TWC numerical model. The results of our study indicate the importance of the intermediate stress on the width of the breakouts.

However, Figure 10 shows that the lateral stress anisotropy has no effect on the depth of the failure zone for the conditions we studied. This may indicate that the extent of the depth of the failure zone might be mainly governed by the axial and maximum lateral stresses for a given material. However, this needs further investigations for other cases to reach a general conclusion.

7. CONCLUSION

The experiments conducted under true triaxial stress conditions in the TTSC were simulated by using ABAQUS program. The methodology to construct 2D and 3D models and comparison with the experimental results were discussed in detail.

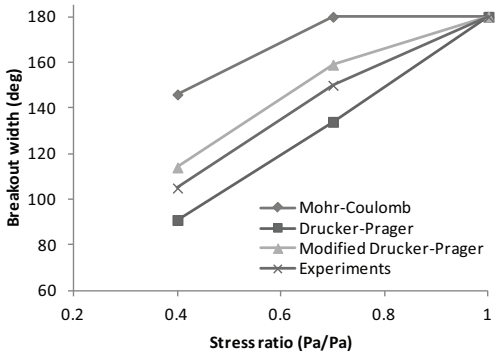

Fig. 9. The failure zone width as a function of stress anisotropy in 3D models.

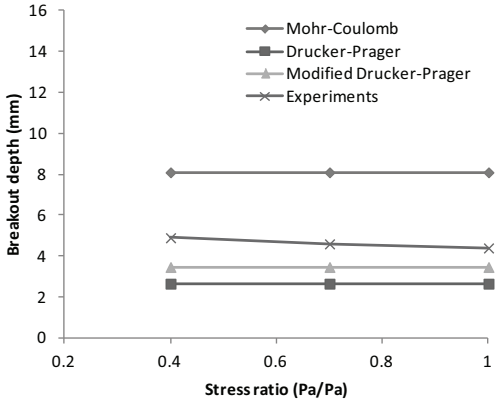

Figure 10. The failure zone depth as a function of stress anisotropy in 3D models.

The results of simulations in 2D and 3D were compared. It was shown that if the magnitude of the axial stress in 3D is relatively close to the magnitude of the out of plane stress in 2D (calculated from Hook's law) the results are reasonably similar to each other.

Using different failure criteria it was concluded that for the tested samples the modified Drucker-Prager with 0.8 flow stress ratio has the best correlation with experimental results.

The results also indicated that the lateral stress ratio has a significant impact on the width of failure zone (breakout), while the depth of the failure zone is mainly influenced by the maximum lateral stress and axial stress.

8. REFERENCES

1. Bratli, R.K., And Risnes, R., 1981 - Stability and failure of sand arches. SPE Journal, Vol. 21, No. 2, pp. 236-248, 8427-PA.
2. Perkins, T.K., And Weingarten, J.S., 1988 - Stability and failure of spherical cavities in unconsolidated sand and weakly consolidated rock. 63rd annual technical conference, Houston, Texas, SPE 18244.
3. Nouri, A., Vaziri, H., Belhaji, H., And Islam, R., 2004 - Sand production prediction: a new set of criteria for modeling based on large-scale transient experiments and numerical investigation. SPE annual technical conference and exhibition, Houston, Texas, SPE 90273.
4. Euripides Papamichos, Johan Tronvoll, Anne Skjærstein, Tor Erling Unander 2010 - 2010_Hole stability of Red Wildmoor sandstone under anisotropic stresses and sand production criterion, Journal of Petroleum Science and Engineering, 72 (2010) 78–92.
5. Vriezen, P.B., Spijker, A., And Van Der Vlis, A.C., 1975 - Erosion of perforation tunnels in gas wells. 50th annual fall meeting, Dallas, Texas, SPE 5661
6. Khodaverdian, M.F., Abou-Sayed, A.S., Ramos, R., Guo, Q., And Mclennan, J.D., 1998 - Laboratory simulation of liner loading and near-wellbore permeability variation in poorly consolidated sandstones. SPE/ISRM Eurock '98, Trondheim, Norway, SPE 47291.
7. Papamichos, E., Vardoulakis, I., Tronvoll, J., And Skjaerstein, A., 2001 - Volumetric sand production model and experiment. Int. J. Numer. Anal. Meth. Geomech., Vol. 25, pp. 789-808.
8. Younessi A., Rasouli V., Wu B. 2012- The effect of stress anisotropy in sanding: An experimental study, the 46th US Rock Mechanics / Geomechanics Symposium held in Chicago, IL, USA, 24-27 June 2012.
9. Risnes, R., Bratli, R.K., And Horsrud, P., 1982 – Sand stresses around a wellbore. SPE journal.
10. Younessi A., Rasouli V., Wu B. 2012- Proposing A Sample Preparation Procedure For Sanding Experiments, Southern Hemisphere International Rock Mechanics Symposium SHIRMS 2012
11. Rasouli, V., And Evans, B., 2010 - A true triaxial stress cell to simulate deep downhole drilling condition. APPEA journal 2010, 50th Anniversary Issue, pp. 61-70.
12. Sadd, M.H., 2010 - Elasticity: theory, applications, and numerics. Academy press.
13. Detournay, E., And Fairhurst, C., 1987 – Two-dimensional elastoplastic analysis of long, cylindrical cavity under non-hydrostatic loading. Int. J. Rock Mech. Min Sci. & Geomech. Abstr, Vol. 24, No. 4, pp. 197-211.

Paper 6 A fracture sliding potential index for wellbore stability analysis

International Journal of Rock Mechanics & Mining Sciences 47 (2010) 927–939

Contents lists available at ScienceDirect

International Journal of Rock Mechanics & Mining Sciences

journal homepage: www.elsevier.com/locate/ijrmms

A fracture sliding potential index for wellbore stability analysis

A. Younessi, V. Rasouli *

Department of Petroleum Engineering, Curtin University of Technology, ARRC Building, 26 Dick Perry Avenue, Kensington, Perth, WA 6151, Australia

ARTICLE INFO

Article history:
Received 2 August 2009
Received in revised form
12 February 2010
Accepted 31 May 2010
Available online 15 June 2010

Keywords:
Rock engineering system
Fracture sliding potential
Wellbore stability

ABSTRACT

Sliding failure along the fractures intersecting a wellbore is one of the major wellbore instability mechanisms. This kind of failure is similar to the slope instabilities, a well-known phenomenon in mining and civil engineering. During drilling operations the drilling fluid can penetrate through fractures and lead to fracture reactivation and wellbore instability. The rock engineering systems (RES), initially introduced in the mining- and civil-related geomechanics problems, is an approach to analyze the interrelationship between the parameters affecting rock engineering activities. In this study, after discussing the sliding mechanism along a fracture in a wellbore during drilling, and identifying all the effective parameters, an interaction matrix is introduced to study the sliding failure mechanism. Thereafter, the interaction intensity and dominance of each parameter in the system is determined to classify these parameters. A systematic approach was used to determine the relative interactive intensity and value of each contributing parameter in the fracture sliding mechanism. As a result, an index is presented to estimate the fracture sliding potential. The results indicate the ability of this method to analyse wellbore instability due to fracture reactivation mechanism. This will assist in finding a better engineering action to mitigate or eliminate potential fracture sliding during drilling. The results show a good agreement with those obtained using Mohr–Coulomb failure analysis and field observations.

1. Introduction

In the oil and gas industries, dealing with wellbore instability problems are both time consuming and costly. Different wellbore failures have been introduced and discussed in the literature [1], the most common ones being breakouts, induced fractures and fracture reactivation. Instabilities may occur in different modes of shear, tensile failure or sliding along the interface of weak planes [2]. A comprehensive knowledge of these failure mechanisms and the parameters triggering each failure mode helps in a proper design of the wellbore, drilling, completion and production program of the well. Sliding along a fracture plane is a common failure reported during drilling oil and gas wellbores. In this paper, a new approach is presented to understand sliding mechanism better and identify the interrelation between different parameters contributing in this failure to occur.

Rock engineering system (RES) is an engineering approach introduced to study the interrelationship between various parameters involved in an engineering project [3]. In this approach the main parameters are arranged along the diagonal elements of a matrix, a so-called interaction matrix, and the interrelations between pairs of parameters are identified in off-diagonal elements. Previously, the interaction matrix corresponding to wellbore stability has been developed in order to study different failure mechanisms [4]. In that study, the parameters affecting fracture reactivation in a wellbore were used to build the corresponding interaction matrix. The interaction matrix was quantified using an expert semi-quantitative (ESQ) coding system to allow the assessment of the amount of cause and effect of each parameter within the system to be made [3]. In addition, by plotting the parameters in the cause–effect diagram the interaction intensity and dominance of each principal parameter in the system was studied [5].

Fracture reactivation is a common failure in oil and gas wellbores, which may occur in three different stages during the life of a wellbore: fracture sliding during drilling operation [6], during production from the reservoir and later on as a result of injection into the reservoir [7]. It is important to note that the sliding initiation mechanisms are different in each of these scenarios [4]. Here, in this study, the sliding mechanism during drilling operation is studied using the RES approach where the conventional Mohr–Coulomb criteria will be applied to assess the shear strength of the fracture. Moreover, using the RES approach a fracture sliding potential index (FSPI) is proposed to evaluate the sliding potential of a fracture intersecting a wellbore during drilling operation. In over balance drilling the wellbore pressure is larger than reservoir pressure, which is similar to injecting into a reservoir. This suggests that the FSPI has the potential to be used for fracture reactivation analysis during fluid injection stage.

* Corresponding author.
E-mail address: v.rasouli@curtin.edu.au (V. Rasouli).

1365-1609/$ - see front matter Crown Copyright © 2010 Published by Elsevier Ltd. All rights reserved.
doi:10.1016/j.ijrmms.2010.05.014

2. Sliding mechanism along the fracture planes

Formation failure in the vicinity of the wellbore may have serious consequences on drilling operations [8]. Breakout, breakdown and fracture sliding are the most common failures observed around a wellbore. An optimised well engineering design should take the impact of these failure modes into account in order to ensure the integrity of the well to be maintained during long term production period [9].

A wellbore drilled to get access to the reservoir formation, which is usually few hundreds to few thousands meters below the surface, intersects different formations, rock masses and also discontinuities at various scales (from faults at large scale to bedding planes at small scale). These planes of weakness have the potential to slide as soon as a drilled wellbore intersects them.

Fracture sliding initiates as the induced shear stress applied on a given plane inside the rock mass exceeds the shear strength along that plane. Formations are usually inhomogeneous and anisotropic; hence sliding tends to take place along the weakest plane within the rock mass, i.e. a fracture plane if any exists. If the rock mass contains no discontinuity plane, large stress magnitudes may create fractures along the weak planes within the rock mass.

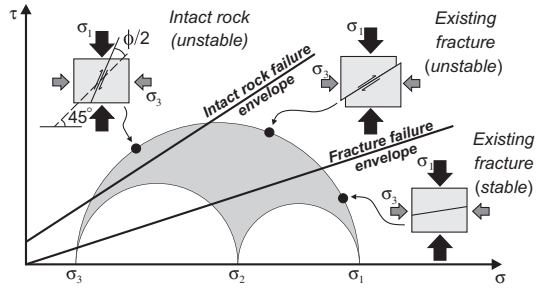

Fig. 1. The state of stress is demonstrated by Mohr's circle. The envelopes are the boundaries between the stable and unstable conditions [10].

Earthquakes and faults movement are events that can induce large stresses enough to exceed the intact rock strength [7].

The Mohr–Coulomb criterion is the most conventional sliding failure envelope used in geomechanics (Fig. 1) and is written in the form of

$$\tau = C_d + \sigma'_n \tan \phi_d \quad (1)$$

where τ and σ'_n are the shear and effective normal stresses (MPa) applied on a discontinuity plane with cohesion C_d (MPa) and friction angle ϕ_d (deg).

Fracture reactivation may occur in three different stages during the life of a wellbore: fracture sliding during drilling operation, sliding during production phase due to reservoir depletion, and sliding during fluid injection (e.g. waste disposal applications, enhance recovery such as water flooding and fracture stimulation). Sliding occurs in each of these cases with a different mechanism, although the sliding term is used commonly in all cases [4]. In this study, using the interaction matrix associated with Mohr–Coulomb criteria the sliding mechanisms correspondent to drilling operation is studied.

The initiation failure mechanism during drilling operation is rather simple and its concept is well known in rock mechanics (e.g. in slope stability analysis). If the drilling fluid invades into the formation due to no (or very thin) mud cake, then fluid will penetrate through the existing fractures and increase the pressure along the plane of fracture [6]. This results in the effective stress applied normal to the fracture plane to decrease. According to the Mohr–Coulomb criterion the new state of stress may exceed the fracture shear strength and cause sliding of fracture plane as depicted in Fig. 2.

This type of failure is very common in drilling oil and gas wellbores, in particular in naturally fractured formations. The early impact of sliding failure could be tight hole-related problems, e.g. over torque and over pull forces, which is observed during running in hole (RIH) and pooling out of hole (POOH). This problem can be cured by reaming and back reaming of the tight hole interval. The later problems associated with sliding failure are more serious and include pipe stuck, drillstring collapse and difficulties in running the casings. These problems cannot be

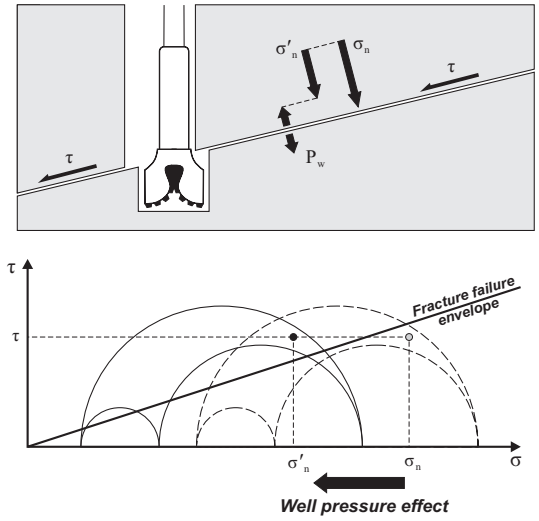

Fig. 2. Fracture plane shearing due to the invasion of drilling mud and reduction in normal stress.

mitigated by conventional methods such as increasing the mud weight, as this could cause further problems in this situation [6].

3. Rock engineering systems

The parameters and variables involved in a rock engineering project may have a certain effect on other parameters and the whole system and, inversely, may be affected by other parameters to a certain extent. This shows the need for studying the interrelationship between different parameters within a rock engineering project and to understand the way they interact with each other within the system. Rock engineering systems (RES), introduced by Hudson [3], is a methodology which allows studying the interrelationship of parameters involved in a rock engineering design and construction. In this study the RES was used to evaluate and analyse the sliding mechanism along a fracture plane during drilling a wellbore.

The first step in this study is to determine the parameters which encounter in a fracture sliding analysis. We start with a simple case by firstly introducing three main parameters: fracture properties, stresses and engineering activities.

The first two parameters are rock mechanical parameters, which will be turned into a rock engineering concept of fracture sliding analysis when their interaction with the third parameter (i.e. the engineering activities which is drilling the wellbore in this case) is taken into account simultaneously. Interactions between these parameters as depicted in Fig. 3 are listed as follows:

1. *Interaction 1 (fracture properties/in situ stress)*: Fractures change the distribution of stress.
2. *Interaction 2 (fracture properties/engineering activities)*: Drilling fluid is invaded into the fracture plane.
3. *Interaction 3 (in situ stress/fracture properties)*: High stresses can induce fractures.
4. *Interaction 4 (in situ stress/engineering activities)*: Pore pressure and minimum in situ stress delineate the safe mud weight window.
5. *Interaction 5 (Engineering activities/fracture properties)*: High fluid pressure can reactivate fractures.
6. *Interaction 6 (Engineering activities/in situ stress)*: State of stress is changed around the wellbore.

A useful way of representing the interaction between these parameters is to arrange them in a square matrix form known as the Hudson Interaction Matrix. In this case the interaction matrix is a 3×3 matrix as shown in Fig. 4. In this matrix the main parameters are arranged along the diagonal elements with their interactions shown in off-diagonal elements. The importance of parameters used in this study is discussed below.

3.1. Fracture properties

Undertaking a fracture sliding analysis requires a good knowledge of the physical and mechanical properties of the fracture plane. Fracture dip and dip direction, surface roughness and aperture are perhaps important properties to be considered and briefly discussed here.

3.1.1. Dip and dip direction

Any plane in space is represented by two attributes, dip and dip direction. The orientation of a fracture plane with respect to the direction of the principal stresses determines the magnitude of induced stresses acting onto the plane [11]. Using any failure

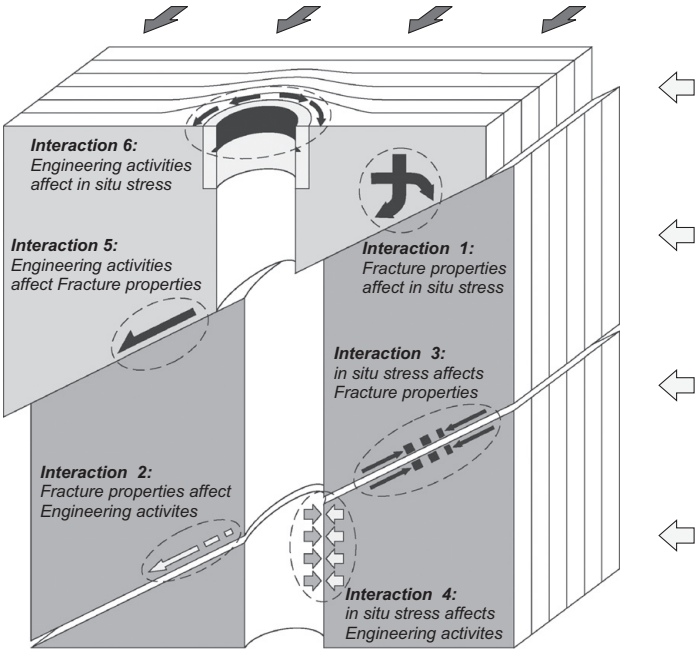

Fig. 3. Interactions between three main parameters involved in a fracture sliding analysis.

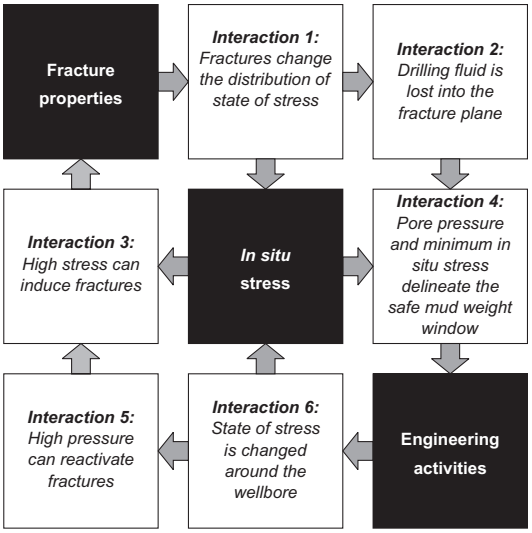

Fig. 4. Interactions between fracture properties, in situ stresses and engineering activities illustrated in an interaction matrix form.

criterion, such as Mohr–Coulomb, the critical shear stress that initiates the failure on a weak plane can be estimated [12] and the critical oriented fractures can be identified in any state of stress.

3.1.2. Roughness

Surface roughness could have a significant influence on the mechanical properties of the fractures. In general, the shear strength of a fracture increases as the fracture morphology becomes rougher. Therefore, a direct correlation is expected to exist between surface roughness and sliding potential of a fractured surface: the rougher the fracture surface, the lower the sliding potential due to stress changes along the surface of the fracture. It should be noted that the effect of surface roughness becomes negligible at high normal stress levels as the asperities are degraded in this situation [13].

3.1.3. Aperture

In general, fractures with larger apertures (or openings) are less stable in shear mode, which is partly due to the lesser effect of roughness. If the aperture is more than the maximum height of the roughness, the fracture behavior will be directed by the properties of the filling material. In this situation, at small displacements the shear strength is mainly governed by the properties of the filling material, whereas at larger shear displacements the impact of roughness is dominant [14].

3.2. In situ stress

Perhaps stress concentration and relaxation could be considered as one of the main causes of fracture sliding. As the stress concentration or relaxation exceeds the shear fracture strength the failure initiates and sliding occurs along the fracture plane. Regardless of the state of stress, considering the porous structure and the fluid inside this porous media, the total stress is applied to the rock matrix and the pore fluids.

3.2.1. Effective stress

This is part of the total stress which is applied to the matrix and grains of the formation. The state of stress in a field can be defined by knowing the direction and magnitude of the principal effective stresses [15]. One of the principal stresses is usually assumed to be vertical whereas the other two are horizontal [16], i.e. the maximum and minimum horizontal stresses. The vertical effective stress is due to the weight of the overburden layers, and the horizontal effective stresses are induced from the lateral strain of the formations and from tectonic effects.

3.2.2. Pore pressure

This is part of the total stress which is taken by the fluid inside pores. Generally in shallow depths, as long as the pores or fractures are permeable and interconnected up to the surface, the pore pressure at any point is the hydrostatic pressure of the water column above that point. However, at larger depth the situation may be different and some zones could be over or under pressured.

3.3. Engineering activities

Parameters considered under this category include those related to constructions that disturb the stress balance in the field. These parameters can be divided into three classes of drilling-, production- and injection-related parameters in the context of petroleum engineering applications. However, in this paper the drilling-related parameters were studied.

Amongst drilling-related parameters, perhaps drilling fluid is the most important parameter affecting the stresses. Aside from wellbore trajectory (which is often constrained by logistical factors), drilling fluid properties are the only variables in drilling which could be changed whereas stresses and rock properties are intrinsic properties of the field and formations.

3.3.1. Drilling fluid

It influences the instability of a wellbore mechanically or chemically. The mud weight should be kept within a certain window to ensure stability: it must be greater than pore pressure gradient to avoid kick and shear failures known as breakouts and it must be less than formation fracture gradient to avoid mud loss into the formation and eventually tensile failure of the formation. A high mud weight can also reactivate the existing natural open fractures by invading drilling fluid into the fractures and cause severe problem during drilling operation. On the other hand, the chemical interaction between the mud and formation could cause instabilities in shaly zones [8].

4. The interaction matrix and coding system

To fully understand the overall reaction of an engineering system, the interrelationship between various parameters needs to be taken into consideration. Each parameter can affect the system and also be affected by the system to a certain extent. The interaction matrix developed by Hudson allows studying the interrelationship between different parameters within a RES. The interaction matrix is a square matrix. The main parameters are arranged along the diagonal elements of the matrix whereas the off-diagonal elements are filled with quantitative numbers representing the amount of interaction between each pairs of parameters. The interactions are to be read clockwise, as they could be path dependent. Also the matrix is usually asymmetric.

Dip & dip direction	*Roughness is different in different direction* [16]	*No interaction in fracture sliding*	*Stress orientations and magnitudes are perturbed by presence of a fracture* [17]	*No interaction in fracture sliding*	*No interaction in fracture sliding*
No interaction in fracture sliding	**Roughness**	*Fracture aperture depends upon roughness* [18, 19]	*No interaction in fracture sliding*	*No interaction in fracture sliding*	*Rough fractures yield lower fluid loss rates* [20]
No interaction in fracture sliding	*The effect of roughness faded in fractures with larger aperture* [14]	**Aperture**	*No interaction in fracture sliding*	*No interaction in fracture sliding*	*Mud loss is higher in fracture with larger aperture* [21]
Fracture orientation affected by principal stress directions [3]	*Fracture roughness generally decreases in higher normal stresses* [22]	*Fracture aperture decreases as the effective normal stress increases* [23]	**Effective stress**	*Elevated in situ stress due to tectonic can lead to over-pressure* [24]	*No interaction in fracture sliding*
No interaction in fracture sliding	*No interaction in fracture sliding*	*Elevated pore pressure increases fracture aperture* [3]	*Effective stress reduced by increasing pore pressure* [3]	**Pore pressure**	*Higher mud weight is used for higher pore pressure* [26]
No interaction in fracture sliding	*Fracture roughness may reduce due to mechanical erosion of fluid flow* [25]	*Higher fluid pressure increases fracture aperture* [3]	*Drilling fluid changes the state of stress around th borehole* [26]	*Invaded fluid increases the fluid pressure inside fracture* [27]	**Drilling fluid**

Fig. 5. FSP interaction matrix developed for this study. Numbers shown are references that support the stated interaction.

Fig. 5 shows the interaction matrix constructed for the six parameters involved in the analysis of fracture sliding potential (FSP) corresponding to the case explained in the previous section. This is a 6×6 matrix, where the main parameters are located along the diagonal elements. The interaction between each two parameters is described qualitatively in the corresponding off-diagonal element (this element results from the intersection of a horizontal and a vertical line passing through the first and second parameters, respectively). The off-diagonal elements were quantified later on, using coding systems to allow the assessment of the amount of cause and effect of each parameter within the system to be made. In this way, the sum of each row passing through a parameter indicates the total influence of the parameter on the system (cause) whereas each column (passing through the parameter) describes the influence of the system on the parameter (effect).

For the purpose of the present work, an expert semi-quantitative (ESQ) coding system was adopted. In this coding system the interaction between each two parameters is quantified using numbers between zero (no interaction) and four (critical interaction). Coding numbers of 1, 2 and 3 show weak, medium and strong interactions, respectively. Fig. 6 shows the results of coding the interaction matrix corresponding to Fig. 5 using the ESQ coding system. As can be recognized, matrix coding is not an easy process. In this study the matrix coding was carried out mainly based on the information obtained from previous studies [16–26], analytical formulas and the authors experiences. However, the coding numbers can be moderated to suit best for a specific project based on the available information from the off-set wells (e.g. structural geology reports, drilling reports) and past experiences from similar fields.

Cause

Effect							
	DD	2	0	3	0	0	5
	0	***Rgh***	2	0	0	1	3
	0	2	***Apr***	0	0	3	5
	3	3	3	***ES***	2	0	11
	0	0	3	4	***PP***	2	4
	0	2	3	3	4	***DF***	12
	3	9	11	10	6	6	

DD-Dip & dip direction ***ES***-*Effective* stress
Rgh-Roughness ***PP***-Pore pressure
Apr-Aperture ***DF***-Drilling fluid

Fig. 6. Semi-quantitative coding of the FSP interaction matrix.

5. Cause–effect diagram and histogram of interactive intensity

The cause value (total influence of the parameter on the system) is obtained as the sum of the off-diagonal rows corresponding to the given parameter. Similarly, the effect value (total influence of system or other parameters on a certain parameter) is the sum of off-diagonal columns corresponding to the given parameter. The cause and effect values corresponding to each parameter can be represented as a point in a cause–effect

coordinate system. This is shown in Fig. 7 for the FSP interaction matrix discussed earlier. Note that in this space the diagonal of the diagram is the locus of $C=E$. Along this diagonal and as we move away from the centre of the coordinate system, the summation of cause and effect ($C+E$) increases. The lines of equal interaction intensity (i.e. $C+E$ values) can be plotted on the diagram allowing discrimination between 'less interactive' and 'more interactive' parameters. The parameters located in the bottom right portion of the diagram are 'dominant' in the system, as they have increasing $C-E$ values as we move further away from the diagonal line. In a similar manner, the 'subordinate' parameters are defined as those which are highly dominated by the system and are located in the top left corner of the diagram. These parameters will have decreasing $C-E$ values (taking the sign into account) moving away from the diagonal line.

The cause–effect plot is a helpful tool in understanding the behavior of each parameter individually as well as studying the whole system. For example, the points tend to distribute perpendicularly to the $C=E$ diagonal show low level of interactivity between parameters, whereas a high interactivity will result in the points being distributed along the main diagonal line [5]. In Fig. 7, it can be seen that the effective stress has the most interaction in the system, whereas dip and dip direction show the least interaction within the system. The diagram also shows that drilling fluid has the most impact on the system, i.e. the whole system is more sensitive to drilling fluid changes than other parameters. In practical sense this is very beneficial, as the most readily controlled parameter during drilling operations is the mud weight and as such by choosing the right mud density FSP could be mitigated or minimized.

The sum of the cause and effect percentage ($C+E\%$) corresponding to each parameter describes the relative interactive intensity (RII) of that parameter in the system. In Fig. 8, the histogram of RII corresponding to parameters considered in FSP

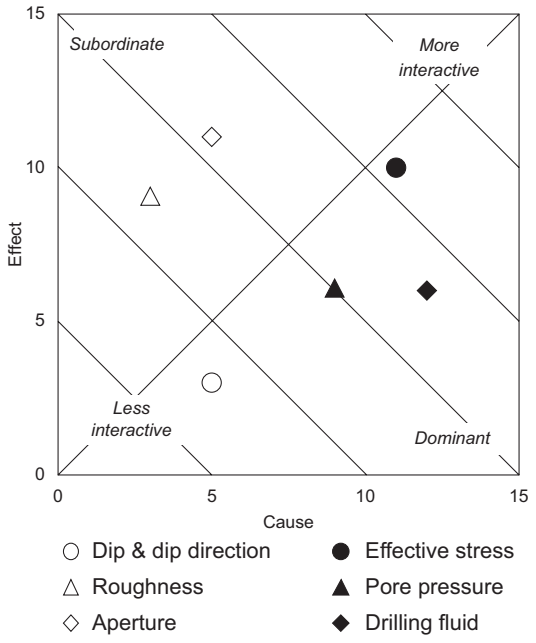

Fig. 7. Cause–effect diagram corresponding to parameters involved in FSP study.

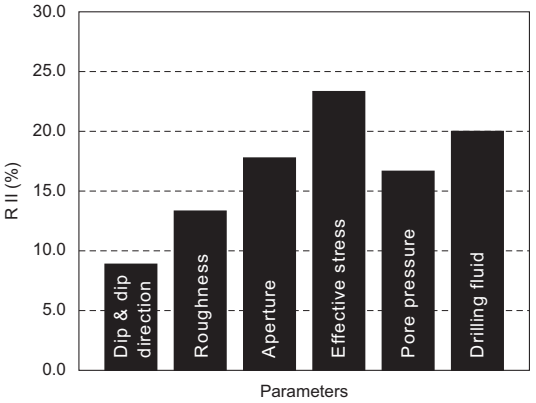

Fig. 8. Histogram of interactive intensity corresponding to parameters involved in FSP study.

analysis is shown. The interaction of each individual parameter is high enough to contribute in fracture sliding to occur. As a result, all the selected parameters will be used in FSP analysis. The RII will be used to incorporate the contribution, or weight, of each parameter in the FSP study.

6. Developing the 'pull-down menus' for FSP

In order to assess the sliding tendency of a fracture plane we need to multiply the RII corresponding to each parameter by corresponding value (Ω) of that parameter and then add these values. RII can be easily obtained through the process explained in the previous section. However, as the dimension of each parameter is different from others, the value of individual parameters cannot be used directly as an input to the analysis. Furthermore, the value Ω for those parameters which is expressed qualitatively in the literature needs to be quantified. To do so, we implemented a semi-quantitative approach to identify Ω corresponding to each of six parameters involved in the FSP analysis. In this approach the parameters are rated as 0 for "low contribution", 1 for "contributory" and 2 for "strong contribution". The following sections explain how Ω is determined for each of six parameters.

6.1. Fracture dip and dip direction

In order to establish a quantitative base methodology to obtain Ω corresponding to dip and dip direction of a fracture, in this work, an extensive sensitivity analysis was carried out on number of fracture sets with different dip and dip directions. The poles of 621 fractures used for this analysis plotted on the hemispherical projection shown in Fig. 9 (bottom). As is seen from this figure, the data are distributed uniformly. Performing range of sensitivity analysis on each fracture plane while changing the magnitude of the three principal stresses, it would be possible to identify potentially unstable fracture planes. This was simply done using Mohr–Coulomb criteria; the planes above the line of fracture shear strength are unstable, as shown in Fig. 9 (top). In this figure, for simplicity, the normalized values of shear and normal stresses are plotted. It should be noted that in Fig. 9 (bottom) the azimuthal dip direction of a plane is measured with respect to the minimum horizontal stress direction (not from North, as is a

common practice). This is to consider the effect of the horizontal stresses direction, which is one of the key parameters in the FSP analysis.

Using this approach the failure probability of fractures under three stress regimes of normal, reverse and strike-slip was calculated and based on the results five zones with different probability for sliding were identified. This is shown in Fig. 10 from which it is clear that the critical fracture sliding direction changes depending on the given stress regime. These probability zones were used to take into account the effect of fracture dip/dip direction in the FSP analysis.

6.2. Roughness

In the conventional rock classification systems, the conditions of fracture surfaces are described by three main parameters of roughness, separation and weathering [27]. These classifications are originally developed for the applications in civil and mining engineering, which are generally representing shallow depth environments. The majority of instabilities occurred along the fracture planes intersecting a wellbore in petroleum applications are located hundreds of meters below the surface. At this depth the weathering effect can be neglected due to the considerable difference between the surface and deep underground conditions. Similar to other rock mass classification systems roughness could be classified as smooth, slightly rough and rough with semi-quantitative coding values of 0, 1 and 2 to be used to quantify roughness, respectively. The effect of aperture is considered as a separate parameter below.

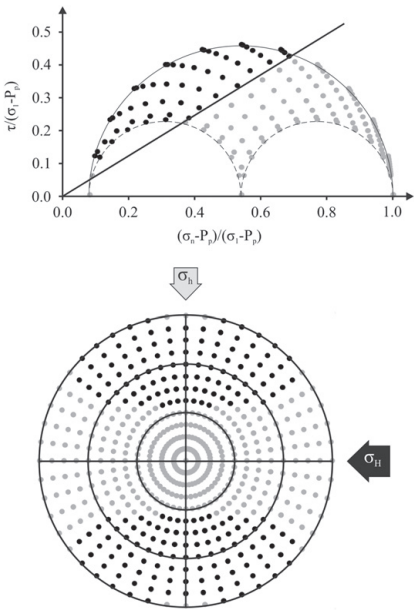

Fig. 9. The hemispherical projection corresponding to 621 fracture planes (left) and the corresponding plot of Mohr's circle (right).

6.3. Aperture

Aperture or opening is the distance between the two walls of a fracture. Measuring the aperture of a fracture is rather a simple practice when the fracture is visible such as fractures exposed to the tunnel wall or intersecting rock slopes. Core samples could be used to obtain some information about the fractures underground. Core sampling in oil and gas wells, where the reservoir formations are located few hundreds of meters below the surface, is not always economical. Instead, image logs are useful sources which could be used in order to retrieve the geometrical properties of the fractures. In Fig. 11 seven examples of image logs acquired using ultrasonic borehole imager (UBI) tool are shown using which some geometrical properties of fractures downhole have been retrieved. In specific, aperture is conventionally classified as "closed", "partially closed" and "open" [28] and thus corresponding semi-quantitative coding values for aperture used in this study are 0, 1 and 2, respectively.

6.4. In situ stresses

The state of stress is identified by determining the magnitude and direction of the three principal stresses σ_1, σ_2 and σ_3. In Section 6.1 the effect of stress orientation was considered by referencing fracture azimuth with respect to the minimum horizontal stress direction. Performing a sensitivity analysis on the magnitude of the three principal stresses the impact of various combinations of stress magnitudes on FSP analysis for fractures shown in Fig. 9 was studied. This allowed assigning an appropriate Ω to this parameter for each fracture plane. For the sake of simplicity, σ_2 and σ_3 are normalized against σ_1 to reduce the number of variables from three to two. The sensitivity analysis was then conducted on non-dimensioned parameters σ_2/σ_1 and σ_3/σ_1 and the results are shown in Fig. 12.

The results show that by decreasing the value of σ_3/σ_1 the sliding potential along the fracture planes increases. The closer value of σ_3/σ_1 to 1 represents more isotropic stress regime and lesser potential for the sliding to occur along the fracture plane, or

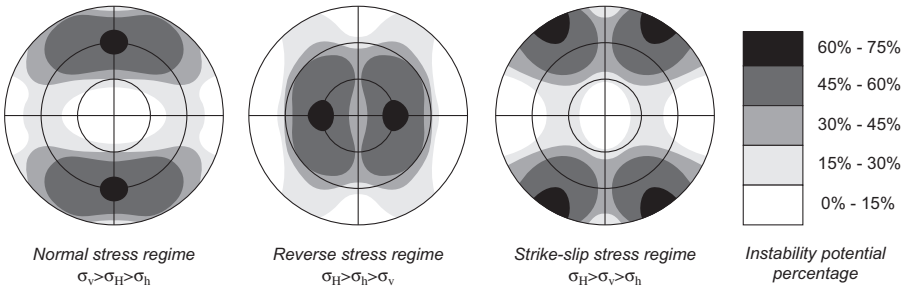

Fig. 10. The effect of fracture dip and dip direction in FSP analysis.

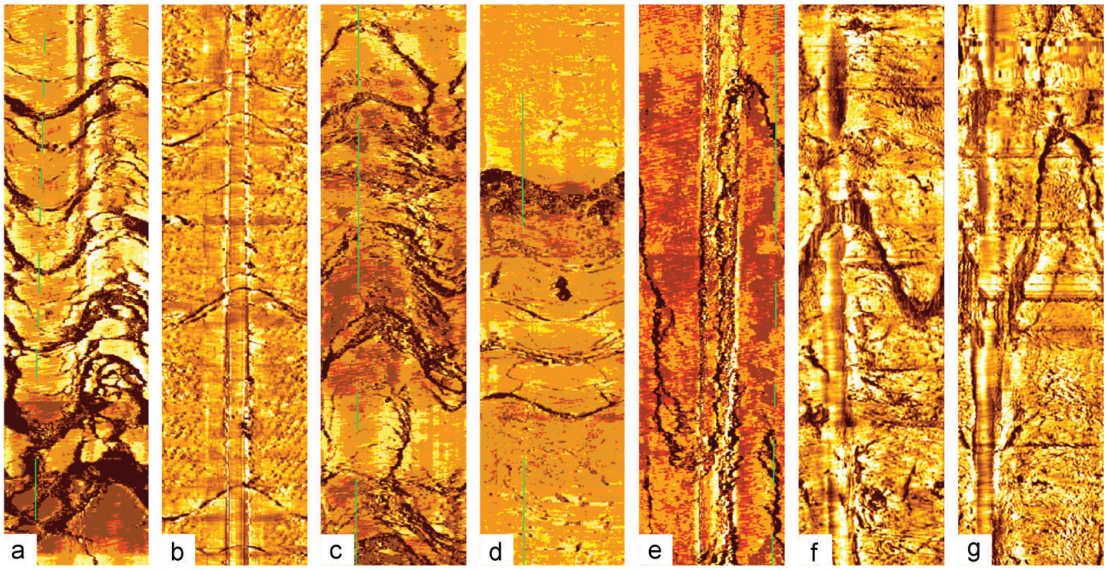

Fig. 11. Examples of fractures detected by UBI; (a) the aperture varied from closed to open from top to bottom, (b) a set of closed fractures, (c) a set of open and rough fractures, (d) partially closed fractures, (e) a high angle rough fracture, (f) an open smooth fracture and (g) open and slightly rough fracture. Dark colors represent low amplitude ultrasonic reflections (indicative of fracturing).

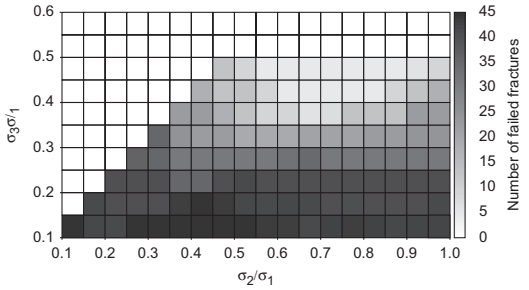

Fig. 12. The impact of magnitude of in situ stresses on FSP.

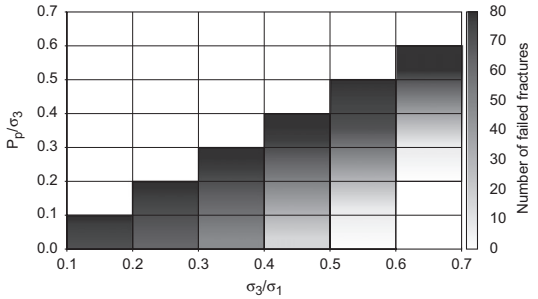

Fig. 13. The effect of pore pressure on FSP.

more stable condition. From Fig. 12, it is also seen that the sliding potential of a fracture is less sensitive to σ_2/σ_1 than σ_3/σ_1, which shows lesser importance of intermediate stress in the FSP analysis, as expected from Mohr–Coulomb criteria too. Therefore, the sensitivity of fracture reactivation to intermediate stress is negligible and, hence, was ignored to simplify the analysis. Accordingly, the Ω corresponding to the stress magnitude is chosen as 0, 1, and 2 for the values of σ_3/σ_1 being greater than 0.5, between 0.5 and 0.3 and less than 0.3, respectively.

6.5. Pore pressure

Pore pressure has the same dimension as the stress, and therefore here, with the same analogy to in situ stresses, the ratio of pore pressure over the minimum stress (P_p/σ_3) was used to investigate the pore pressure effect on FSP. It is worthwhile mentioning that both pore pressure and minimum horizontal stress magnitudes increase with depth and that the ratio of P_p/σ_3 would be independent from depth.

Fig. 13 illustrates the results of the sensitivity analysis of P_p/σ_3 ratio on FSP for 621 studied fracture sets. From this figure it is seen that the FSP increase as P_p/σ_3 ratio becomes larger. Theoretically, an increase in pore pressure reduces the effective stresses and shifts the Mohr's circle to the left, closer to the failure envelope, i.e. higher sliding potential along the fracture surface. Based on the results of Fig. 13, Ω corresponding to pore pressure is chosen as 0, 1, and 2 for the values of P_p/σ_3 being less than 0.3, between 0.3 and 0.6 and greater than 0.6, respectively.

6.6. Drilling fluid

In this study, only the mechanical effect of drilling fluid was considered in studying the FSP. During drilling operation the

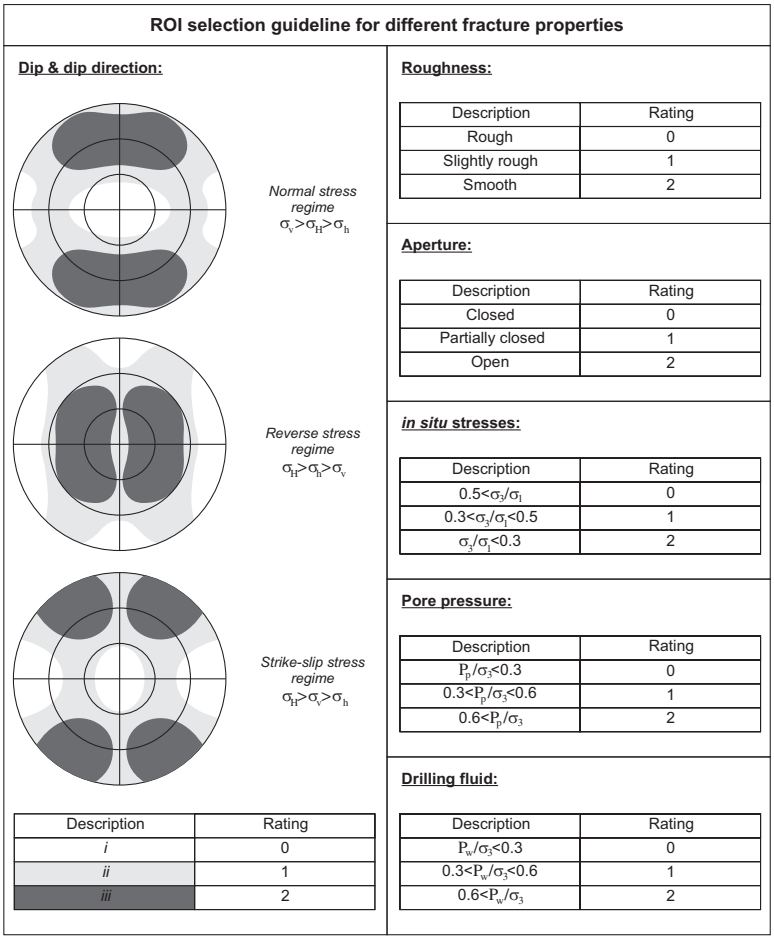

Fig. 14. 'Pull-down menus' for FSP analysis.

drilling mud invades into the open fractures and reduces the magnitude of the normal stress applied perpendicular to the plane of fracture and consequently may lead to fracture reactivation to take place. This is similar to the effect of elevated pore pressure (discussed in Section 2) which moves the Mohr circle to the left closer to the sliding envelop. Therefore, similar to pore pressure the value of Ω corresponding to the drilling fluid is 0, 1, and 2 for the values of P_w/σ_3 being less than 0.3, between 0.3 and 0.6 and greater than 0.6, respectively.

7. Fracture sliding potential index (FSPI)

Fig. 14 summarizes the values of Ω corresponding to the parameters discussed in the previous section which will be used to analyse the fracture sliding potential (FSP). In Table 1, maximum Ω, RII and scaled relative interactive intensity (SRII) of each parameter are listed. As the maximum Ω for these parameters were 2, it was decided to use a scaled relative interactive intensity (SRII) parameter equal to half of RII as given in the last column of Table 1.

Table 1
Maximum Ω and RII corresponding to each parameter.

	Maximum Ω	**II** $C+E$	**RII** $C+E\%$	**SRII** $(C+E\%)/2$
Dip and dip direction	2	8	8.89	4.44
Roughness	2	12	13.33	6.67
Aperture	2	16	17.78	8.89
In situ stresses	2	21	23.33	11.67
Pore pressure	2	15	16.67	8.33
Drilling fluid	2	18	20.00	10.00
Total	**12**	**90**	**100.00**	**50.00**

The fracture sliding potential index (FSPI) can be expressed as

$$FSPI = \sum_{i=1}^{n} SRII_i \times \Omega_i \quad (2)$$

where n is the number of the parameters. Larger values for FSPI indicate higher potential for the fracture to slide. In order to establish a classification scheme for the FSP, by which the sliding

potential of the fracture could be estimated, FSPI was used to assess the stability of a wide range of systematically generated individual fractures with different properties at different state of stresses. The sliding potential for each fracture was also assessed using commonly used Mohr–Coulomb criteria. In general a good agreement is seen between the results of both methods; however, it is clear that the new approach is more advantageous in terms of being able to take into account a wider range of input data which can be interchangeably used in the analysis. As an example of the above analysis, in Appendix A, 20 of these fractures are shown to compare the results of the FSPI and Mohr–Coulomb analysis.

According to these results Table 2 is proposed as a general guideline to estimate the probability of fracture sliding based on its calculated FSPI values. As it is seen three classes of I, II and III are proposed with corresponding FSPI values of less than 30, between 30 and 60 and greater than 60. These classes refer to "stable", "nearly stable" and "unstable" fractures, respectively. The definition for each class is also provided in the last column of Table 2.

In terms of practical applications, it is important to identify the sliding potential for any existing fracture after being intersected by a drilled wellbore. The FSPI value is an index which shows this possibility. Consequently, the drilling program may need justification in order to mitigate or minimize this effect as it could cause mud loss through the fracture plane. As the mud property is the only controllable variable, the driller may choose to change the drilling fluid weight or add lost circulation material (LCM) to mud for drilling across the interval where any fracture plane exists. In worse scenario the driller may have to complete drilling the current interval and set the casing immediately.

8. Case study

In this section, the proposed methodology will be applied to analyse the FSP during drilling operation in an oilfield. The formation is a Carbonate rock and the fracture properties as interpreted from UBI image are shown in Table 3. Using conventional log-based approach, as adopted in oil and gas industries, the magnitude of three principal stresses as well as pore pressure were estimated (explaining this workflow is out of the scope of this paper and is not the objective of this study). The orientation of minimum and maximum horizontal stresses was also estimated from the image logs. These results are summarized in Table 4. The real wellbore pressure which was used in drilling the section of interest is 45 MPa. A reverse fault stress regime is expected from the order of magnitude of principal stresses.

Using given information in Tables 3 and 4, the FSPI value corresponding to the existing fracture was calculated. The details of calculating the RII and Ω values corresponding to each

Table 2
Fracture sliding estimation based on FSPI value calculated for a fracture.

Fracture sliding potential index (FSPI)	Class	Sliding probability	Definition
FSPI < 30	I	Stable	The fracture is stable and is not likely interfere with drilling operations
30 < FSPI < 60	II	Nearly stable	The fracture may become reactivated due to unfavourable drilling practices. Caution is required while intersecting fracture
60 < FSPI	III	Unstable	The fracture is unstable and it is highly recommended to modify well planning to avoid intersecting the fracture if possible

Table 3
Fracture properties required for FSP analysis.

Dip (deg)	Dip direction (deg)	Friction angle (deg)	Cohesion (MPa)	Roughness (dimensionless)	Aperture (dimensionless)
25	45	23	0	Smooth	Partially closed

Table 4
Stresses and pore pressure data calculated for FSP analysis.

Vertical stress (MPa)	Maximum horizontal stress (MPa)	Minimum horizontal stress (MPa)	Minimum horizontal stress direction (deg)	Pore pressure (MPa)	Wellbore pressure (MPa)
60.4	91.1	69.7	150	44.8	45

Table 5
Pull-down menus calculated for FSP analysis.

	Dip and dip direction	Roughness	Aperture	In situ stresses	Pore pressure	Wellbore pressure	FSPI
Description	*iii*	Smooth	Partially closed	$\sigma_3/\sigma_1=0.66$	$P_p/\sigma_3=0.74$	$P_w/\sigma_3=0.74$	
Ω	2	2	1	0	2	2	
SRII	4.44	6.67	8.89	11.67	8.33	10.00	
SRII × Ω	**8.89**	**13.33**	**8.89**	**0**	**16.67**	**20.00**	**68**

parameter are given in Table 5. Based on this table the FSPI value calculated for this fracture is 68, which lies in class III of Table 2, i.e. the fracture tends to be unstable and slide.

Fig. 15 shows the results of shear strength analysis of the fracture which clearly confirms the results obtained using FSP approach, as the fracture plane in above the fracture failure envelope, i.e. failure region. The observations from image logs also

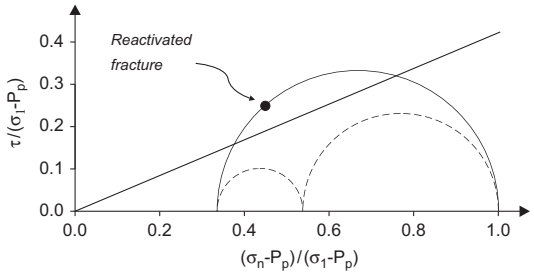

Fig. 15. Mohr–Coulomb analysis indicates that the fracture is unstable.

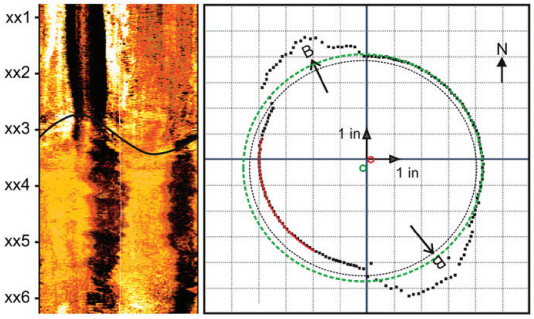

Fig. 16. The UBI image log and the cross-section of the wellbore indicates that the fracture becomes unstable when is intersected by the wellbore wall.

are in agreement with this result. The cross-section of the UBI image log, as shown in Fig. 16, confirms that the fracture slides towards the wellbore and is unstable.

The results of this analysis could be used as a predictive sliding potential guide in drilling nearby wells which intersect the same fracture plane. During drilling a new well, the interaction matrix can be modified using data obtained real time to calculate a more accurate FSPI. This enables the driller to adjust and modify the drilling program and mud design for the depth interval where the fracture plane exists.

9. Conclusions

In this paper a new approach based on the rock engineering systems (RES) was developed in order to analyse the sliding potential of a fracture which intersects a wellbore during drilling operation.

Did and dip direction, roughness and aperture of the fracture as well as the effective induced stresses, pore pressure and drilling mud density were found to be the six parameters which play the major role in controlling fracture sliding potential. The interaction matrix corresponding to these parameters were constructed. The cause–effect diagram indicated that the effective stresses have the most significant influence on sliding potential. It also showed that drilling fluid is the dominant parameter in the system, which is a fortunate coincidence as it is the only parameter that typically in a practical sense can be controlled during drilling.

The scaled relative interactive intensity (SRII) together with the value (Ω) associated with each parameter were used to develop a fracture sliding potential index (FSPI). FSPI ranges between 0 and 100; FSPI < 30 indicates stable fracture, 30 < FSPI < 60 corresponds to a nearly stable fracture and FSPI > 60 refers to an unstable fracture.

RII was determined using an expert semi-quantitative (ESQ) coding system in this work. However, this could be more accurately determined employing different expert system approaches such as neural network, fuzzy logic or intelligent systems, or a combination of these methods.

In comparison to Mohr–Coulomb approach wider range of input data can be interchangeably used in the FSPI method. This method

Table A1
Input data used for FSP analyses of 20 selective fractures.

	Dip (deg)	Dip direction (deg)	Friction angle (deg)	Cohesion (MPa)	Roughness (dimensionless)	Aperture (dimensionless)	σ_V (MPa)	σ_H (MPa)	σ_h (MPa)	σ_h direction (deg)	Pore pressure (MPa)	Wellbore pressure (MPa)	FSPI
1	12	100	23	0	Rough	Open	76	63	54	12	24	25	32
2	46	43	27	0	Slight rgh.	Open	54	76	49	37	37	37	48
3	24	27	26	0	Smooth	Closed	98	26	23	123	10	10	48
4	78	80	25	0	Smooth	Part clos.	62	64	49	30	12	12	20
5	15	58	20	0	Rough	Part clos.	46	74	23	56	9	9.5	52
6	65	67	30	0	Rough	Closed	75	57	44	82	10	11	9
7	36	176	21	0	Slight rgh.	Open	57	36	23	10	7	7.2	70
8	27	29	25	0	Smooth	Open	89	96	41	79	26	26.1	64
9	34	41	25	0	Rough	Part clos.	92	45	31	1	23	23	77
10	5	92	20	0	Slight rgh.	Closed	38	28	27	127	7	7.9	13
11	71	45	30	0	Rough	Part clos.	85	63	50	171	34	36	50
12	59	31	20	0	Smooth	Closed	41	47	41	63	12	12	22
13	29	107	28	0	Slight rgh.	Open	47	80	55	79	25	27	43
14	83	139	23	0	Slight rgh.	Part clos.	86	79	25	81	9	11	68
15	41	156	22	0	Smooth	Part clos.	90	80	33	24	17	17.2	57
16	76	112	21	0	Smooth	Open	100	21	20	53	11	11.9	87
17	50	43	27	0	Rough	Closed	73	54	36	69	15	15	46
18	45	76	24	0	Slight rgh.	Closed	26	57	33	152	20	21	64
19	21	82	22	0	Smooth	Part clos.	48	88	30	176	21	26	71
20	10	91	20	0	Rough	Open	42	91	24	34	17	18.5	91

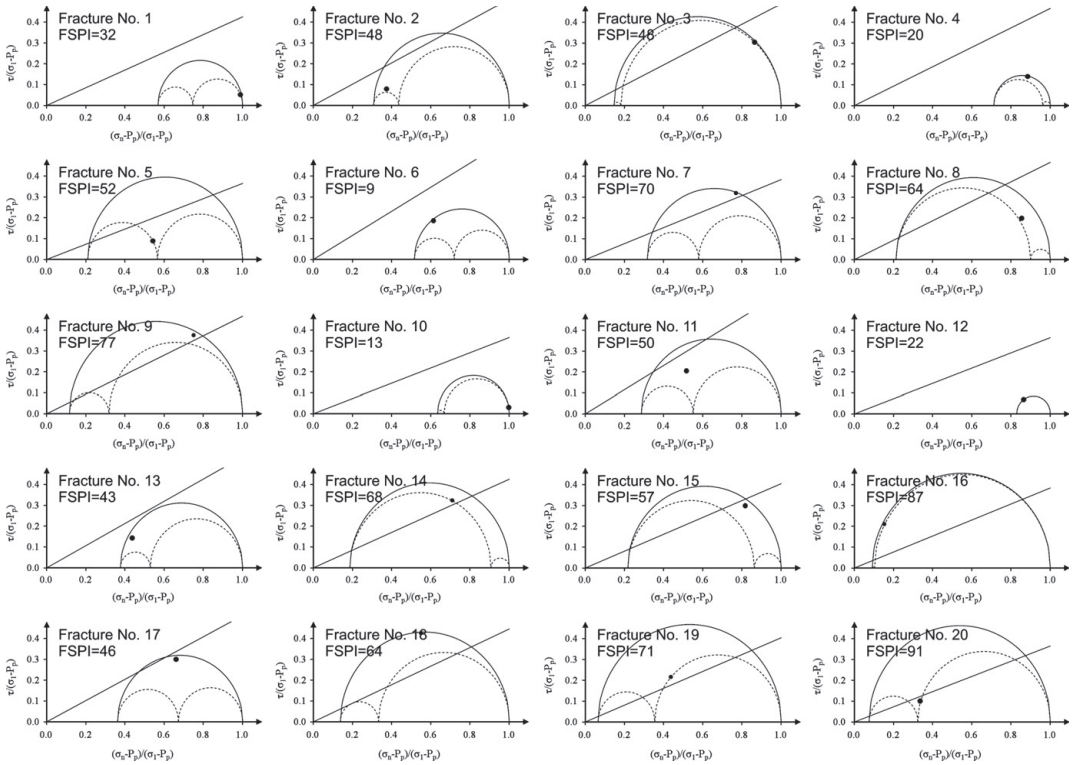

Fig. A1. Mohr–Coulomb and FSPI results for 20 selective fractures.

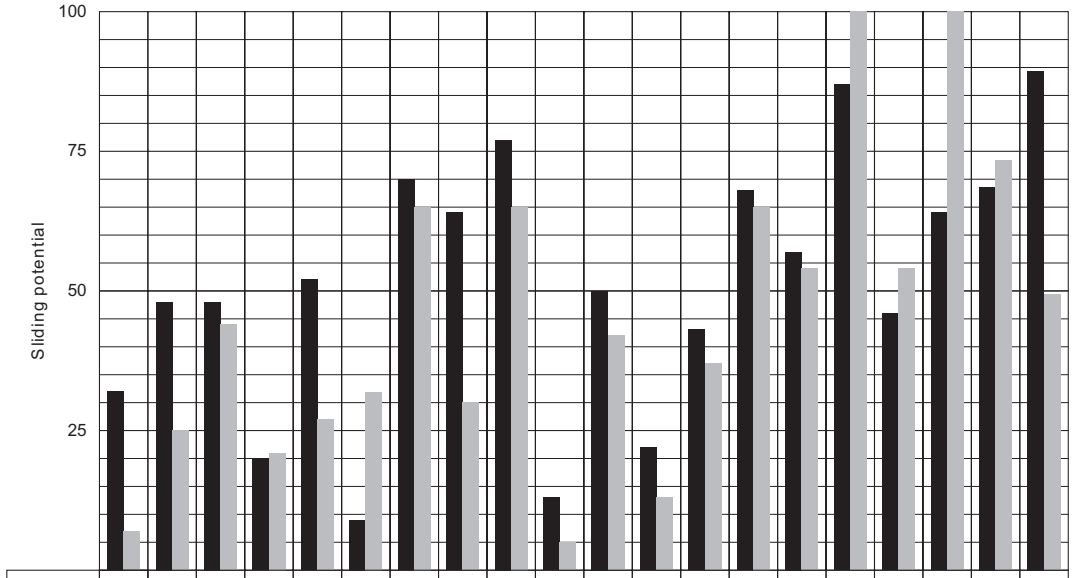

Fracture No.	1	2	3	4	5	6	7	8	9	10	11	12	13	14	15	16	17	18	19	20
FSPI	32	48	48	20	52	9	70	64	77	13	50	22	43	68	57	87	46	64	71	91
SSR_n	7	25	44	21	27	32	65	30	65	5	42	13	37	65	54	218	54	105	74	50

Fig. A2. Comparison of Mohr–Coulomb against FSPI results for 20 selective fractures.

can be easily adjusted for specific project by including additional effective parameters contributing in the system, changing the matrix code values, etc. In FSPI approach the effect of an uncertain value used for one parameter will be moderated by the effect of other parameter values. In contrary, in the Mohr–Coulomb approach a small change in input data (mainly cohesion and friction angle) could result in a large change in the output results.

The presented case study using this approach demonstrated how the results are in good agreement with analytical Mohr–Coulomb and real observation obtained from image logs.

Acknowledgment

The authors would like to express their sincere thanks to John Hudson for his valuable comments and input to the original manuscript of this work.

Appendix A

In order to show the comparison results of FSPI with those obtained from Mohr–Coulomb approach, 20 fractures were selected from a wide range of analysed fractures generated systematically with different properties at different state of stresses (Table A1). The results of the Mohr–Coulomb criteria and FSPI for these fractures are shown in Fig. A1. Qualitative comparison of the results from this table indicates a reasonable agreement between the two approaches. However, in order to allow a more quantitative comparison, the shear stress–shear strength ratio (SSR) from Mohr–Coulomb is used as an indicator for FSP to be compared against FSPI, proposed in this paper. SSR is defined as

$$SSR = \frac{\tau}{C_d + \sigma'_n \tan \phi_d} \tag{A1}$$

or alternatively the normalized value of SSR can be used as

$$SSR_n = \frac{Average\ FSPI \text{ for } 20\ fractures}{Average\ SSR \text{ for } 20\ fractures} \times SSR \tag{A2}$$

The results of SSR_n and $FSPI$ for 20 generated fractures are shown in Fig. A2. Overall, and in more than 90% of cases both methods are consistent in their final results, which confirms the validity of our developed approach based on RES.

References

[1] Chen X, Tan CP, Haberfield CM. Wellbore stability analysis guidelines for practical well design. In: Proceedings of the SPE Asia Pacific oil & gas conference, Adelaide, 1996.
[2] Bratton T, Bornemann T, Li Q, Plumb D, Rasmus J, Hess A. Logging-while-drilling images for geomechanical, geological and petrophysical interpretations. In: Proceedings of the SPWLA 40th annual logging symposium, Oslo, 1999, paper JJJ.
[3] Hudson JA. Rock engineering systems: theory and practice. Chichester: Ellis Horwood; 1992.
[4] Younessi A, Rasouli V. Representing a Rock Engineering System to analyze wellbore instability due to fracture reactivation. In: Proceedings of the first Southern Hemisphere international rock mechanics symposium (SHIRMS), Perth, 2008.
[5] Mazzoccola DF, Hudson JA. A comprehensive method of rock mass characterization for indicating natural slope instability. Q J Eng Geol 1996;29:37–56.
[6] Maury V. Rock failure mechanisms identification: a key for wellbore stability and reservoir behavior problem. In: Proceedings of the European rock mechanics symposium, 1994, p. 175–82.
[7] Dusseault MB, Bruno MS, Barrera J. Casing shear: causes, cases, cures. In: Proceedings of the SPE international oil & gas conference, Beijing, 2–6 November 2001, paper SPE 72060.
[8] Tare UA, Mody FK. Managing borehole stability problems: on the learning, unlearning and relearning curve. In: Proceedings of the AADE 2002 technical conference on "Drilling and Completion Fluids and Waste Management", Texas, 2–3 April 2002, paper AADE-02-DFWM-HO-31.
[9] Hawkes CD, McLellan PJ. Coupled modeling of borehole instability and multiphase flow for underbalanced drilling. In: Proceedings of the IADC/SPE drilling conference, Dallas, 26–28 February 2002, paper SPE 74447.
[10] Hudson JA, Harrison JP. Engineering rock mechanics: an introduction to the principles. Oxford: Elsevier; 2000.
[11] Jaeger JC, Cook NGW, Zimmerman RW. Fundamentals of rock mechanics, 4th ed. Oxford: Wiley-Blackwell; 2007.
[12] Streit JE, Hillis RR. Estimating fault stability and sustainable fluid pressure for underground storage of CO_2 in porous rock. Energy 2004;29:1445–56.
[13] Barton N. A relationship between joint roughness and joint shear strength. In: Proceedings of the international symposium on rock mechanics, Nancy, 1971.
[14] Indraratna B, Haque A. Shear behavior of rock joints. Rotterdam: Balkema; 2000.
[15] Addis MA, Last NC, Yassir NA. The estimation of horizontal stresses at depth in faulted regions and their relationship to pore pressure variation. Rock mechanics in petroleum engineering (Proceedings of the EUROCK). Rotterdam: Balkema; 1994. p. 887–95.
[16] Aadnoy BS, Hansen AK. Bounds on in-situ stress magnitudes improve wellbore stability analyses. In: Proceedings of the IADC/SPE drilling conference, Dallas, 2–4 March 2004, paper SPE 87223.
[17] Jing L, Hudson JA. Fundamentals of the hydro-mechanical behaviour of rock fractures: roughness characterization and experimental aspects. Int J Rock Mech Min Sci 2004;41(3):383.
[18] Sharifzadeh M, Mitani Y, Esaki T. Rock joint surfaces measurement and analysis of aperture distribution under different normal and shear loading using GIS. Rock Mech Rock Eng 2006;41(2):299–323.
[19] Barton N. Modelling rock joint behaviour from in situ block tests: implications for nuclear waste repository design. Report ONWI-308. Columbus, OH: Office of Nuclear Waste Isolation; 1982. 96 p.
[20] Ozdemirtas M, Babadagli T, Kuru E. Effects of fractal fracture surface roughness on borehole ballooning. Vadose Zone J 2009;8(1):250–7.
[21] Majidi R, Miska SZ, Yu M, Thompson LG. Fracture ballooning in naturally fractured formations: mechanism and controlling factors. In: Proceedings of the SPE annual technical conference and exhibition, Denver, 21–34 September 2008, paper SPE 115526.
[22] Jiang Y, Li B, Tanabashi Y. Estimating the relation between surface roughness and mechanical properties of rock joints. Int J Rock Mech Min Sci 2006;43:837–46.
[23] Matsuki K, Wang EQ, Giwelli AA, Sakaguchi K. Estimation of closure of a fracture under normal stress based on aperture data. Int J Rock Mech Min Sci 2008;45:194–209.
[24] Zhang B, Wu H, Liu C, Han F, Ma Y. The effect of stress on pore pressure in rocks and the mechanism of water table anomaly before earthquakes. Acta Seismol Sinica 1992;5(1):153–9.
[25] National Research Council. Rock fractures and fluid flow. Washington, DC: National Academies Press; 1996.
[26] Fjaer J, Holt RM, Horsrud P, Raaen AM, Risnes R. Petroleum related rock mechanics, 2nd ed. Amsterdam: Elsevier; 2008.
[27] Bieniawski ZT. Engineering rock mass classification. New York: Wiley; 1989.
[28] Mäkel GH. The modeling of fracture reservoirs: constraints and potential for fracture network geometry and hydraulic analysis. In: Structurally complex reservoirs, Geological Society Special Publication, vol. 292. London: Geological Society; 2007. p. 375–405.

Paper 7 Rock engineering systems adopted for sanding prediction in perforation tunnels.

Lead author
Ahmadreza Younessi

ROCK ENGINEERING SYSTEMS ADOPTED FOR SANDING PREDICTION IN PERFORATION TUNNELS

A. Younessi and V. Rasouli
Department of Petroleum Engineering
Curtin University of Technology
613 (Rear), Level 6, ARRC
26 Dick Perry Ave, Kensington
Perth WA 6151
Ahmadreza.YounessiSinaki@postgrad.curtin.edu.au
V.Rasouli@curtin.edu.au

ABSTRACT

Sand production is an important issue in reservoirs with weak or unconsolidated sand formations. Production of sand not only causes several problems in maintaining wellbore integrity but also is a problem during production where damages through the tubing and surface facilities are likely to occur due to the sand grains being transported along this path.

The rock engineering systems (RES), initially introduced in mining and civil related geomechanics problems, is one approach to analysing the interrelationship between different parameters involved in a rock engineering project. This is the approach that was adopted in this work to study and predict the sanding potential in perforation tunnels.

Sanding mechanism in perforation tunnels during production was reviewed and all effective parameters were identified. An interaction matrix was introduced to study the sanding mechanism through the interrelation between pairs of parameters. The interaction matrix was coded using a semi-quantitative rating approach to determine the interaction between each pair of parameters. The interaction intensity and dominance of each parameter in the system were studied through the cause-effect diagram to classify the parameters. This will assist in finding a better engineering action to mitigate or eliminate instabilities.

A sensitivity analysis was conducted on a data set, and major parameters playing in sand production in a perforation tunnel were identified using analytical formulae. The results of sensitivity analysis were compared with the cause-effect diagram derived from the interaction matrix. A good agreement between the two methods was observed. This shows the usefulness of RES for identifying potential sanding solutions through the interaction matrix analysis.

KEYWORDS

Rock engineering system, sanding prediction, wellbore integrity, perforation tunnel.

INTRODUCTION

The different process of sedimentation of the formations composes a wide range of unconsolidated to consolidated sand reservoirs. The completion design of sand reservoirs depends on the formation consolidation. On the top limit in consolidated formations the sand is strong enough to resist failures; hence, no sand control systems are required in these reservoirs. On the other hand, unconsolidated sands are weak and sand will produce as soon as production begins; sand control is needed for these kinds of reservoirs. The behaviour of the reservoirs located in weak consolidated sands is predictable and needs to be studied in more detail. Hence the completion system can be optimised to reduce the costs corresponding to sand production (Veeken et al, 1991).

The onset of sanding occurs in two stages: failure and transportation. The stresses are perturbed around the perforation tunnel and the maximum stresses are expected in the boundary of the perforation path. This, if it exceeds the compressive strength of the sand formations surrounding the perforation tunnel, will cause failing the sands in shear mode. The flow of hydrocarbon into the perforation tunnel and then inside the borehole will transport the sand towards the surface. The sand production can be prevented by predicting and mitigating the failure stage.

Sanding mostly occurs along perforation tunnels in cased holes. Production of sand not only causes several problems in maintaining wellbore integrity but is also a problem during production where damages through the tubing and surface facilities are likely to occur due to sand grains being transported along this path.

This paper introduces failure mechanisms and the main parameters contributing to sand production. To understand the interrelationship between these parameters, rock engineering systems (RES)—developed originally with its applications in rock mechanics by Hudson (1992)—are used. RES allows us to investigate the interaction between pairs of parameters affecting sanding; it also aids in the understanding of these effects on the overall response of the system—i.e. sand production.

FAILURE MECHANISMS

Perforation involves penetrating the reservoir rock using explosives and jets. The perforation tunnel generated after shooting the jet results in the removal of the rock formation and its replacement with either the fluid from the wellbore or reservoir formation. Consequently, the replaced fluid supports the stresses that have been sustained by removed rock. As a result, the stresses around the perforation tunnel are disturbed—that is, stress redistribution around the perforation tunnel has occurred.

The stresses induced around a perforation tunnel follow the same pattern of any cavity. Stress concentration occurs in the direction of the minimum stress, perpendicular to the perforation tunnel. The stress concentration can exceed the compressive strength of the formation, and leads to formation failure in a shear mode. This failure happens due to high drawdown pressure and low formation strength.

Tensile failure is another possible failure mechanism. Around the perforation tunnel wall, the radial stress and the pore pressure are both equal to the wellbore pressure, which implies that the effective radial stress is zero at the perforation tunnel wall. If the pore pressure gradient is larger than the radial stress gradient at the cavity wall, the effective radial stress becomes less than zero, and the condition for tensile failure may be fulfilled at some point around the wellbore wall (Fjaer et al, 2008).

The other failure mechanism that initiates the sand production is the cohesive failure. This mechanism is the typical failure in the case of poorly consolidated sands. Cohesive failure occurs when the drag force, due to fluid velocity, exceeds the cohesive strength of formation at the perforation tunnel wall (Abbas et al, 2003). The cohesive strength in unconsolidated sands is close to zero; therefore cohesive failure is the main failure mechanism in these formations.

Of the three mechanisms explained above, the shear failure mode is the mechanism most likely to happen in perforation tunnels, which may cause sand production in the presence of flow of reservoir fluid.

To study sanding in a perforation tunnel several parameters need to be taken into consideration such as: rock physical and mechanical properties, fluid properties, in-situ stresses and perforation tunnel geometry. The interaction between these parameters could determine whether the sand grains are going to fail and then be transported. Such a study is essential to obtain a reasonable estimation of sanding initiation. In this work, the RES is proposed and will be used as a tool for studying the interaction between parameters involved in sanding.

ROCK ENGINEERING SYSTEM

The parameters and variables involved in a rock engineering project can have certain effects on other parameters and the whole system and, inversely, may be affected by other parameters by a certain percentage. This shows the need to study the interrelationship between different parameters in a rock engineering project and the way they interact with each other within the system. Hudson (1992) introduced the RES and presented it in a wider context to integrate all the relevant information in rock engineering design and construction. The RES approach aims to identify the parameters relevant to a problem—and their interactions—and provide a better understanding of a rock engineering problem. In the context of petroleum applications this approach was first used to analyse the wellbore instabilities related to fracture reactivation (Younessi and Rasouli, 2008). In this study the RES is used to evaluate and analyse the onset of sanding that occurs in perforation tunnels.

The first step is to determine the parameters that are encountered in sand production in perforation tunnels. We start with a simple concept in which a low-density matrix is considered. To do this, three main parameters are selected to introduce all possible failure mechanisms. These are: reservoir characteristics, boundary loads and engineering activities.

The first two parameters can be considered as rock mechanical parameters, which will be turned into a rock engineering concept of sand production analysis when their interaction with the third parameter (i.e. the engineering activities) is simultaneously taken into account. Interactions between these parameters, as given in Figure 1, are as follows:

- Interaction 1 (reservoir characteristics/boundary loads): horizontal stresses magnitudes are related to reservoir characteristics.
- Interaction 2 (reservoir characteristics/engineering activities): perforation design depends on the reservoir characteristics.
- Interaction 3 (boundary loads/reservoir characteristics): induced stresses can change the reservoir characteristics.
- Interaction 4 (boundary loads/engineering activities): drawdown pressure is a function of reservoir characteristics.
- Interaction 5 (engineering activities/reservoir characteristics): reservoir characteristics are changed around perforation tunnels.
- Interaction 6 (engineering activities / boundary loads): the state of stress is changed around the wellbore and perforation tunnels.

These interactions can be illustrated systematically in a matrix form known as the Hudson interaction matrix, depicted in Figure 2. The importance of each of these parameters in the context of this work is discussed here in detail.

Reservoir characteristics

Knowledge of the petrophysical and mechanical properties of the formation is needed to conduct a sand production prediction. Understanding these properties assists in obtaining a better knowledge of the formation behaviour under different states of stresses. We discuss these properties individually in the following sections of this paper.

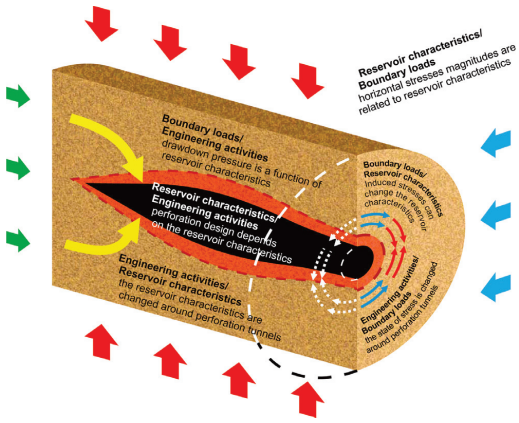

Figure 1. Interactions between three main parameters involved in a sand production prediction.

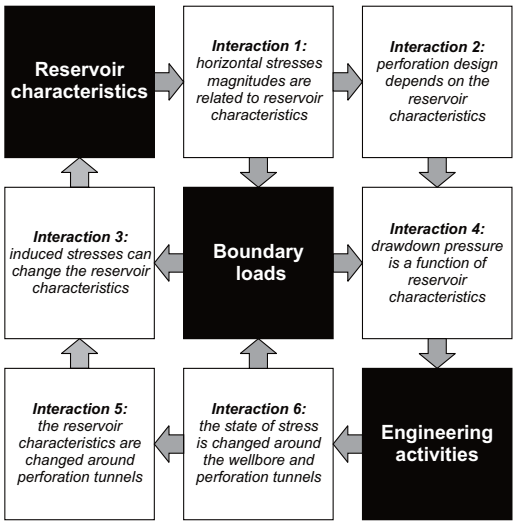

Figure 2. Interactions between the reservoir characteristics, boundary loads and engineering activities illustrated in an interaction matrix form.

PETROPHYSICAL PROPERTIES OF ROCK

Porosity is the most important petrophysical parameter that significantly influences the onset of sanding. Parameters such as permeability and density are considered in relation to other parameters. For example, the density of the formation is directly proportional to the in situ stresses, or the permeability is proportional to the effective porosity. Many articles have been published on the effect of porosity on formation instability, all of which confirm a larger failure potential in formation with higher porosity (Abbas et al, 2003; Gil et al, 2005).

MECHANICAL PROPERTIES OF ROCK

These properties are defined by the deformation moduli and strength properties of the formation. Deformation moduli refer to the slope of stress-strain curve of a rock in a triaxial test at different stages of loading. However, at the failure stage the strength properties of the rock are more critical. Uni-axial compressive strength (UCS), internal friction angle and tensile strength are the primary parameters that are used in sand production prediction studies (Chin and Ramos, 2002). The failure initiation in perforation tunnels is strongly dependent on the mechanical strength of the formation (Tronvoll and Fjaer, 1994).

FORMATION FLUID PROPERTIES

After the bond forces between sand grains are collapsed, the fluid flows through the perforation tunnel and transports the sand to the wellbore and surface facilities. The fluid drag force itself can be high enough to erode weak sand formations. This force is directly related to the fluid flow rate and fluid viscosity (Chin and Ramos, 2002). It is also observed that water cut has an impact on sand grain failure in perforation tunnels and hence affects the sand production (Bailin Wu et al, 2006).

Boundary loads

One of the main causes of initiation of sand failure is the stress concentration and relaxation during production and injection operations. As the stress concentration or relaxation exceeds the formation strength the failure initiates and, as a result, instability occurs. Regardless of the state of the stress, considering the porous structure and the fluid inside this porous media, the stresses are divided into two categories: the stress that is applied to the matrix and grains of the formation (known as effective stress), and the stress that is applied to the fluid inside the porous media of the formation (known as pore pressure). These stresses are introduced briefly in the following subsections.

IN SITU STRESSES

The state of stress in a field can be defined using the direction and magnitude of the principal stresses. In geomechanics studies one of the principal stresses is usually assumed to be vertical and the other two principal stresses to be horizontal (Aadnoy et al, 2004). The vertical principal stress is due to the weight of the overburden layers, and the horizontal stresses are induced from the lateral strain of the formations and from tectonic effects; however, the complete state of stress is defined by knowing the magnitudes of the three principal stresses and their corresponding directions (Addis et al, 1994).

RESERVOIR PRESSURE

Generally in shallow depths—as long as the pores or fractures are interconnected and permeable up to the surface—the pore pressure is normally the hydrostatic pressure of the water column above the study depth. This situation could be different in deeper sections of the field, for example in reservoir section (they are mainly located hundreds of meters below the surface, and some zones could be over or under pressured). The onset of sanding is related to the reservoir pressure and the changes of fluid pressure during time, for example with reservoir depletion.

Engineering activities

These include parameters related to engineering activities (both perforation and production) that disturb the stress balance in the field. The most important parameters in this category are briefly reviewed below.

PERFORATION GEOMETRY

The geometry of perforation tunnels depends on the type of explosive charge used for perforation. It is observed that small perforation tunnels are more stable than large holes. Deep penetrating charges generally perforate a smaller hole, and hence make a more stable perforation tunnel (Venkitaraman et al, 2000).

PERFORATION DIRECTION AND PHASING

The failure zone around a single perforation tunnel may extend to a degree where there is a large unstable zone induced around the wellbore as a result of number of perforation shots close to each other. This could lead to large amount of sands produced. The distance between the perforation tunnels can be dictated by shot density and phasing. Therefore, a minimum perforation to perforation distance may need to be defined to have a stable wellbore. Moreover, in a situation where the difference between the in-situ stresses (vertical and horizontal) are considerable, the perforation tunnels should be in the direction of maximum stability—that is, the direction where the difference between the two stresses is lower (Venkitaraman et al, 2000).

DRAWDOWN PRESSURE

The fluid flows from a high pressure to a lower pressure environment. In order to produce from a well, the wellbore pressure must be less than that of the reservoir pressure. The pressure difference between the wellbore and reservoir is known as drawdown pressure. The production rate of a wellbore is controlled by the drawdown pressure. A critical drawdown pressure needs to be sustained to avoid sand production. The critical drawdown pressure changes during the life of a reservoir when the other parameters change. (Qiu et al, 2006).

INTERACTION MATRIX AND PARAMETERS CLASSIFICATION

To fully understand the overall reaction of an engineering system, the interrelationship between various parameters needs to be taken into consideration. Each parameter can affect the system and also be affected by the system to a certain degree. The interaction matrix developed by Hudson allows the study of the interrelationship between different parameters in a RES. The interaction matrix is a square matrix. The main parameters are located along the diagonal elements of the matrix whereas the off-diagonal elements are filled with quantitative numbers, each showing the amount of interaction between two parameters. The interactions are to be read clockwise, as they could be path dependent. Also, the matrix is not necessarily symmetric.

Figure 3 shows the interaction matrix constructed for the eight parameters involved in the sand production case explained in the previous section. This is an 8x8 matrix, where the main parameters are located along the diagonal elements. The interaction between each two parameters is described qualitatively in the corresponding off-diagonal element (this element results from the intersection of a horizontal and a vertical line passing through the first and second parameters, respectively). The off-diagonal elements will be quantified later on, using coding systems to allow the assessment of the amount of cause and effect of each parameter in the system. In this way, the sum of each row passing through a parameter indicates the total influence of the parameter on the system (cause) whereas each column (passing through the parameter) describes the influence of the system on the parameter (effect).

Coding the matrix

For the purpose of the present work, a semi-quantitative coding system is adopted in which the interaction between each two parameters is ranges between zero (no interaction) and four (critical or very high interaction). Coding numbers of one, two and three show minor, moderate and high interactions, respectively. Figure 4 shows the results of coding the interaction matrix constructed in Figure 3 using this semi-quantitative coding method. As can be recognised, matrix coding is not an easy process and requires gathering all available information from the off-set wells (structural geology reports, drilling reports etc) and past experiences in similar fields to be able to quantify the interactions with more certainty.

Cause-effect diagram

The cause (total influence of the parameter on the system) is obtained as the sum of the off-diagonal rows corresponding to that parameter (Fig. 4). Similarly, the effect (total influence of system or other parameter on a certain parameter) is the sum of off-diagonal columns corresponding to that parameter. The cause and effect values corresponding to each parameter can be represented as a point in a cause-effect coordinate system. This is shown

Petrophysical properties *Density, Porosity, Permeability, Grain size*	*Mechanical properties are directly related to petrophysical properties*	*Larger permeability has larger fluid rate*	*Vertical stress is directly related to density*	*No interaction in onset of sanding*	*Smaller grainsize lesser stable geometry*	*Less perforation tunnels are needed in high permeable zones*	*Drawdown pressure is less in permeable formations*
No interaction in onset of sanding	**Mechanical Properties** *UCS, Poisson ratio, Biot's factor*	*No interaction in onset of sanding*	*Horizontal stresses are related to mechanical properties*	*No interaction in onset of sanding*	*The average diameter of perforation tunnel is a function of formation strength*	*The minimum stable distance between perforation is related to formation strength*	*Stronger formations can sustain higher drawdown pressure*
Erosion can change the porosity and permeability	*Erosion can change the mechanical properties*	**Fluid Properties** *Viscosity, Flow rate, Density*	*No interaction in onset of sanding*	*No interaction in onset of sanding*	*No interaction in onset of sanding*	*No interaction in onset of sanding*	*No interaction in onset of sanding*
Induce stresses during depletion change the density and porosity	*The mechanical properties are changed in the plastic zone induced around perforation tunnels*	*No interaction in onset of sanding*	**Effective Stresses** *in situ and induced stresses*	*Reservoir pressure increases in with increase of stresses*	*High stresses induce failure and enlarge the perforation geometry*	*It is preferable to perforate in the direction of minimum stress*	*No interaction in onset of sanding*
high reservoir pressure increases the porosity	*No interaction in onset of sanding*	*Pressure increases the fluid viscosity and density*	*Effective stresses have revers relation with reservoir pressure*	**Reservoir pressure**	*No interaction in onset of sanding*	*No interaction in onset of sanding*	*Drawdown pressure is a function of reservoir pressure*
The crush zone is a function of the perforation diameter	*The crush zone is a function of the perforation diameter*	*Larger perforation diameter increase fluid rate*	*The stresses are induced around a perforation tunnel is a function of perforation geometry*	*No interaction in onset of sanding*	**Perforation geometry** *Shape, Diameter and length*	*The shot density and perforation diameter have reverse relations*	*No interaction in onset of sanding*
No interaction in onset of sanding	*No interaction in onset of sanding*	*Larger number of shots increase fluid rate*	*The magnitude of induce stresses around a perforation tunnel relates to its direction*	*No interaction in onset of sanding*	*The shot density and perforation diameter have reverse relations*	**Perforation Direction & Density**	*Drawdown pressure is less in higher shot density*
No interaction in onset of sanding	*No interaction in onset of sanding*	*Fluid rate is a function of drawdown pressure*	*Drawdown pressure induces stresses*	*No interaction in onset of sanding*	*No interaction in onset of sanding*	*No interaction in onset of sanding*	**Drawdown pressure**

Figure 3. A complete sand prediction production interaction matrix.

								Cause
PP	4	3	3	0	3	1	3	17
0	***MP***	0	2	0	3	2	4	11
1	4	***FP***	0	0	0	0	0	5
3	3	0	***ES***	4	2	4	0	16
1	0	1	4	***RP***	0	0	4	10
1	3	3	3	0	***PG***	0	0	12
0	0	3	4	0	2	***PDD***	2	11
0	0	3	3	0	0	0	***DP***	6
Effect 6	14	13	19	4	10	9	13	

PP-Petrophysical Properties ***RP***-Reservoir Pressure
MP-Mechanical Properties ***PG***-Perforation Geometry
FP-Fluid Properties ***PDD***-Perforation Direction & Density
ES-Effective Stresses ***DP***-Drawdown Pressure

Figure 4. Semi-quantitative coding of the sand production prediction interaction matrix.

in Figure 5 for the sand production interaction matrix, earlier discussed. Note that in this space the diagonal of the diagram is the focus of C=E. Along this diagonal and as we move away from the centre of the coordinate system, the summation of C+E increases. Then, the lines of equal interaction intensity (i.e. C+E values) can be plotted on the diagram allowing discrimination between less interactive and more interactive parameters. The parameters plotting in the bottom right of the diagram are the ones that dominate the system, as they have increasing C–E values further away from the diagonal line. In a similar manner, the subordinate parameters are defined as those that are highly dominated by the system and are located in the top left of the diagram. These parameters will have decreasing C–E values (taking the sign into account) moving away from the diagonal.

The cause-effect plot is helpful in understanding the behaviour of each parameter individually as well as in studying the whole system. The cause-effect diagram for onset of sanding corresponding to the interaction matrix obtained from the previous section is shown in Figure 5. The average parameter value (C/8,E/8) lies close to the centre of the diagram, indicating the sand production interaction matrix represents a system that is 50% interactive.

It can be seen that the effective stresses is the most interactive parameter in the system. As it was expected, the system can be controlled by controlling this parameter. In other words, the onset of sanding can be delayed by controlling the stresses around the perforation tunnel. For instance, directional perforation can control the magnitude of induced stresses around the perforation tunnel and delay the onset of sanding. On the other hand, reservoir pressure has the least interaction in onset of sanding. This parameter cannot be controlled during the sand production and has the lowest impact on the other parameters.

The petrophysical properties are always important in any geomechanics study. This parameter is the dominant parameter and has the largest cause value among all

parameters. In contrast, fluid properties and drawdown pressure are the most subordinate parameters in the system. They also have the lowest cause value in the effective parameters in onset of sanding. The drawdown pressure was expected to be the subordinate parameter since it is one of the construction design parameters. Since fluid rate is considered as part of fluid properties, this parameter is expected to behave similar to drawdown pressure.

SENSITIVITY ANALYSIS

In addition to the parameter characterisation as performed using the cause-effect diagram in the previous section, a sensitivity analysis was conducted to study the effect of each parameter on the onset of sanding. Here, the onset of sanding initiated under shear failure mechanism is studied for a perforation tunnel in a permeable reservoir under production. In this condition the radial (σ_r) and tangential (σ_θ) stresses induced around a perforation tunnel are expressed as

$$\sigma_r = p_w$$

$$\sigma_\theta = a\sigma_v + b\sigma_H + c\sigma_h - p_w + \alpha\frac{1-2\nu}{1-\nu}(p_w - p_r)$$

where σ_v, σ_H and σ_h are the vertical, maximum and minimum horizontal stresses, respectively. Also, υ is Poisson ratio, α is Biot's factor, p_w and p_r are wellbore and reservoir pressure, respectively. The stress coefficients a, b and c are to transfer the principal in situ stresses into the perforation tunnel direction. For a vertical perforation tunnel a, b and c are 0, 3 and -1, respectively.

In order to calculate the effective stresses around the perforation tunnel wall, the pore pressure is considered to be equal to wellbore pressure, p_w. Hence, the critical wellbore pressure (p_{cw}) is expressed as

$$p_{cw} = \frac{a\sigma_v + b\sigma_H + c\sigma_h - UCS - \alpha\frac{1-2\nu}{1-\nu}p_r}{(a+b+c) - \alpha\frac{1-2\nu}{1-\nu}}$$

The sensitivity analysis is done using the latter equation. In order to illustrate the results of the sensitivity analysis in a diagram, the wellbore pressure is plotted versus the reservoir pressure, as is shown in Figure 6. The well produces if the wellbore pressure is less than the reservoir pressure. This condition is the focus of the points below the diagonal of the diagram illustrated in Figure 6 where $p_w = p_r$. The critical drawdown pressure is the difference between the reservoir pressure and critical wellbore pressure. In Figure 6 the area between the critical wellbore pressure and the diagonal of the diagram shows the critical drawdown pressure. Generally, the critical drawdown pressure reduces as the reservoir depletes.

The sensitivity analysis is conducted based on a set of data obtained from the reservoir section of a vertical well. The data is shown in Table 1. The results are discussed in more detail in the following sections and compared with the cause-effect results obtained from the RES analysis.

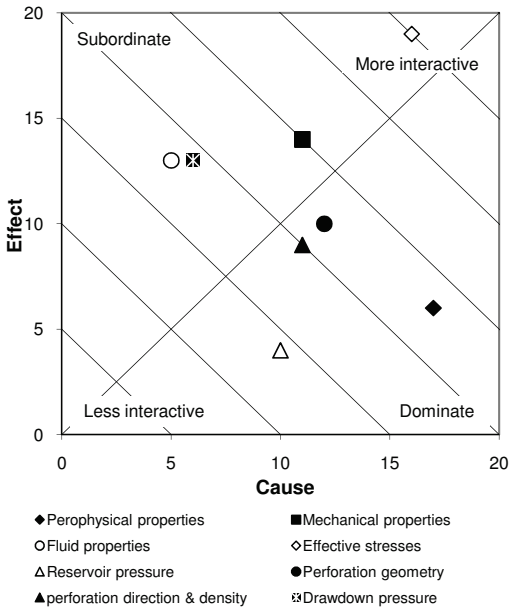

Figure 5. Cause-effect diagram corresponding to parameters involved in sand production prediction study.

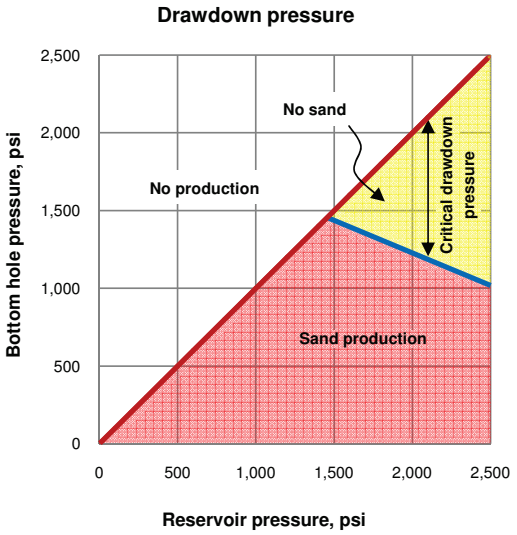

Figure 6. Illustration of critical drawdown pressure.

Formation strength

The critical drawdown pressure was calculated for six different formation strengths (UCS) and plotted in Figure 7. The critical wellbore pressure changes as expected—that is, it reduces as the UCS decreases.

Stress anisotropy

To evaluate the impact of the stress anisotropy, a sensitivity analysis was conducted on a horizontal perforation tunnel perforated along the minimum horizontal stress, the results of which are shown in Figure 8. Therefore, the vertical stress was kept constant and the maximum horizontal stress was changed between the range of minimum horizontal and vertical stresses. The results show that an increase in the stress anisotropy ratio decreases the critical drawdown pressure.

Table 1. Parameter used for sensitivity analysis.

Vertical stress (σ_v)	4,000 psi
Maximum horizontal stress (σ_H)	3,800 psi
Minimum horizontal stress (σ_h)	2,600 psi
σ_H azimuth	0 deg (North)
Reservoir pressure (p_r)	2,500 psi
Poisson ratio (v)	0.25
UCS	5,500 psi
Wellbore azimuth	0 deg
Wellbore deviation	0 deg (vertical)
Perforation azimuth	90 deg
Biot's factor	0.9

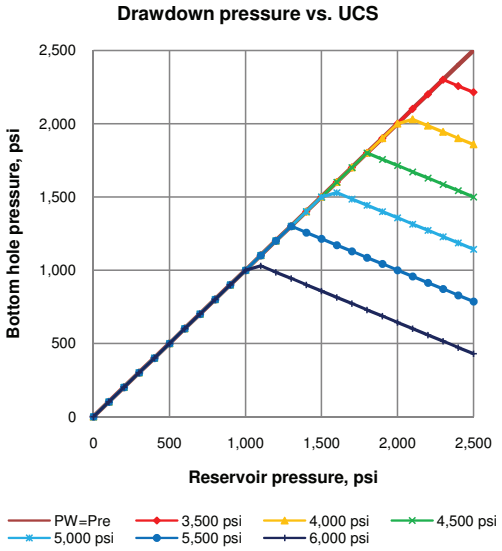

Figure 7. Sensitivity analysis of UCS.

Perforation direction

The critical wellbore pressure was calculated for perforation tunnels in different directions. The results are plotted in Figure 9. Since the wellbore is vertical, all the perforation tunnels are horizontal. From the data given in Table 1 it can be seen that the stress regime is normal ($\sigma_v > \sigma_H > \sigma_h$). Hence, here the stress anisotropy around the perforation tunnel is maximised when the tunnel is perforated along the maximum horizontal stress direction (i.e. 0 degree towards North). As it was shown in the previous section, stress anisotropy increases the formation instability; hence, in this case the perforation tunnel along the maximum horizontal stress is more unstable than that of perforated along the minimum horizontal stress, as seen from Figure 9.

CONCLUSION

In this paper, the mechanisms of onset of sanding in a perforation tunnel under production were reviewed. Thereafter, the main, previously identified, parameters governing the instability and sand production were identified and tested.

The RES methodology was implemented to study the interaction between different parameters involved in sanding and to study how they affect sand production.

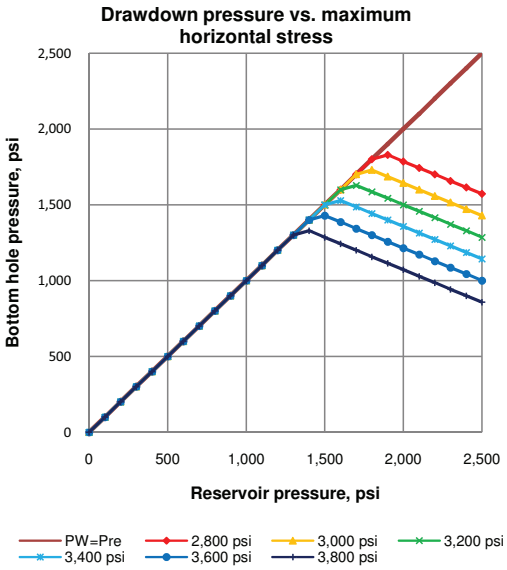

Figure 8. Sensitivity analysis of stress anisotropy ratio.

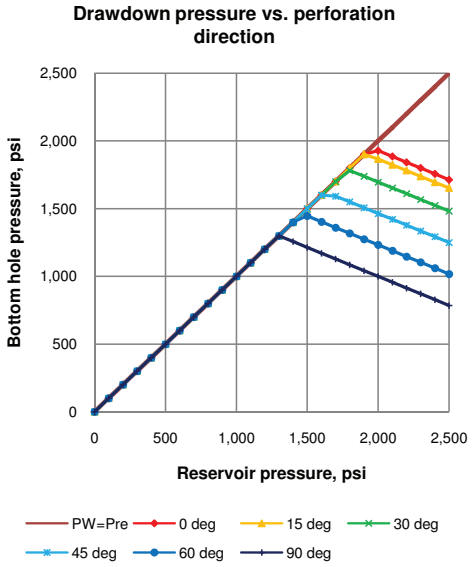

Figure 9. Sensitivity analysis of perforation direction.

In the RES approach the parameters are structured in an interaction matrix and the effect of each parameter on the system is demonstrated.

It was shown that effective stresses is the most interactive parameter in the system; it is concluded, therefore, that the onset of sand production can be delayed by controlling this parameter. In addition, petrophysical properties is the most dominant parameter, whereas fluid properties and drawdown pressure are subordinate parameters.

To evaluate the accuracy of the cause-effect diagram, a sensitivity analysis on three different parameters was conducted in a vertical wellbore. The results showed that due to reservoir depletion and as a result of an increase in the stress anisotropy ratio the critical drawdown pressure reduces, whereas increasing the formation strength increases the critical drawdown pressure. In addition, it was concluded that in a normal stress regime horizontal perforation along the minimum horizontal stress is more stable than perforating along the maximum horizontal stress.

REFERENCES

AADNOY, B.S. AND HANSEN, A.K., 2004—Bounds on in-situ stress magnitudes improve wellbore stability analyses. In: The IADC/SPE Drilling Conference, Dallas, 2–4 March, SPE 87223-MS.

ABBAS, H.H., HABBTAR, A.H. AND SHEBATALHAMD, A., 2003—Sand control during drilling, perforation, completion and production. SPE 13th Middle East Oil Show and Conference, Bahrain, 9–12 June, SPE 81492.

ADDIS, M.A., LAST, N.C. AND YASSIR, N.A., 1994—The estimation of horizontal stresses at depth in faulted regions and their relationship to pore pressure variation, in Rock mechanics in petroleum engineering. In: Eurock 1994 proceedings, A.A. Balkema, Rotterdam, pp. 887–95.

CHIN, L.Y. AND RAMOS, G.G., 2002—Predicting volumetric sand production in weak reservoirs. In: SPE/ISRM Rock Mechanics Conference held in Irving, Texas, 20–23 October, SPE/ISRM 78169.

FJAER, E., HOLT, R.M., HORSRUD, P., RAAEN, A.M. AND RISENES, R., 2008—Petroleum related rock mechanics 2nd edition. Developments in petroleum science, 53.

HUDSON, J.A., 1992—Rock engineering systems: theory and practice. Chichester: Ellis Horwood.

MONTGOMERY, C.T., RAMOS, R., GIL, I., ORMARK, K. AND SOERENSEN, C., 2005—Failure mechanisms in deepwater chalks rock stability as function of pore pressure and water saturation. In: International Petroleum Technology Conference, Doha, Qatar, 21–23 November, IPTC 10321-MS.

QIU, K., MARSDEN, J.R., ALEXANDER, J., RETNANTO, A., ABDELKARIM, O.A. AND SHATWAN, M., 2006—Practical approach to achieve accuracy in sanding prediction. In: 2006 SPE Asia Pacific Oil and Gas Conference and Exhibition, Adelaide, Australia, 11–13 September, SPE 100944.

TRONVOLL, J. AND FJAER, E., 1994—Experimental study of sand production from perforation cavities. In: International Journal of Rock Mechanics and Mining Sciences and Geomechanics Abstracts, 31 (5), 394–410.

VEEKEN, C.A.M., DAVIES, D.R., KENTER, C.J. AND KOOIJMAN, A.P., 1991—Sand production prediction review: developing an integrated approach. In: 66th Annual Technical Conference and Exhibition of the Society of Petroleum Engineers held in Dallas, TX, 6–9 October, SPE 22792.

VENKITARAMAN, A., BEHRMANN, L.A. AND NOORDERMEER, A.H., 2000—Perforating requirements for sand prevention. 2000 SPE International Symposium on Formation Damage Control, Lafayette, Louisiana, 23–24 February, SPE 58788.

WU, B., TAN, C.P. AND LU, N., 2006—Effect of water cut on sand production—an experimental study. 2005 Asia Pacific Oil and Gas Conference and Exhibition, Jakarta, Indonesia, 5–7 April, SPE 92715.

YOUNESSI, A. AND RASOULI, V., 2008—Representing a Rock Engineering System to analyze wellbore instability due to fracture reactivation. In: First Southern Hemisphere International Rock Mechanics Symposium (SHIRMS), Perth, Australia.

Paper 8 Representing rock engineering system to analyse sand production in perforation tunnels

Rock Mechanics in Civil and Environmental Engineering – Zhao, Labiouse, Dudt & Mathier (eds)
© 2010 Taylor & Francis Group, London, ISBN 978-0-415-58654-2

Representing rock engineering system to analyse sand production in perforation tunnels

A. Younessi & V. Rasouli
Department of Petroleum Engineering, Curtin University of Technology, Perth, Australia

ABSTRACT: Several sophisticated analytical and numerical models have been proposed to study the sanding initiation mechanisms. The Rock Engineering Systems (RES), initially introduced in mining and civil related geomechanics field, is an approach used in this study to analyse the interrelationship between the parameters playing in sand production mechanisms. After discussing all possible failure mechanisms in a perforation tunnel and identifying all parameters contributing in sand production, an interaction matrix is introduced to study the failure mechanisms. Thereafter, the interaction intensity and dominance of each principal parameter in the system is established to classify the parameters. The other aspect of the systems approach is establishing when positive feedback within the system can occur, which leads to sand production. The results indicate the ability of this method to analyse sand production and assist in applying a better engineering action to mitigate or eliminate instabilities resulting in sanding.

1 INTRODUCTION

Production of sand, not only causes several problems in maintaining wellbore integrity but also is a problem during production where damages through the tubing and surface facilities are likely to occur due sand grains being transported along this path.

A wide range of unconsolidated to consolidated sand reservoirs exists, each require a different well completion system. In consolidated formations the sand is strong enough to resist against the failures. Hence, no sand control systems are required in these reservoirs. On the other hand, the unconsolidated sands are weak and sand will produce as soon as the production begins. Sand control is essential for these kinds of reservoirs. However, the response of the reservoirs in weak consolidated sands needs to be studied in more details to optimise the completion system in order to reduce the costs associated with sand production (Veeken et al., 1991).

The onset of sanding occurs in two stages: failure and transportation. After perforation the stresses are perturbed around the perforation tunnel. This, if exceeds the compressive strength of the sand formations surrounding the perforation tunnel, will cause failing the sands in shear mode. Thereafter, the flow of hydrocarbon into the perforation tunnel and then inside the borehole will transport the sand towards the surface. Thus, The sand production can be prevented by predicting and mitigating the failure stage.

In this paper, after introducing the failure mechanisms, the effective parameters contributing in sand production are introduced. In order to understand the interrelationship between these parameters Rock Engineering Systems (RES), developed originally with its applications in rock mechanics by Hudson (1992), are used. RES allows investigating the interaction between pairs of parameters affecting sanding and then combining these effects to understand the overall response of the system, i.e. sand production.

2 FAILURE MECHANISMS

The perforation tunnel generated after shooting the jet results in removing the rock formation and replacing it with either the fluid from the wellbore or reservoir formation. As a result, the stresses around the perforation tunnel are disturbed i.e. stress redistribution around the perforation tunnel is occurred.

Stress concentration around a perforation tunnel, similar to any other circular opening, occurs in the direction of the minimum stress perpendicular to the plane passing through the perforation tunnel. The stress concentration can exceed the compressive strength of the formation, and leads to formation failure in a shear mode. This failure happens due to high drawdown pressure and low formation strength.

Tensile failure is another possible failure mechanism. If the pore pressure gradient is larger than the radial stress gradient at the perforation tunnel wall, the effective radial stress will become negative, and the condition for tensile failure may be fulfilled at some point inside the wall (Fjaer et al. 2008).

The other failure mechanism which initiates the sand production is the cohesive failure. This mechanism is the typical failure in the case of poorly consolidated sand. Cohesive failure occurs when the

drag force due to fluid velocity exceeds the cohesive strength of formation at the perforation tunnel wall (Abbas et al., 2003).

In order to study sanding in perforation tunnel several parameters need to be taken into consideration: these are parameters related to rock physical and mechanical properties, fluid properties, in situ stresses and perforation tunnel geometry. The interaction between these parameters could determine whether the sand grains are going to fail and then produced. In this work, the RES, which is introduced in the following section is proposed and used as a tool for studying the interaction between parameters involved in sanding and their effects on the whole system will be analysed.

3 ROCK ENGINEERING SYSTEMS

The parameters and variables involved in a rock engineering project can have a certain effect on other parameters and the whole system and, inversely, may be affected by other parameters by a certain percentage. This shows the need for studying the interrelationship between different parameters within a rock engineering project and the way they interact with each other within the system. The rock engineering systems (RES) introduced and presented within the wider context of an approach to integrate all the relevant information in rock engineering design and construction by Hudson (1992). The RES approach aims at identifying the parameters relevant to a problem, and their interactions, thus providing overall coherency in approaching rock mechanics and rock engineering problems. In the context of petroleum applications this approach was firstly used to analyase the wellbore instabilities related to fracture reactivation (Younessi & Rasouli, 2008). In current study the RES is used to evaluate and analyse the onset of sanding, specifically in perforation tunnels.

We start with a simple concept in which a low-density matrix is considered. To do this three main parameters are selected to introduce all possible failure mechanisms. These are reservoir characteristics, boundary loads and engineering activities.

The first two parameters can be considered as rock mechanical parameters, which will be turned into a rock engineering concept of sand production analysis when their interaction with the third parameter (i.e. the engineering activities) is taken into account simultaneously. Interactions between these parameters are as follows:

- Interaction 1 (Reservoir characteristics/boundary loads): horizontal stresses magnitudes are related to reservoir characteristics.
- Interaction 2 (Reservoir characteristics/engineering activities): perforation design depends on the reservoir characteristics.
- Interaction 3 (Boundary loads/reservoir characteristics): induced stresses can change the reservoir characteristics.

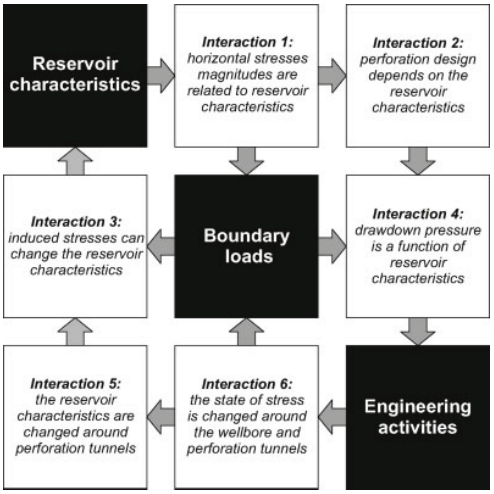

Figure 1. Interactions between three main parameters involved in a sand production prediction study.

- Interaction 4 (Boundary loads/engineering activities): drawdown pressure is a function of reservoir characteristics.
- Interaction 5 (Engineering activities/reservoir characteristics): reservoir characteristics are changed around perforation tunnels.
- Interaction 6 (Engineering activities / boundary loads): the state of stress is changed around the wellbore and perforation tunnels.

These interactions can be illustrated systematically in a matrix form known as the Hudson Interaction Matrix depicted in Figure 1.

In order to study the onset of sanding in perforation tunnels in more details the main parameters needs to be broken into more detailed. The main parameters can be divided to 8 parameters: petrophysical properties, mechanical properties, fluid properties, effective stresses, reservoir pressure, perforation direction and density, perforation geometry and drawdown pressure.

The interaction matrix is described in more detail in the following section.

4 INTERACTION MATRIX AND MATRIX CODING

To fully understand the overall reaction of an engineering system, the interrelationship between various parameters needs to be taken into consideration. Each parameter can affect the system and also be affected by system to a certain degree. The interaction matrix developed by Hudson allows studying the interrelationship between different parameters within a RES. The interaction matrix is a square matrix. The main parameters are located along the diagonal elements of the matrix whereas the off-diagonal elements show

Petrophysical properties *Density, Porosity, Permeability, Grain size*	*Mechanical properties are directly related to petrophysical properties*	*Larger permeability has larger fluid rate*	*Vertical stress is directly related to density*	*No interaction in onset of sanding*	*Smaller grainsize lesser stable geometry*	*Less perforation tunnels are needed in high permeable zones*	*Drawdown pressure is less in permeable formations*
No interaction in onset of sanding	**Mechanical Properties** *UCS, Poisson ratio, Biot's factor*	*No interaction in onset of sanding*	*Horizontal stresses are related to mechanical properties*	*No interaction in onset of sanding*	*The average diameter of perforation tunnel is a function of formation strength*	*The minimum stable distance between perforation is related to formation strength*	*Stronger formations can sustain higher drawdown pressure*
Erosion can change the porosity and permeability	*Erosion can change the mechanical properties*	**Fluid Properties** *Viscosity, Flow rate, Density*	*No interaction in onset of sanding*	*No interaction in onset of sanding*	*No interaction in onset of sanding*	*No interaction in onset of sanding*	*No interaction in onset of sanding*
Induce stresses during depletion change the density and porosity	*The mechanical properties are changed in the plastic zone induced around perforation tunnels*	*No interaction in onset of sanding*	**Effective Stresses** *in situ and induced stresses*	*Reservoir pressure increases in with increase of stresses*	*High stresses induce failure and enlarge the perforation geometry*	*It is preferable to perforate in the direction of minimum stress*	*No interaction in onset of sanding*
high reservoir pressure increases the porosity	*No interaction in onset of sanding*	*Pressure increases the fluid viscosity and density*	*Effective stresses have revers relation with reservoir pressure*	**Reservoir pressure**	*No interaction in onset of sanding*	*No interaction in onset of sanding*	*Drawdown pressure is a function of reservoir pressure*
The crush zone is a function of the perforation diameter	*The crush zone is a function of the perforation diameter*	*Larger perforation diameter increase fluid rate*	*The stresses are induced around a perforation tunnel is a function of perforation geometry*	*No interaction in onset of sanding*	**Perforation geometry** *Shape, Diameter and length*	*The shot density and perforation diameter have reverse relations*	*No interaction in onset of sanding*
No interaction in onset of sanding	*No interaction in onset of sanding*	*Larger number of shots increase fluid rate*	*The magnitude of induce stresses around a perforation tunnel relates to its direction*	*No interaction in onset of sanding*	*The shot density and perforation diameter have reverse relations*	**Perforation Direction & Density**	*Drawdown pressure is less in higher shot density*
No interaction in onset of sanding	*No interaction in onset of sanding*	*Fluid rate is a function of drawdown pressure*	*Drawdown pressure induces stresses*	*No interaction in onset of sanding*	*No interaction in onset of sanding*	*No interaction in onset of sanding*	**Drawdown pressure**

Figure 2. A complete sand prediction production interaction matrix.

the interaction between two parameters. The interactions are to be read clockwise, as they could be path dependent. Also the matrix is not necessarily symmetric.

Figure 2 shows the interaction matrix constructed for the eight parameters involved in sand production. This is an 8×8 matrix, where the main parameters are located along the diagonal elements. The interaction between each two parameters is described qualitatively in the corresponding off-diagonal element. The off-diagonal elements need to be quantified using a coding system to allow the assessment of the amount of cause and effect of each parameter within the system. In this way, the sum of each row passing through a parameter indicates the total influence of the parameter on the system (cause) whereas each column (passing through the parameter) describes the influence of the system on the parameter (effect).

For the purpose of the present work, a semi-quantitative coding system in which the interaction between each two parameters is ranged between zero (no interaction) to four (critical or very high interaction) is adopted. Coding numbers of 1, 2 and 3 show minor, moderate and high interactions, respectively. Figure 3 shows the results of coding the interaction matrix constructed in Figure 2 using this semi-quantitative coding method. As can be recognized, matrix coding is not an easy process and requires gathering all available information from the off-set wells (structural geology reports, drilling reports) and past experiences within similar fields to be able to quantify the interactions with more certainty.

Cause

	PP	4	3	3	0	3	1	3	17
	0	***MP***	0	2	0	3	2	4	11
	1	4	***FP***	0	0	0	0	0	5
	3	3	0	***ES***	4	2	4	0	16
	1	0	1	4	***RP***	0	0	4	10
	1	3	3	3	0	***PG***	2	0	12
	0	0	3	4	0	2	***PDD***	2	11
	0	0	3	3	0	0	0	***DP***	6
Effect	6	14	13	19	4	10	9	13	

PP-Petrophysical Properties ***RP***-Reservoir Pressure
MP-Mechanical Properties ***PG***-Perforation Geometry
FP-Fluid Properties ***PDD***-Perforation Direction & Density
ES-Effective Stresses ***DP***-Drawdown Pressure

Figure 3. Semi-quantitative coding of the sanding prediction interaction matrix.

5 CAUSE-EFFECT DIAGRAM

The cause (total influence of the parameter on the system) is obtained as the sum of the off-diagonal rows corresponding to that parameter (Fig. 3). Similarly, the effect (total influence of system or other parameter on a certain parameter) is the sum of off-diagonal columns corresponding to that parameter. The cause and effect values corresponding to each parameter can be represented as a point in a Cause–Effect coordinate system (Fig. 4).

The Cause–Effect plot is helpful in understanding the behavior of each parameter individually as well as studying the whole system. It can be seen that the "effective stresses" is the most interactive parameter

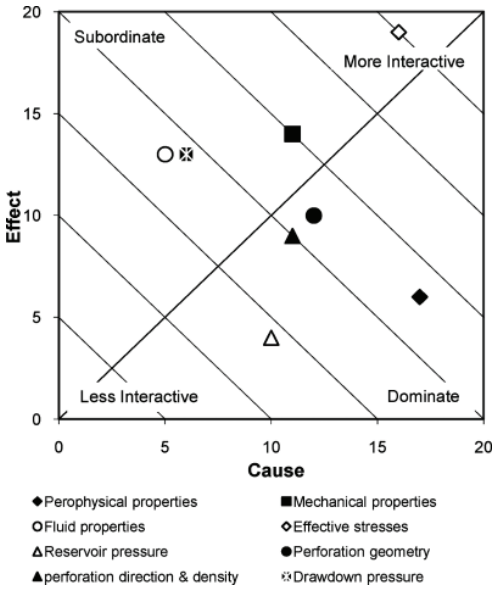

Figure 4. Cause–Effect diagram corresponding to parameters involved in sanding prediction study.

in the system. As it was expected, the system can be controlled by changing this parameter. For instance, directional perforation can control the magnitude of induced stresses around the perforation tunnel and delays the onset of sanding. On the other hand, "Reservoir pressure" has the less interaction in onset of sanding. This parameter cannot be controlled during the sand production and has the lowest impact on the other parameters.

The "Petrophysical properties" is the dominant parameter and has the highest cause value among the parameters. In contrast, "Fluid properties" and "Drawdown pressure" are the most subordinate parameters in the system. They also have the lowest cause value within the parameters. The "Drawdown Pressure" was expected to be the subordinate parameter since it is one of the construction design parameters.

6 SAND PRODUCTION ANALYSIS

As an application example, the interaction matrix reflecting the shear failure mechanism is shown in Figure 5, which shows that the disturbance commences after perforating a tunnel and progresses till it arrives back to the same parameter completing a loop. In rock

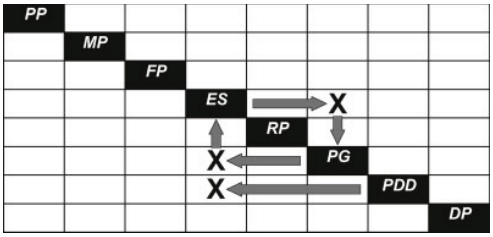

Figure 5. Interaction mechanism path due to shear failure.

engineering such loops are generally attenuated and die out (negative feedback). However, loops with positive feedback can occur (Hudson 1992), in which case the loop could continue till the stresses exceed the shear strength of sand and thus the sand production occurs in this way.

7 CONCLUSION

Different failure mechanisms of sanding were reviewed and the effective parameters involved were discussed.

The RES methodology was implemented to study the onset of sanding. The interactions between parameters and the system response were studied by constructing the interaction matrix and through cause-effect diagram interpretation. The results demonstrated the capability of the interaction matrix in studying different failure mechanisms simultaneously and in parallel.

REFERENCES

Abbas, H.H., Habbtar, A.H. & Shebatalhamd, A. 2003. Sand control during drilling, perforation, completion and production. *SPE 13th Middle East Oil Show & Conference*, Bahrain, 9–12 June, SPE 81492.

Fjaer, E., Holt, R.M., Horsrud, P., Raaen, A.M. & Risenes, R. 2008. *Petroleum related rock mechanics 2nd edition. Developments in petroleum science 53*.

Hudson, J.A. 1992 – *Rock engineering systems: theory and practice*. Ellis Horwood, Chichester.

Veeken, C.A.M., Davies, D.R., Kenter, C.J. & Kooijman, A.P. 1991. Sand production prediction review: developing an integrated approach. *66th Annual Technical Conference and Exhibition of the Society of Petroleum Engineer.* Dallas, TX, October 6–9, SPE 22792.

Younessi, A., Rasouli, V. 2008. Representing a Rock Engineering System to analyze wellbore instability due to fracture reactivation. *First Southern Hemisphere International Rock Mechanics Symposium (SHIRMS)*. Perth, Australia.

Appendix: Details of sand production experiments

Two set of experiments were carried out to simulate sand production under true-triaxial stress conditions. In these experiments the mechanism of sanding and the effect of lateral stresses on geometry of the failure zone were investigated (see Chapter 3). The experiments setup is described in detail in Section 3.1. In these experiments the loading and unloading procedure described in Section 3.2 was implemented. The deformation of the borehole wall was not monitored during these experiments. However, failure was detected by monitoring the amount of produced sand at the outlet of TTSC (see Figure 3.3). At the end of each experiment, after the sample was removed from TTSC, the shape of the failure zone was captured precisely using a borescope. The detail of the results of these experiments is presented in this section.

Set 1 of experiments

In the first set of experiments the target axial and maximum lateral stresses were set to 8 and 14 MPa respectively. The target minimum lateral stress, which was the intermediate boundary stress, was different in each experiment. Hence, the minimum lateral stress was 8, 10, 12 and 14 MPa in experiments B1401 to B1404 respectively (see Table 3.1). The target boundary pore pressure applied to all of these experiments was 4 MPa. It must be noted that the target stresses and pore pressure are the final loads that was applied to the boundary of the sample at it was reached by increasing the loads in several steps described in Section 3.2.

The first experiment was test B1404 where both lateral stresses were 14 MPa, and hence the stress distribution around the borehole was axisymmetric. The loading and unloading path along with the cumulative amount of produced sand in test B1404 is plotted in Figure A.1. During the loading stage of this experiment no sand was observed in the measurement tube at the outlet of TTSC. However, as soon as the fluid flow was stopped, at the end of loading stage, a small amount of sand was observed in the measurement tube.

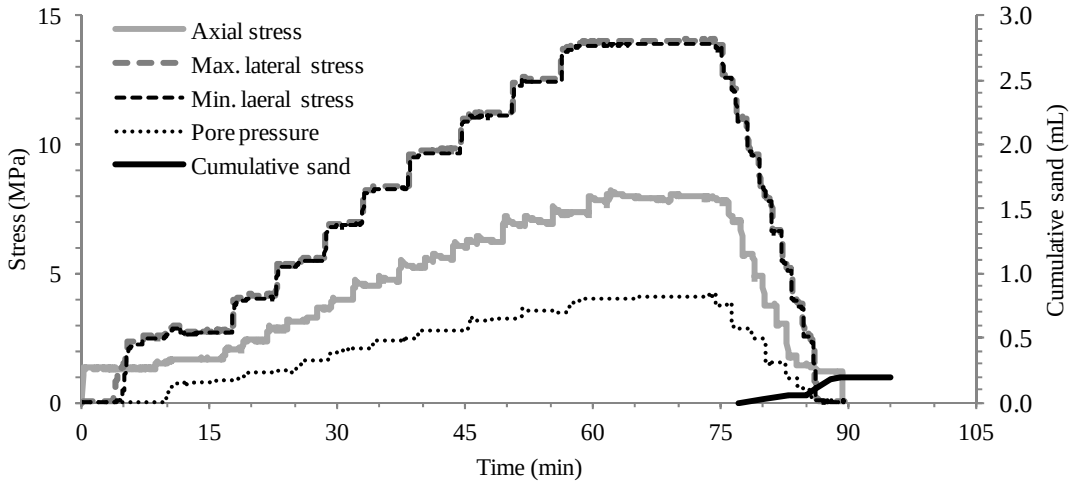

Figure A.1. Loading diagram and cumulative sand volume produced in test B1404.

After unloading the sample, the sample was removed from TTSC. A large amount of failed sand grains were still attached to the borehole wall due to residual strength. These grains were removed from the borehole wall by blowing pressurized air. This was done under free-stress state condition, so the cavity did not expand further. The shape of the failure zone was then captured precisely using a borescope. The geometry of the failure around the borehole of test B1404 is shown in Figure A.2.

For the rest of the experiments in Set 1 it was decided to stop the fluid pump at the end of each loading steps to make sure that all the produced sands are collected in the measurement tube. Figure A.3 shows the loading paths of the rest of experiments in Set 1 along with the cumulative produced sands. Figure A.4 shows the failure zones developed around the borehole for the rest of experiments in Set 1.

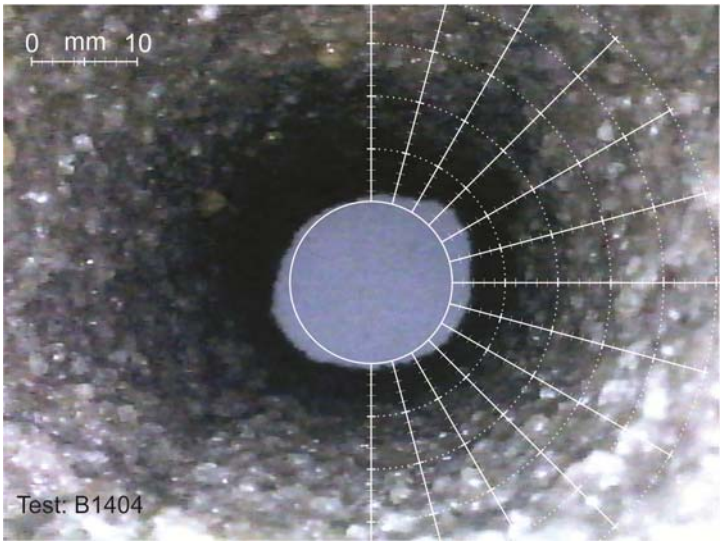

Figure A.2. Failure zone developed in experiment B1404.

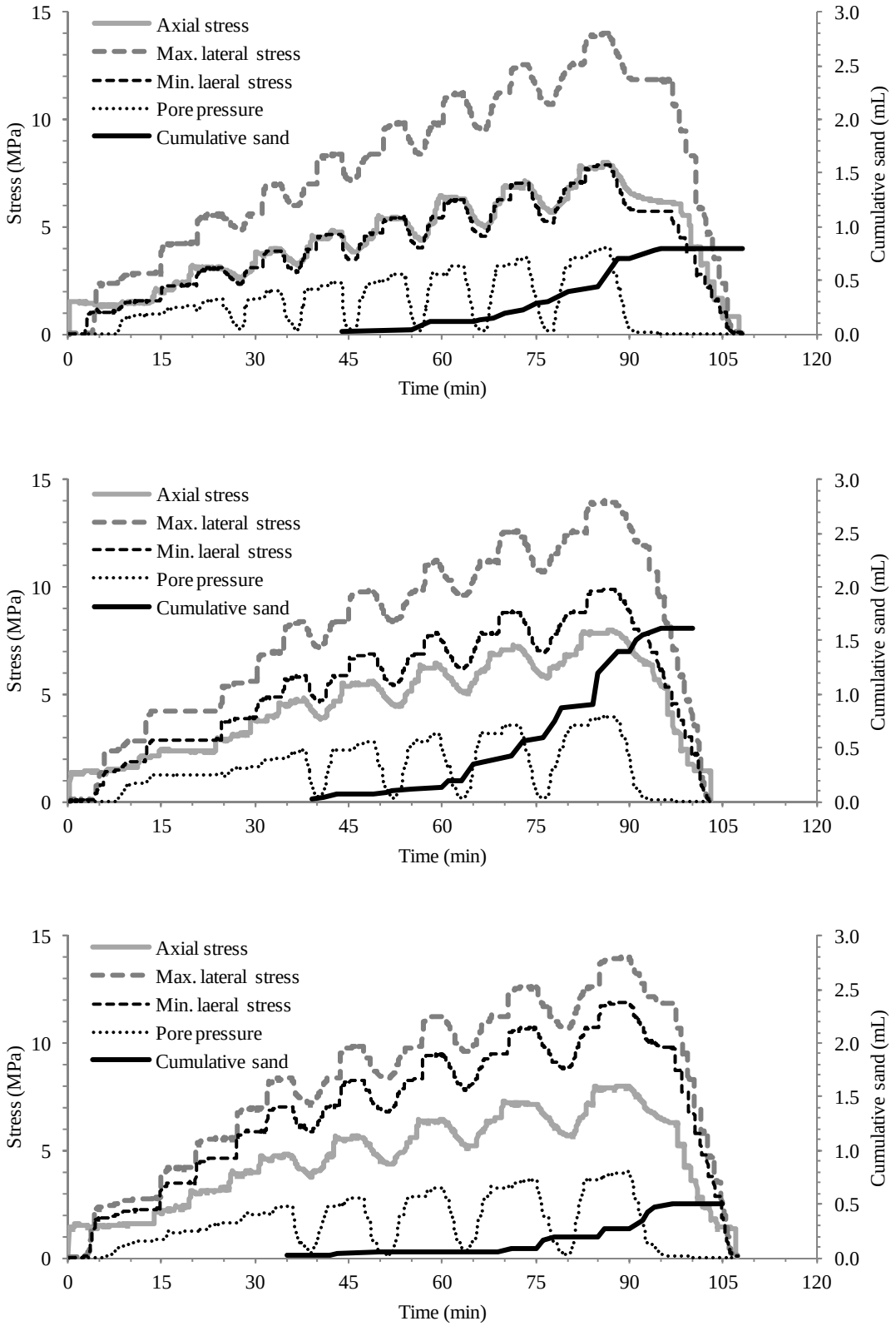

Figure A.3. Loading diagram and cumulative sand volume produced in tests B1401, B1402 and B1403 (from top to bottom).

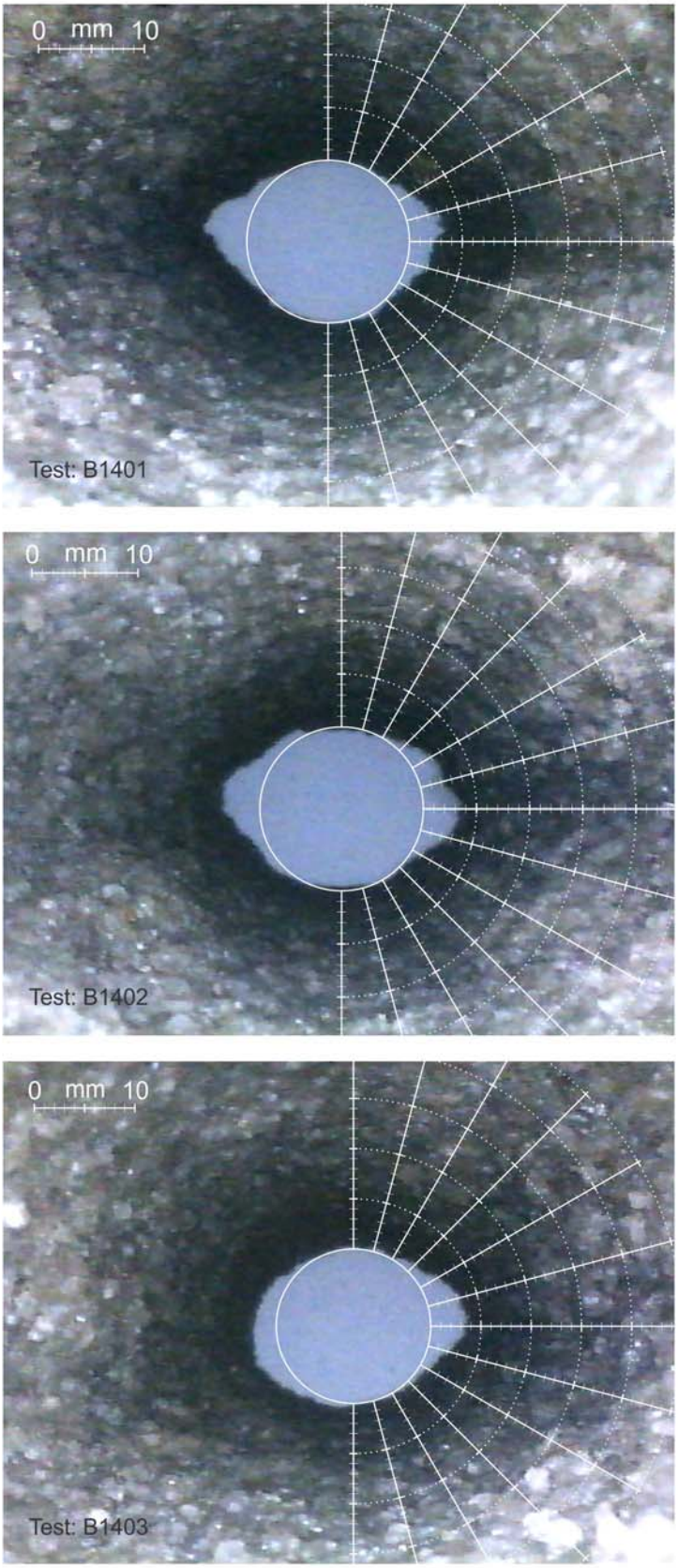

Figure A.4. Failure zone developed around the borehole in tests B1401, B1402 and B1403 (from top to bottom).

Set 2 of experiments

In the second set of sand production experiments the target boundary pore pressure, axial and maximum lateral stresses were initially set to 4, 8 and 20 MPa respectively. Similar to Set 1 The target minimum lateral stress was different in each test. However, in the first test (test B1600) of this set of experiments the specimen was totally failed due to high boundary stresses and progressive sand production (where the target minimum lateral stress was 8 MPa). Therefore, the target boundary stresses were changed for the rest of these experiments. The target boundary pore pressure, axial and maximum lateral stresses were changed to 3.2, 6.4 and 16 MPa respectively. And the minimum lateral stresses were changed to 6.4, 11.2, 16 MPa in experiments B1601 to B1603, respectively.

The loading path and cumulative produced sand for experiment B1600 is presented in Figure 3.8. In test B1600, because the sample totally failed by the end of the loading stage, the experiment was terminated immediately without following the unloading procedure. Large deformations were observed at the borehole wall in the direction of maximum lateral stress after the sample was removed from the TTSC (Figure A.5).

Figure A.6 shows the loading paths and cumulative produced sands for the rest of tests of Set 2 of experiments. In overall, it can be seen that the amount of produced sands were increased in the second set of experiments. This is obviously due to the larger failure zone induced around the borehole in the second set of experiments. The geometries of the failure zone induced around the borehole of the rest of tests in Set 2 of experiments are presented in Figure A.7.

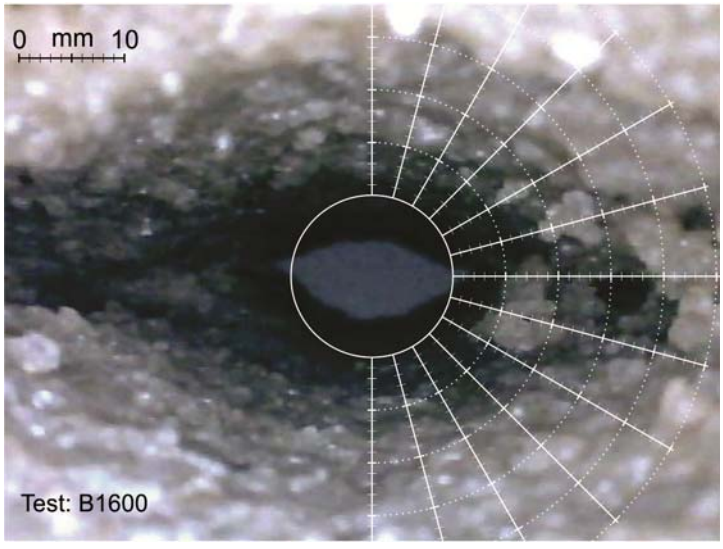

Figure A.5. Deformation and Failure zone induced around the borehole in test B1600.

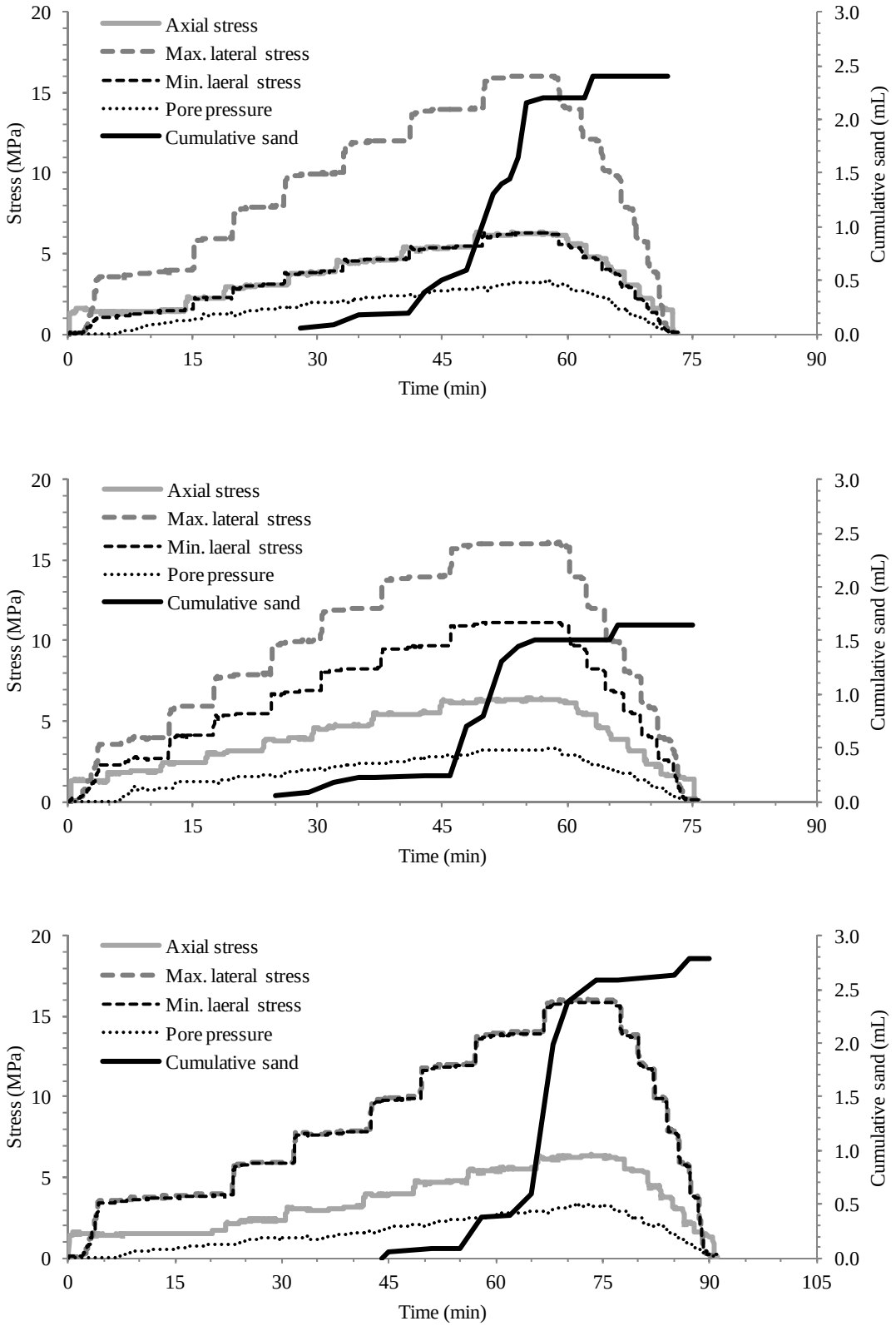

Figure A.6. Loading diagram and cumulative sand volume produced in tests B1601, B1602 and B1603 (from top to bottom).

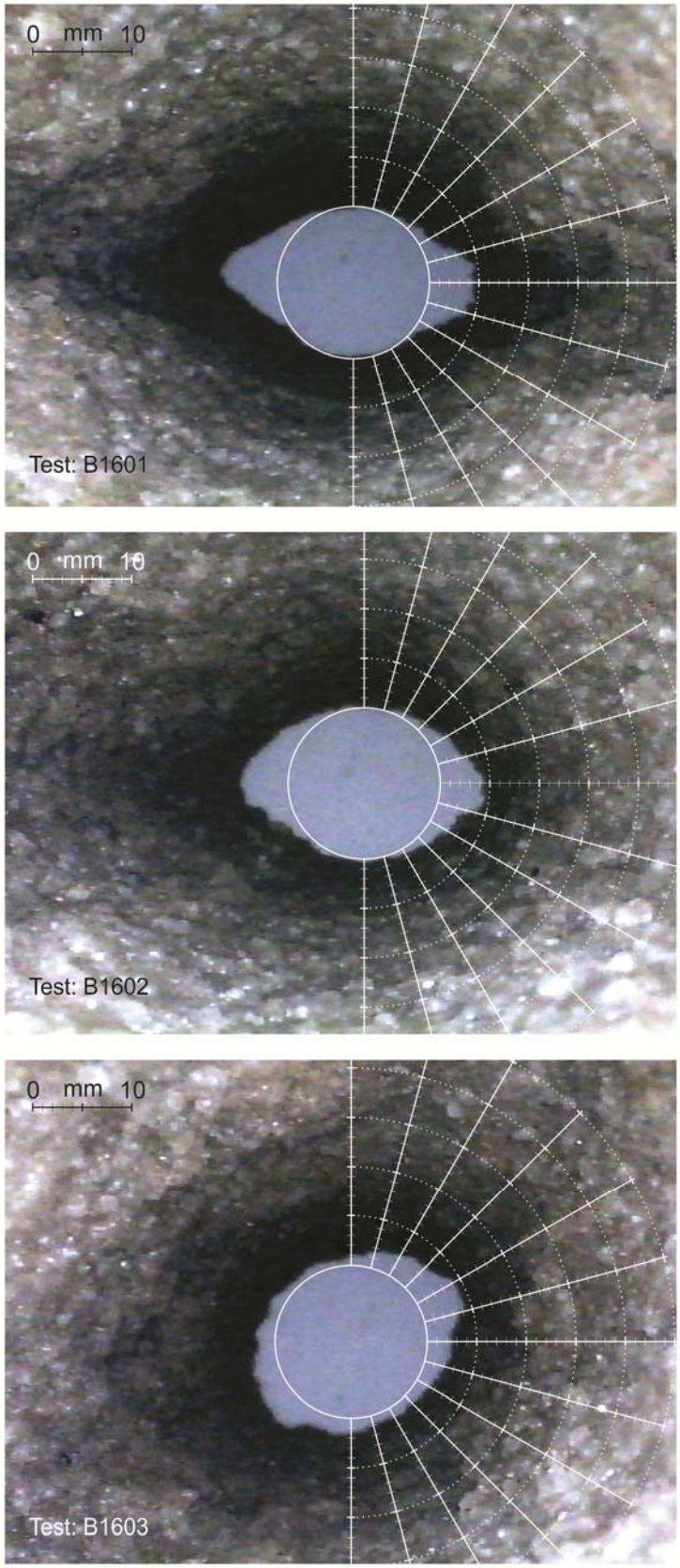

Figure A.7. Failure zone developed around the borehole in tests B1601, B1602 and B1603 (from top to bottom).